FOSSIL ENERGY

DOE/BC/15190-2
(OSTI ID: 800796)

3-D RESERVOIR AND STOCHASTIC FRACTURE NETWORK MODELING FOR ENHANCED OIL RECOVERY, CIRCLE RIDGE PHOSPHORIA/TENSLEEP RESERVOIR, WIND RIVER RESERVATION, ARAPAHO AND SHOSHONE TRIBES, WYOMING

Semi-Annual Report
November 1, 2000-April 31, 2001

By:
Paul R. La Pointe
Jan Hermanson

Date Published: September 2002

Work Performed Under Contract No. DE-FG26-00BC15190

Golder Associates, Inc.
Redmond, Washington

National Energy Technology Laboratory
National Petroleum Technology Office
U.S. DEPARTMENT OF ENERGY
Tulsa, Oklahoma

DISCLAIMER

This report was prepared as an account of work sponsored by an agency of the United States Government. Neither the United States Government nor any agency thereof, nor any of their employees, makes any warranty, expressed or implied, or assumes any legal liability or responsibility for the accuracy, completeness, or usefulness of any information, apparatus, product, or process disclosed, or represents that its use would not infringe privately owned rights. Reference herein to any specific commercial product, process, or service by trade name, trademark, manufacturer, or otherwise does not necessarily constitute or imply its endorsement, recommendation, or favoring by the United States Government or any agency thereof. The views and opinions of authors expressed herein do not necessarily state or reflect those of the United States Government.

This report has been reproduced directly from the best available copy.

DOE/BC/15190-2
Distribution Category UC-122

3-D Reservoir and Stochastic Fracture Network Modeling for Enhanced Oil Recovery, Circle Ridge Phosphoria/Tensleep Reservoir, Wind River Reservation, Arapaho and Shoshone Tribes, Wyoming

By
Paul R. La Pointe
Jan Hermanson

September 2002

Work Performed Under DE-FG26-00BC15190

Prepared for
U.S. Department of Energy
Assistant Secretary for Fossil Energy

Virginia Weyland, Project Manager
U.S. Department of Energy
National Energy Technology Laboratory
National Petroleum Technology Office
One West Third Street, Suite 1400
Tulsa, OK 74103

Prepared by
Golder Associates Inc.
18300 NE Union Hill Road, Suite 200
Redmond, WA 98052

Table of Contents

List of Graphical Materials

List of Tables

ABSTRACT

This report describes the progress and results made in fulfillment of contract DE-FG26-00BC15190, "3-D Reservoir and Stochastic Fracture Network Modeling for Enhanced Oil Recovery, Circle Ridge Phosphoria/Tensleep Reservoir, Wind River Reservation, Arapaho and Shoshone Tribes, Wyoming" during the first 6 months of the project. The goal of this project is to improve the recovery of oil from the Circle Ridge Oilfield, located on the Wind River Reservation in Wyoming, through an innovative integration of matrix characterization, structural reconstruction, and the characterization of the fracturing in the reservoir through the use of discrete fracture network models. Progress and results have been obtained during this period for several tasks: Task 2.1 – Compilation of existing data; Task 2.2 – Core/FMI data analysis; Task 2.4 – Construction of Balanced Cross-sections; Task 2.5 – Validation of cross-sections; Task 2.6 – Generation of DFN model; Task 3.1 – DFN model flow validation; Task 3.2 – Fault block & matrix model development; and Task 5.1 – Project Web Site.

The principal achievement during this period has been the development and completion of the 3D palinspastic reconstruction of the Circle Ridge Field. The successful completion of this critical step in the project has confirmed some of the previous ideas concerning fault block architecture, and has also led to revisions and refinements that will impact the recovery efficiency of secondary or tertiary recovery processes. The 3D palinspastic model also provides the critical link for conditioning fracture intensity and orientation by making it possible to compare the results of the surface outcrop work and the strain field calculated from the 3D reconstructions.

In addition to the completion of the 3D palinspastic reconstruction, Marathon Oil Company (MOC) conducted a nitrogen injection tracer test in which gas breakthrough was monitored in 66 wells. During the course of this test, MOC obtained surface and bottom hole pressure interference data from 5 wells, and an FMI and a spinner log. Preliminary analysis of this data has been completed. The non-uniform breakthroughs observed during the nitrogen injection test indicate that there are pathways of high conductivity trending east-southeast from the injection well. This direction is sub-parallel to oblique to the strike oif the Red Gully Fault and to the hinge of the field anticline.

The fracture data obtained during the fieldwork of June-July 2000 was analyzed, and the results indicate that the fracturing extant in the reservoir appears to be consistent with formation during folding. During the next quarter, the comparison of the fracture data to the strain data calculated from the palinspastic reconstruction will be completed.

The results of the palinspastic reconstruction, the outcrop analyses and the nitrogen injection test results have been used to plan the remaining tracer, pressure interference, transient, image log and spinner log data acquisition for this project.

Preliminary meetings and work has begun on Task 3, the creation of the fully integrated reservoir model. The project website has been updated with data, reports and results obtained since the first reporting period, and project results have been provided informally to the Northern Arapaho and Eastern Shoshone Tribes.

In general, the project is on schedule and budget. The original work scope called for completion of Task 2.1 and 2.2 in the Fall of 2000. These Tasks include the acquisition and analysis of all field test data. Due to field operations scheduling and to take advantage of the results of the outcrop fracture data analysis and palinspastic reconstruction results, some of the additional subsurface data acquisition was deferred until the summer of 2001, which has now been designed and scheduled. Task 2.6, the generation of the preliminary discrete fracture network model, was scheduled to begin

April 1, 2001 and end May 1, 2001. Due to the slightly delayed completion of the 3D reconstruction, Task 2.6 will be completed by the end of June, 2001. Offsetting these small delays has been the initiation of work on various parts of Task 3, which were not scheduled to begin until the third six-month period of this project. On balance, the initiation of Task 3 tasks and the delays on some of the Task 2 tasks should not impact any of the deliverables in this project or for the next six-month project period. In fact, delaying the final field data acquisition until the structural reconstructions and fracture analyses had been completed has greatly improved the planning of these remaining tests and log acquisitions to best benefit the project's goals.

1 INTRODUCTION

The first six months of this project focused on data collection and preliminary analysis. During this period, there were three active main tasks composed of several active subtasks. The main tasks were Task 1 – Petrophysical Analysis (all subtasks active), Task 2 – Development of the structural conceptual model (subtasks 2.1, 2.2 and 2.3 active), and Task 5 – Technology Transfer (all subtasks active). Due to personnel scheduling considerations relative to Marathon Oil Company's ongoing restructuring, substantial work was initiated on Task 2.4 – Construction of balanced cross-sections.

The project's overriding focus for the second six-month period has been the completion of Task 2 – Development of the structural conceptual model and all of its associated subtasks. Task 2 includes the acquisition and analyses of all surface and subsurface geological, fracture and flow data; the development and validation of a fully three-dimensional structural reconstruction of the Field, and the generation of a preliminary DFN model based upon conditioning parameters identified by jointly analyzing the subsurface data, the outcrop studies and the strain field calculated from the palinspastic reconstruction.

Throughout this report, reference is made to the "overthrust block" and "subthrust block". In general, this nomenclature is used to distinguish between rock in the hanging wall of the main Red Gully Fault (overthrust) and rock in the footwall (subthrust). The actual structural geology is much more complex, as shown by the 3D palinspastic reconstruction results, but this terminology has been retained for ease of reference.

This report follows the outline mandated in Section 4.14 (Guidelines for Organization of Technical Reports (May 1999)) as specified in the contract. The discussion of the experimental work is organized by Task, as are the Results and Discussion section.

2 EXPERIMENTAL WORK

2.1 Overview

The experimental work reported for this contract period consists of the acquisition of new subsurface flow and fracture data, the construction of cross-sections for the Circle Ridge Field, the 3D palinspastic reconstruction of the Circle Ridge Field, and the analysis of the orientations, intensity and size of fractures found in outcrops in the Field. Section 2.2 describes the experimental procedures used in the acquisition of the subsurface field data. Section 2.3 describers the analysis techniques used for the construction of balanced cross-sections; Section 2.3.3 describes the techniques for palinspastic reconstruction, while Section 2.4 describes the analysis techniques used to calculate the statistical parameter values for the outcrop fracturing.

2.2 Compilation of Existing Data – Task 2.1

This Task, in spite of its name, includes approximately $98,000 of in-kind contribution from Marathon Oil to acquire various types of new data from well and well tests. Existing data was already compiled, as described in the previous report (La Pointe and others, 2000). The new data to be acquired for this project is shown in Table 2-1.

Description of Data	Number of tests/logs
Fracture image logs run in existing or new open-hole completions	3
Dynamic flow logs	3
Inter-well pressure interference tests	2
Single well pressure build-up or fall-off tests	2
Injected tracer studies	2

Table 2-1. List of subsurface data to be acquired.

The experimental acquisition of this data is described in the following sections. The wells selected for obtaining this data represent joint consideration of quality and availability of the wells, stratigraphic coverage (inclusion of both Tensleep and Phosphoria), structural coverage (inclusion of both subthrust and overthrust blocks; location to facilitate comparison with surface outcrop studies), and field logistics.

2.2.1 FRACTURE IMAGE LOGS

Image logs obtained as part of this project are Fullbore Formation MicroImager™ (FMI - Schlumberger) logs in open-hole intervals. The logs were interpreted by Marathon to calculate the location and orientation of fractures, bedding plane, and borehole breakout information.

2.2.2 DYNAMIC FLOW LOGS

In order to further understand which features provide the flow paths for fluid flow, high resolution injection profiles are obtained. The flow logging is carried out using a Baker-Atlas spinner tool

2.2.3 INTERWELL PRESSURE INTERFERENCE TESTS

The goal of these pressure interference tests is to understand the pattern of connections between wells, and to use these tests to calibrate the geometric and flow properties of the fracture model. The tests involve changing the pressure at one well, and monitoring pressure responses at other wells. The first pressure interference test was carried out at the same time as a nitrogen injection tracer test (see Section 2.2.5) in order to increase the usefulness of both data sets.

2.2.4 SINGLE WELL PRESSURE BUILD-UP OR FALL OFF TESTS

Falloff data has been obtained at Shoshone 65-2, Shoshone 66-69, and Shoshone 66-2 and in the Overthrust Tensleep. Interpretation of this fall-off data is being performed using an Eclipse reservoir simulator and commercially available pressure transient interpretation software.

2.2.5 INJECTED TRACER STUDIES

Tracer tests can take many different forms. One test has already been carried out, and another will be completed during the summer of 2001. The completed test, described first, is termed the Overthrust Tensleep Nitrogen (OTN) Test. The second test, to be completed this summer, is a bromide test.

In an attempt to better understand reservoir flow paths and the potential for improving oil recovery via gas injection, a nitrogen injection tracer test was performed. Approximately 17.9 MMCF of nitrogen was injected into an up-structure Overthrust

Tensleep well, Shoshone 65-2, during September 2000. A total of 66 Circle Ridge wells were monitored for gas breakthrough.
Marathon currently plans (subject to required regulatory approval) to perform a sodium bromide tracer test in subthrust Fault Block 1. The test will be performed by injecting a concentrated slug of sodium bromide into Shoshone 65-20, a subthrust Phosphoria water injection well. Offset subthrust and overthrust producers will be monitored for breakthrough time and bromide concentration. Mass balance calculations, concerning tracer recovery, will also be performed. If problems are encountered, rendering injection into Shoshone 65-20 infeasible, the tracer will be injected into Shoshone 65-12. Shoshone 65-12 is a subthrust Fault Block 1 Tensleep water injector.

2.3 Construction of Balanced Cross-Sections – Task 2.4, and Validation of Cross-Sections Using Retrodeformation Software – Task 2.5

2.3.1 PURPOSE OF TASKS

Task 2.4 and Task 2.5 are closely related. The purpose of Task 2.4 is to provide input to the retrodeformation process in Task 2.5. Task 2.5 ends with the creation of a balanced palinspastic restoration of the Tensleep and Phosphoria reservoir units. In Task 2.6 (Section 3.6), the strain field is calculated from the successful palinspastic reconstruction and compared with the fracture geometry measured in outcrop in the subsurface, in order to determine how the strain field relates to fracture pattern development, as well as to the parameter values necessary to utilize strain information for developing the discrete fracture network (DFN) model.

2.3.2 ANALYSIS TECHNIQUES

Palinspastic reconstructions of folded and faulted stratigraphy have been widely used for the last 20 years. The reconstructions have mainly been based on 2D cross-sections and several different theoretical methods for various types of fold and fault related deformations have been established by a number of authors, of which Suppe (1983, 1985, 1989), Suppe et al (1990), Medwedeff (1989) and Mitra (1986, 1990) have contributed significantly.

In contrast to 2D reconstructions, the complexity of restoring surfaces and volumes of rock requires the use of computers. The methodology to restore folded and faulted formations are essentially the same as has been used for 2D problems, but has been expanded to allow for movement in all three dimensions. The amount of geometric calculations and thus the need for fast computers has until recently limited full reservoir reconstructions. Due to the increase in computer power over the past few years, 3D palinspastic reconstructions are now possible.

2.3.3 AVAILABLE TECHNOLOGY FOR 3D RECONSTRUCTIONS

There are presently two commercial forward and reverse geological modeling packages available at the open market today: 3Dmove by Midland Valley Ltd. and Geosec3D by Paradigm. There also exist a number of 2D and pseudo-3D restoration packages that can handle specific types of restoration techniques. For this study 3DMove has been chosen for its ability to simulate inclined shear, fault parallel flow, flexural slip unfolding and many other reconstruction techniques truly in three dimensions. 3DMove provides all the techniques listed below, which are required for the Circle Ridge restoration:

- Full 3D restoration and forward modeling capability
- Applicable to strike slip, extension, thrusting, salt tectonics and inversion
- Fast restore-to-target-horizon approach for quick look analysis
- Move on fault capability for full kinematical analysis
- Inclined shear and flexural slip capability
- 3D Model building and visualization
- 2D and 3D data as input
- Wells and seismic display
- Fault construction tools
- Displacement analysis
- Cut-off mapping in 3D and through time
- Contour and 2D sectioning of the 3D model
- Strain visualization
- Interactive freehand model editing
- Full 3D volume representation and attribute filling

2.3.4 RESTORING THRUSTS AND FAULTS

The primary method for restoring faults and thrusts in Circle Ridge has been the Fault Parallel Flow algorithm. Below follows a description of the used method and its implications.

2.3.4.1 Fault Parallel Flow

Fault parallel flow is a kinematic restoration method allowing hanging wall surfaces to be moved across faults in such a way that the hanging wall vertices move parallel to the fault segments over which they are flowing.

Fault Parallel Flow involves a two-stage process:

1. Define the hanging walls and faults, specify the transport direction and calculate the flow model.
2. Once the flow model has been calculated, the hanging walls can be moved using a number of different techniques as described later in this section.

The fault parallel flow method in 3Dmove calculates a flow path for every hanging wall vertex. The general procedure is as follows:

For every hanging wall vertex;

- Create a vertical slice through the faults along the specified transport direction. This produces a fault line over which the hanging wall vertex would move.
- Generate the bisectors for the line.
- Calculate and store the flow path of the hanging wall vertex through the bisectors.

An example fault line and flow path are shown in Figure 2-1. The bisectors merge as they intersect with one another, allowing the delineation of dip domains. Each dip domain has a corresponding fault segment. The hanging wall vertex will pass through the bisectors, moving parallel to the fault segment for any given dip domain.

Once this flow path is generated, the hanging wall vertex can be easily moved along it. It is also possible to apply shear to the hanging wall, by applying an additional slip value to the vertices relative to their height above the fault.

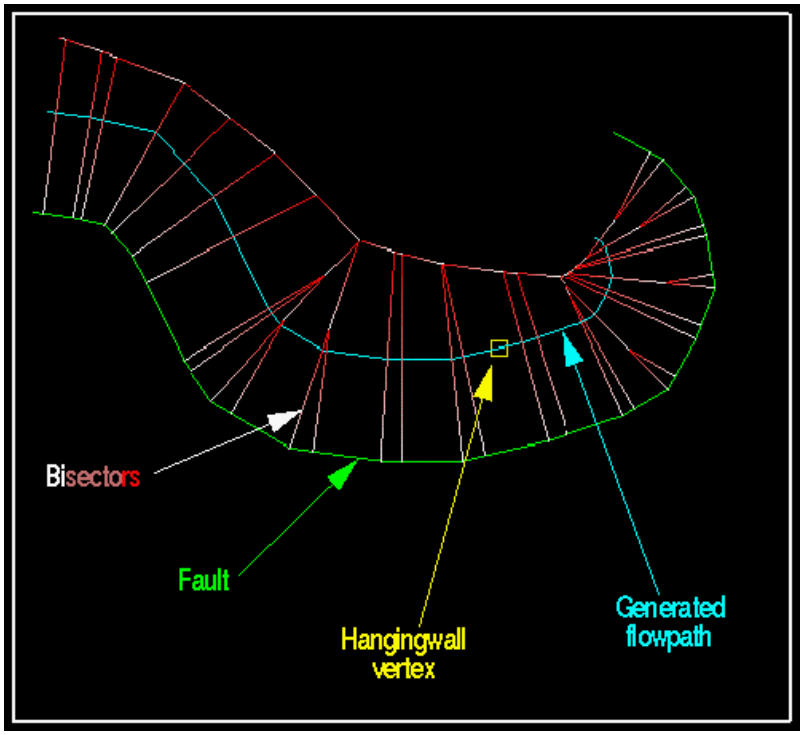

Figure 2-1 Illustration of a cross-section of the calculated flow path along a fault surface (from Midland Valley, 2000)

There are three options for moving the flow model in 3Dmove:

1. Movement by Slip value
2. Movement using Heave bands
3. Restore-to-Surface movement

A slip slider bar is used to change the slip across the whole model (Figure 2-2). A constant slip value is applied to every hanging wall vertex.

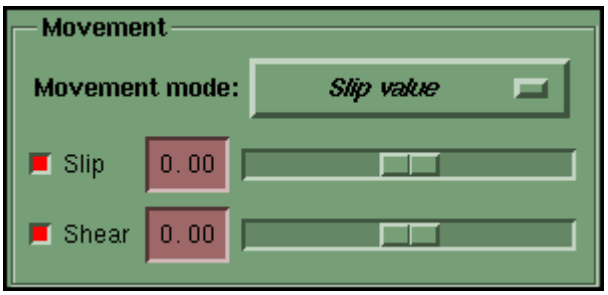

Figure 2-2 Slip slider menu in 3Dmove to perform movement by slip value (from Midland Valley, 2000)

The shear slider is used to change the shear across the model. Using the shear slider applies an additional slip value (on top of the specified slip) relative to the hanging wall vertex's height above the fault. This is illustrated in Figure 2-3.

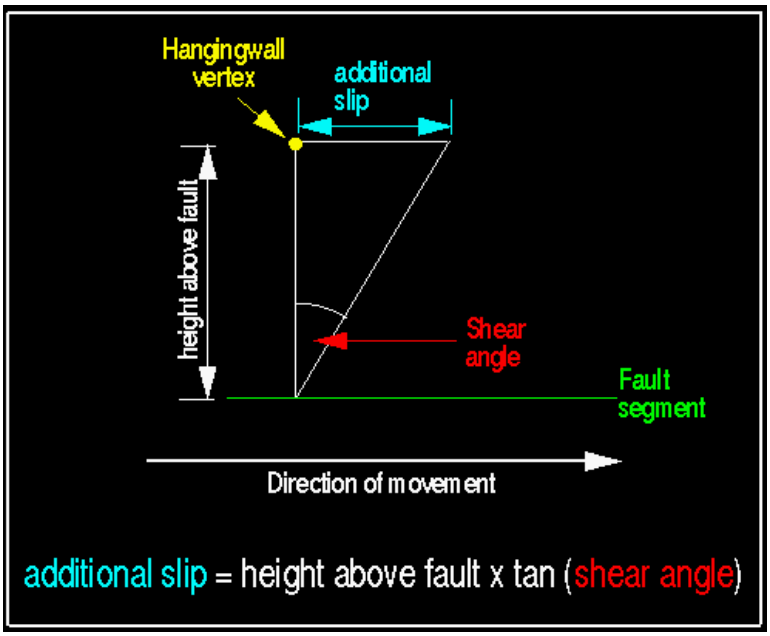

Figure 2-3 Shear calculation using fault parallel flow (from Midland Valley, 2000)

Heave bands movement mode allows the change of slip profile across the fault. Heave bands are usually used to enable different amounts of slip on different sections of the hanging wall formation to match the opposing side of the formation (on the footwall side). This method is desirable when observations show that in order to match the surfaces, variable movements along the fault need to be applied.

The shear slider is also available in this mode, and allows you to independently vary the shear applied to the hanging wall vertices.

The Restore-to-Surface movement mode applies a unique slip value to every hanging wall vertex.

This is done by matching two surfaces on different sides of the fault with each other. 3DMove will calculate - for every flow path in the flow model - the slip distance between the deformed surface and the undeformed surface as shown in Figure 2-4. However, this technique works well only if the fault is relatively steep. If the hanging wall is almost in plane with the fault, the slip lines increase in length back down the fault, as shown in Figure 2-5.

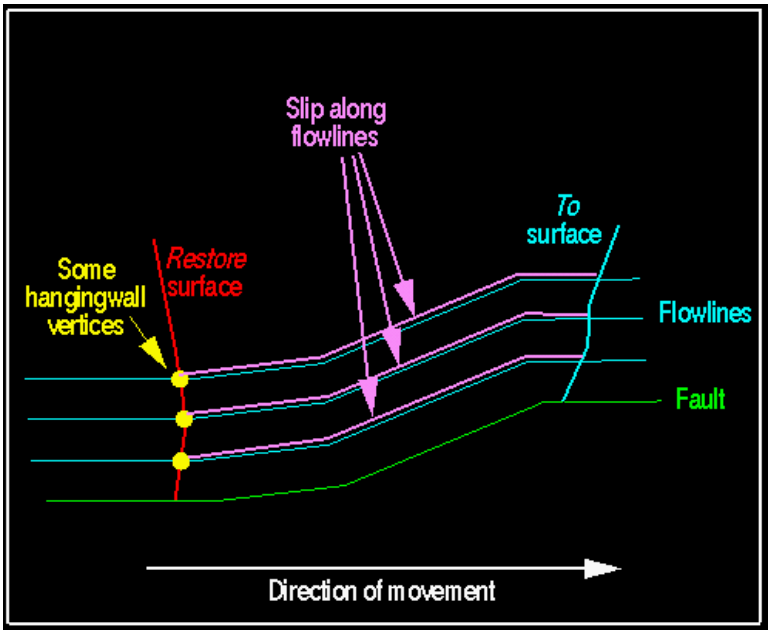

Figure 2-4 Slip along flowlines using the restore to surfaces movement mode (from Midland Valley, 2000)

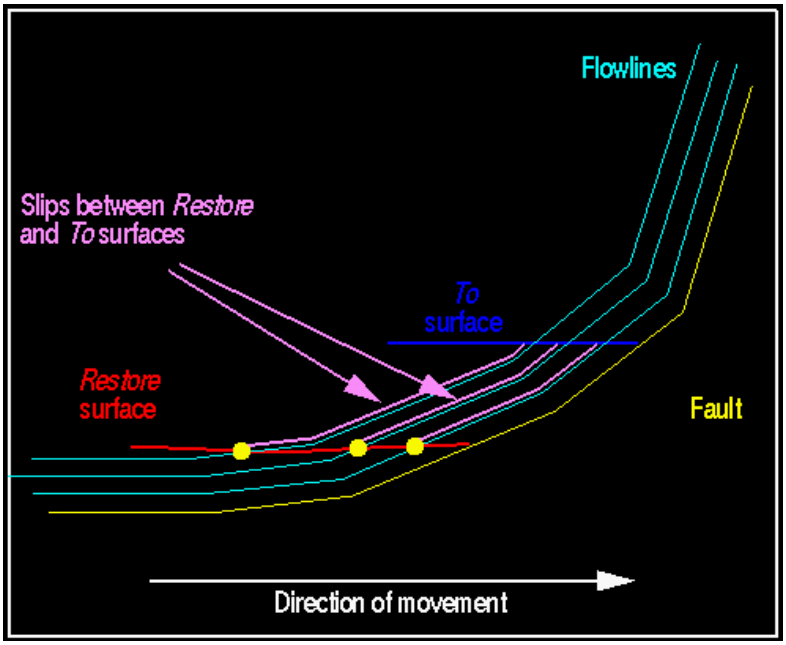

Figure 2-5 Implications of the Restore-to-Surface movement method (from Midland Valley, 2000)

2.3.5 RESTORING FOLDS

Two techniques have been utilized to restore folded strata;

1) Vertical and inclined shear unfolding, and
2) Flexural slip unfolding.

A short explanation of the implications of each restoration technique is presented in the next sections.

2.3.5.1 Vertical and inclined shear unfolding

Vertical and inclined shear balancing preserves the volume of the restored formation. Figure 2-6 shows a black and red surface, which represent a cross-section through a hanging wall fold. The black surface is shown unfolded back to a datum, which represents the pre-deformation geometry (horizontal dotted green line). This datum can be set at any Z depth or elevation.

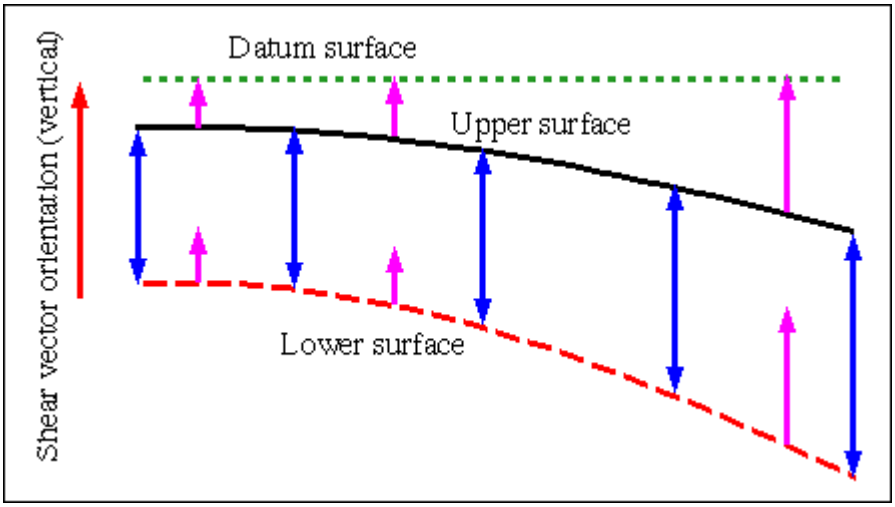

Figure 2-6 Cross-section through a hanging wall fold (from Midland Valley, 2000)

The black and red surfaces are unfolded along a chosen shear vector, in this case a vertical shear vector, represented by the thick, red arrow.

To retro-deform the fold, the black bed is translated vertically to the green datum, with the vertical translation distance varying across the section. The pink arrows represent this distance. The lower red bed is translated the same vertical distance as the black bed that enables volumes to be preserved within the model.

The vertical distance between the black and the red beds is maintained in the orientation of the shear vector. The blue, double-headed arrows in Figure 2-7 represent this distance.

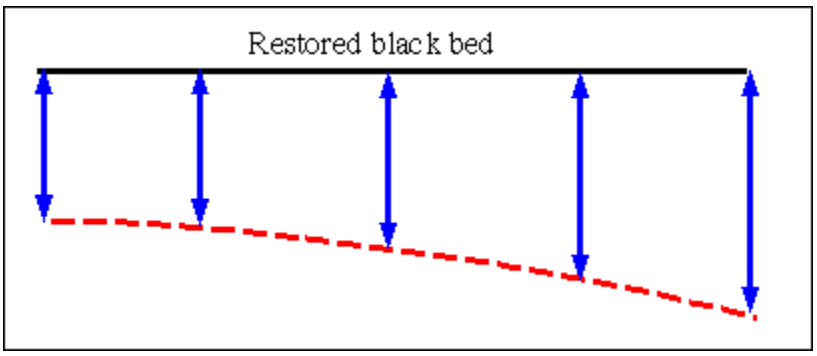

Figure 2-7 Cross-section through the restored hanging wall fold (from Midland Valley, 2000)

Figure 2-7 illustrates how the line length and therefore the surface area of the black surface will change as it is unfolded.

For a constant dip surface using vertical shear, the restored length is shorter than the original length, as shown in Equation 2-1 and Figure 2-8:

$$l = l_o Cos(\theta) \qquad \text{Equation 2-1}$$

where θ is the bed dip,
l is the restored length, and
l_o is the original length.

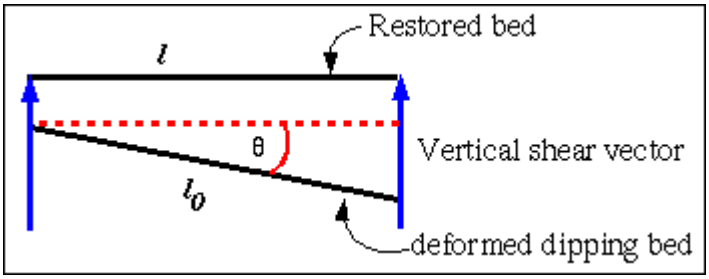

Figure 2-8 The concept of vertical shear and the restored length (l) (from Midland Valley, 2000)

Figure 2-8 illustrates the new area of the restored surface and its relationship with the angle between the restored bed and the deformed dipping bed:

$$A = A_o Cos(\theta) \qquad \text{Equation 2-2}$$

where A_o is the original area of the surface, and
A is the new area.

The area change (ΔA) is given by:

$$\Delta A = A_o - A = A_o(1 - Cos(\theta)) \qquad \text{Equation 2-3}$$

This means that the more steeply dipping the surface is, the greater will be the area change of the restored surface. For a smooth, curved surface, such as a fold, the area change is a complex function, with increasing area change as bedding dip increases.

The key point to note, regarding this technique, is that volume is preserved, but surface area will change. The surface area only remains constant for vertical shear. The map view "footprint" of the surface remains the same.

2.3.5.2 Flexural slip unfolding

The flexural slip unfolding algorithm allows unfolding to occur such that the unfolded model:

- maintains the line length of the template surface in the direction of unfolding;
- maintains the orthogonal bed thickness between the template surface and other passive objects;
- maintains volume of the fold and the model;
- maintains surface area for cylindrical folds with the pin surface coincident with the axial plane; and
- line length and surface area is not maintained in the passive surface (surface area is not maintained in non-cylindrical folds).

For layer-parallel beds, flexural slip unfolding represents flexural slip during fold formation.

The flexural slip unfolding method can be used to validate complex thrust deformations and the cover rocks surrounding intrusive salt structures. As with the inclined shear unfolding mechanism, the methodology of using the flexural slip unfolding algorithm is to unfold the rocks and then to translate the unfolded components to their pre-deformation positions. The structural model is validated if the unfolded rocks can be reassembled to form a coherent geometry.

Analogous to the inclined shear methodology previously described, the shear vector orientation determines the unfolding direction. For example with vertical shear, the beds are unfolded onto a datum (usually horizontal) with the volume of the fold being

preserved. However, the surface area of the fold is not preserved between the folded and unfolded stages. In contrast, the flexural slip unfolding algorithm preserves the line length (Length L shown below in Figure 2-9) in the direction of unfolding and also the surface area.

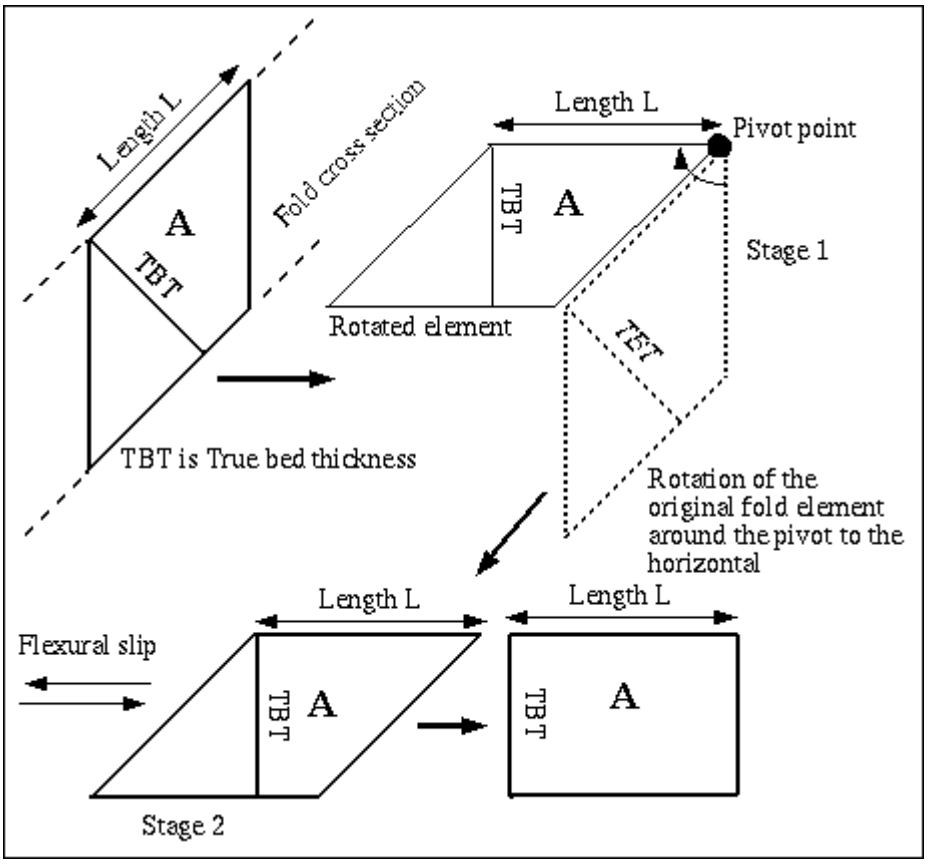

Figure 2-9 Illustration of the flexural slip unfolding algorithm (from Midland Valley, 2000)

Figure 2-9 shows part of a fold as seen in a cross-section. The fold limb dips at 45 degrees and a small volume element of the fold limb has been drawn as a parallelogram. The element has an area, A, which remains constant throughout the unfolding operation. Therefore, the volume of the fold remains constant during restoration.

In addition, the upper surface of the fold element in Figure 2-9 has a line in cross-section with the length L. When unfolded this line length remains constant, as opposed to the inclined shear restoration method where this line length changes. For parallel bedding, the true bed thickness (TBT) remains constant during unfolding, whilst the vertical bed thickness changes.

The flexural slip unfolding process takes place in two stages:

- a rotation of the upper fold surface and fold element to the horizontal (Stage 1 in Figure 2-9)
- a shearing operation to "undo" the flexural slip component of the folding (Stage 2 in Figure 2-9).

In order to carry out flexural slip unfolding, an unfolding direction and a pin surface location and orientation need to be defined. The concept of the pin plane is shown in Figure 2-10.

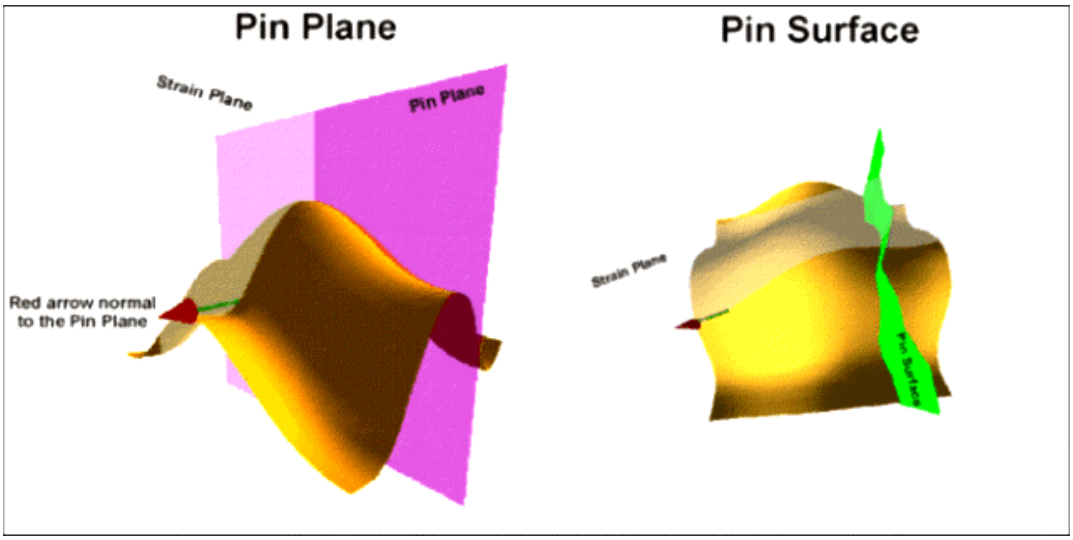

Figure 2-10 Orientation of the pin plane/surface and strain plane. Red arrow indicates the unfolding direction (from Midland Valley, 2000)

The sinuous line length (L in the diagram in Figure 2-11) is measured from the pin plane/surface intersection with the template surface, along the template surface in the direction of unfolding. The sinuous line lengths are measured for all vertices of the template surface. These sinuous distances are then propagated along the pin which may be vertical (as shown) or inclined. The line lengths are then translated along the target/datum in the unfolding direction on intersection with the datum or target surface.

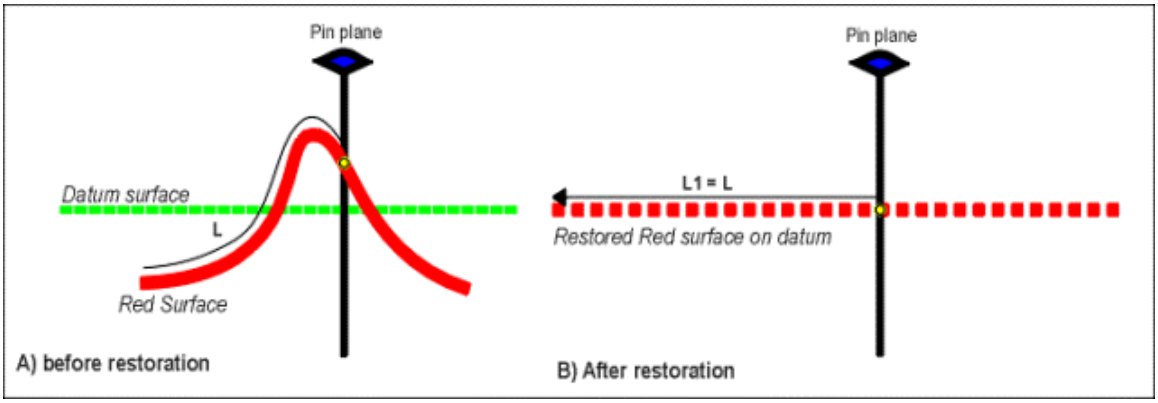

Figure 2-11 Maintaining sinuous line length with a vertical pin (from Midland Valley, 2000)

A slip system (shown in red) is generated from the dip domain bisectors projected from the template horizon (blue). Flow paths are calculated for all vertices of the passive objects in the unfolding direction. These flow paths ensure the orthogonal thickness and therefore fold volume, is maintained between the passive and the template horizons, (this is a similar system to the fault parallel flow algorithm). The sinuous distances to the pin plane of each vertex for all passive surfaces are calculated as illustrated in Figure 2-12. The illustration shows how the flow path (shown in purple) has been calculated for vertex P of the green passive horizon.

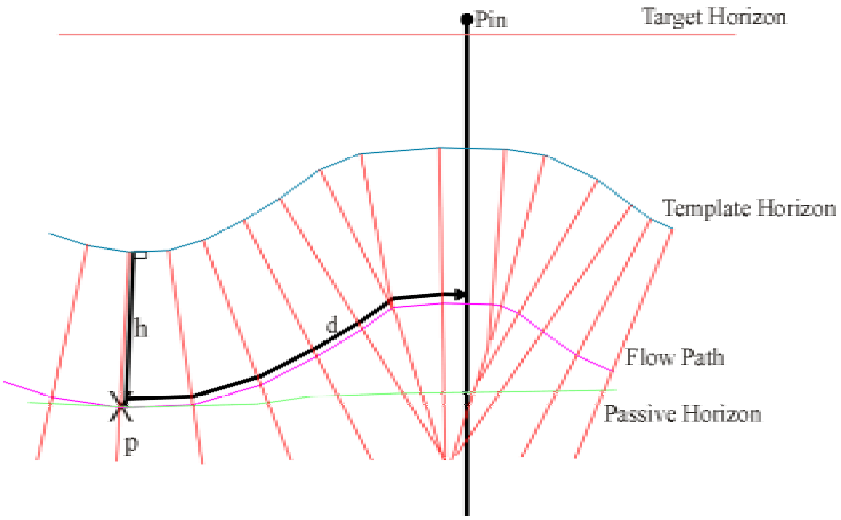

Figure 2-12 Illustration of the bed linkage and the slip system for each vertex in the deformed formation (from Midland Valley, 2000)

When the template horizon has been restored to the target surface or datum, each vertex of the passive horizons is translated along its individual flow path by the sinuous distance calculated in the deformed state. Bed linkage is achieved at the intersection of the template and passive objects with the pin plane and by maintaining orthogonal thickness,

h, between the template and passive surfaces. The flexurally unfolded horizons are shown in Figure 2-13.

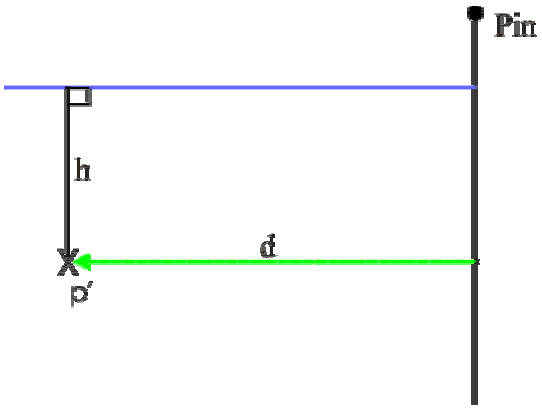

Figure 2-13 Flexurally unfolded template and passive horizons (from Midland Valley, 2000)

2.3.6 STRAIN ANALYSIS MEASURES

Strain can be quantified in terms of a bulk (non-directional) change in the rock volume, which is termed *dilation*, or by several other measures that incorporate anisotropy of changes with direction.

Geological materials that are strained pass through a large number of intermediate states before arriving at a final state. However, it is not possible to observe the intermediate stages of deformation for most, if not all, tectonic geological processes. In general, it is only possible to observe or quantify the initial undeformed state, the final present state, and perhaps one or two intermediate states. The result of the total deformation taking place from the initial state to the final state is termed the *finite state of strain*. In most situations, the finite strain for a volume of rock is not well modeled by a continuum or infinitesimal strain process. Because 3D palinspastic reconstruction produces a model of the geometry in the undeformed state, the final state, and perhaps a few intermediate states (for example, after folding but before faulting), finite strain measures are a useful way to quantify the deformation experienced by the rock. The next two sections describe the quantification of dilatational and directional finite strains.

2.3.6.1 Dilatation measures

Dilatation is the ratio of the change in length, area or volume of the strained object, relative to the unstrained value, this analysis can be applied to lines, surfaces and volumes. For example, the area dilatation for a surface would be calculated as follows:

$$\Delta_{area} = \frac{(a - a_0)}{a_o}$$ Equation 2-4

where Δ_{area} = the area dilation,
a = the area after strain, and
a_o = the area before strain.

Increases in area produce positive area dilatation; decreases lead to a negative area dilatation.

If a surface doubles its area, the area dilatation would become $(2a_o\text{-}a_o)/a_o = 1$;
If a surface quadruples its area, the area dilatation would become $(4a_o\text{-}a_o)/a_o = 3$;
If a surface does not change its area, the area dilatation would become $(a_0\text{-}a_0)/a_0 = 0$;
If a surface halves its area, the area dilatation would become $(a_o/2 - a_o)/a_o = -1/2$.

For a volume, the calculation is similar. Each region of interest is described as a tetrahedron (Figure 2-14). The strain is based on the change in position of each vertex in the tetrahedron relative to its initial position. By default, the X,Y,Z position of each vertex is expressed relative to the centroid of the tetrahedron. The change in position of the vertices of the strained tetrahedron, relative to the unstrained tetrahedron allows the calculation of both a volumetric dilation and also the direction and magnitude of principal strains (Figure 2-14).

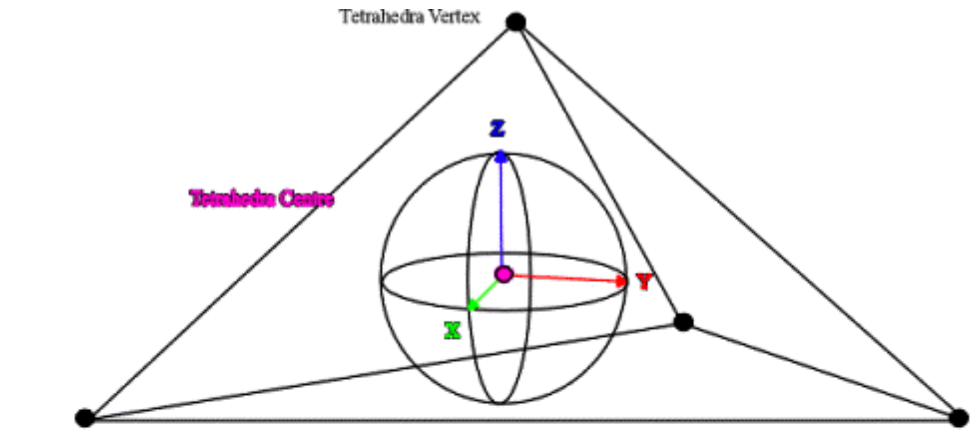

Unstrained tetrahedra with sphere of radius unity.

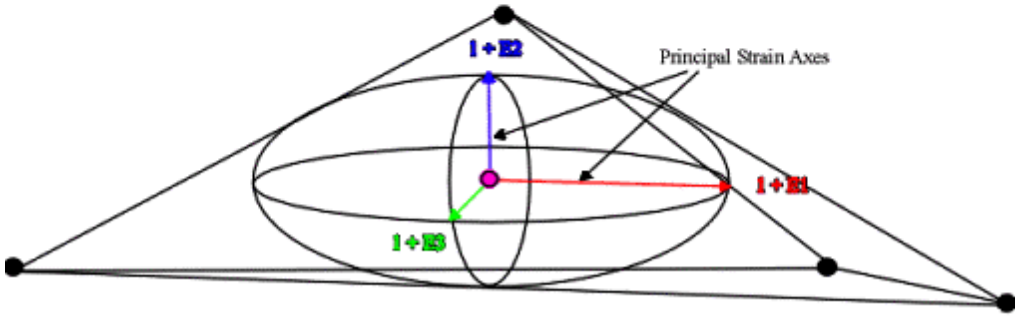

Figure 2-14 Strained tetrahedron with strain ellipsoid. The XYZ axes are eigenvectors of the strain field, and are the principal strain axes.

There are several ways to quantify the volumetric strain that occurs after multiple deformation events. These consist of:

- current dilation,
- absolute, or cumulative dilation, and
- Root Mean Square (RMS) dilation.

Figure 2-15 and Figure 2-16 illustrate these strain measures.

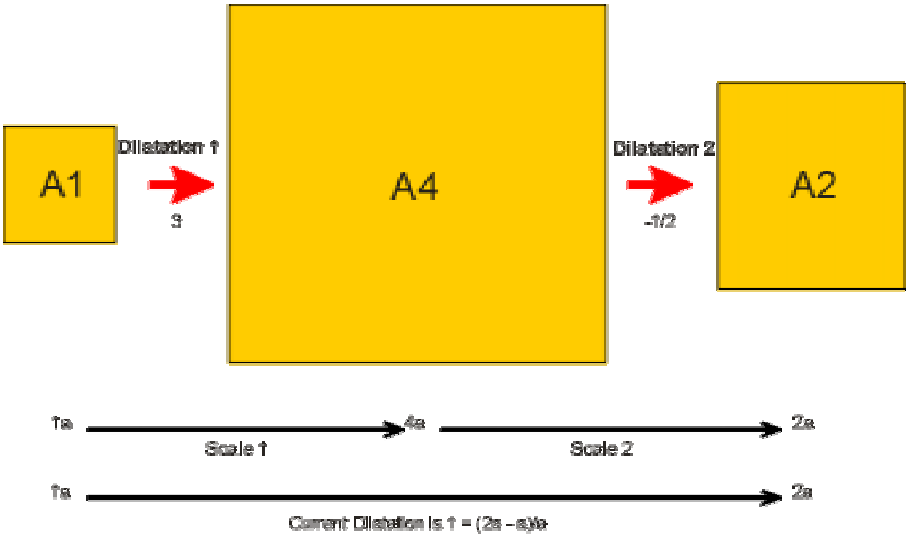

Figure 2-15 Example of the calculation of current dilatation (from Midland Valley, 2000)

Figure 2-15 shows an object A1 with area *a* that undergoes an initial dilatation, becoming object A4 with area *4a*. After a second dilatation, the object becomes A2 with area *2a*. Current dilatation is then a measure of the strain incurred from the change in shape from A1 to A2. This is a change in area from *a* to *2a*, so the current dilation is 1.0.

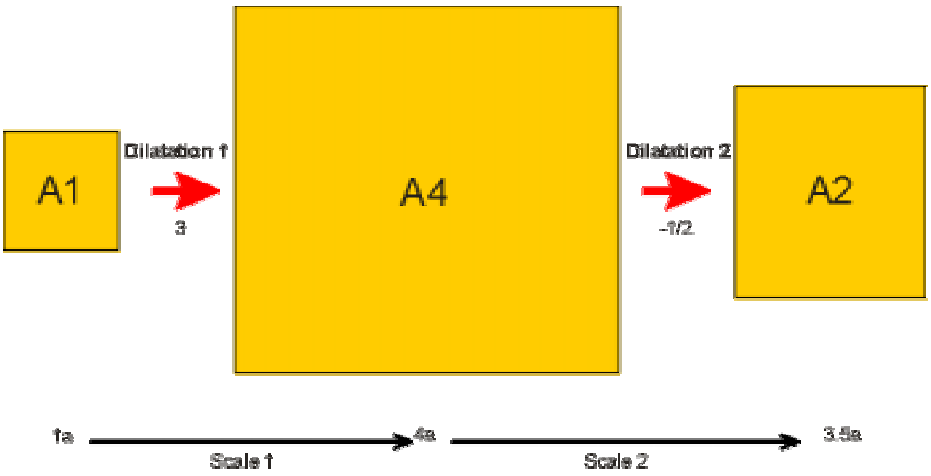

Figure 2-16 Example of absolute and RMS dilation calculations (from Midland Valley, 2000)

The current dilation does not take into account the strain history; it is only a function of the initial state and the current state. The other two measures (absolute and RMS dilation) incorporate the effects of intermediate strain events.

Absolute strain measures the cumulative strain where the summed dilatation is taken as an absolute value:

$$\Delta_{abs} = \sum_{i=1}^{n} \left| \Delta_i \right| \qquad \text{Equation 2-5}$$

where Δ_{abs} = the absolute strain,
Δ_i = the strain after the ith strain event, and
n is the number of strain events.

This means that even if the overall dilatation is negative, i.e. a contraction, the change will be a positive value. In the example above (Figure 2-16), the absolute dilation would be $|3| + |-0.5| = 3 + 0.5 = 3.5$

The RMS dilation is given by:

$$\Delta_{RMS} = \sqrt{\sum_{i=1}^{n} \left(\Delta_i^2 \right)} \qquad \text{Equation 2-6}$$

where Δ_{RMS} = the RMS strain,
Δ_i = the strain after the ith strain event, and
n is the number of strain events.

In the example above (Figure 2-16), the RMS dilation would be $\sqrt{3^2 + (-0.5)^2} = 3.04$.

Absolute strain will always produce a higher value than RMS.

2.3.6.2 Directional strain measures

Let e_i be the strain in the *i-th* direction, where e_i is the change in length divided by the original length, or:

$$e_i = \frac{l - l_0}{l_0} \qquad \text{Equation 2-7}$$

or

$$l = (1 + e_i) * l_0 \qquad \text{Equation 2-8}$$

where l_0 = undeformed length,

l = deformed length, and
e_i = the strain in the *i-th* direction.

Another parameter, the *natural strain* (ε_i), is often calculated from e:

$$\varepsilon_i = \log(1 + e_i) \qquad \text{Equation 2-9}$$

Through knowledge of the magnitudes and directions of strains in three different directions, it is possible to compute the *principal strains*. The principal strains are mathematically equivalent to the eigenvectors and eigenvalues of the strain matrix. These principal strains have the properties that they are:

1) mutually orthogonal; and
2) in directions in which there is no shear strain component.

The principal strains are denoted as e_1, e_2 *and* e_3, where e_1 has the largest magnitude. The corresponding principal strain axes are denoted E1, E2 and E3.

Plane strain ratios are calculated from the ratios of the maximum and intermediate principal strains $(1+e_1 / 1+e_2)$, the intermediate principal strains $(1+e_2 /1+e_3)$ and the minimum and maximum principal strains $(1+e_3/ 1+e_1)$. This information can be used to determine the nature of the strain; plane, constrictional or flattening using a Flinn diagram, (Flinn, 1962), as shown in Figure 2-17

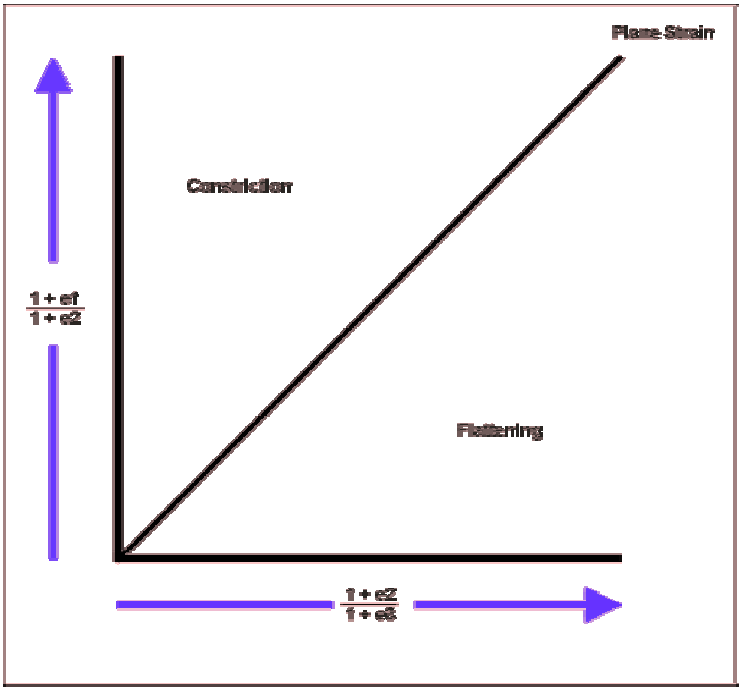

Figure 2-17 Flinn diagram showing the nature of the strain; plane, constrictional or flattening strain ellipsoid.

The volumetric dilation is a measure of the ratio of the change in volume of the strained object, relative to the unstrained volume, and can be written in a manner analogous to the areal strain (Equation 2-4):

$$\Delta_{vol} = \frac{(v - v_0)}{v_o} \qquad \text{Equation 2-10}$$

where Δ_{vol} = the volume dilation or strain,
v = the volume after strain, and
v_o = the volume before strain.

This can easily be re-written in a more common form:

$$\Delta_{vol} = \frac{(1+e_1)*x_1 + (1+e_2)*x_2 + (1+e_3)*x_3 - x_1x_2x_3}{x_1x_2x_3}$$

or Equation 2-11

$$\Delta_{vol} = (1+e_1)*(1+e_2)*(1+e_3) - 1$$

2.4 Experimental Techniques for Calculating Fracture Orientations, Intensity and Size from Outcrop Data

2.4.1 PURPOSE OF TASK

The analysis of fracture orientations, intensity and size is important for two different aspects of this project:

1) determination of how finite strain may control fracture development; and
2) development of statistical models for these quantities in order to create DFN models.

In the Circle Ridge Field, fracture information is very sparse in the subsurface, coming from unoriented core and a few image logs. Since the methodology adopted in this project requires the comparison of the strain field in various structural positions relative to the fracture orientations, intensity and size, subsurface data is not adequate as spatial coverage is very low and there is no direct information on fracture size. On the other hand, the top of the Field is only a few hundred meters below the surface near the crest,

so that the abundant outcrops above the Field should reflect a similar deformation history, at least in those units below the detachment zone afforded by the Gypsum Springs Formation. Thus the fracture parameters necessary for ascertaining the structural controls on fracturing and developing input statistical distributions has been based upon studies of fracturing in outcrop.

2.4.1.1 Scanline Sampling

Figure 2-18. Scanline affixed to Triassic Red Peak Member.

Figure 2-19 shows the measurement of the trace length for one specific fracture crossing the scanline, while Figure 2-20 summarizes the data collected and the form it was collected in. Note that orientation information about each scanline, as well as the prevailing bedding orientation, was collected in addition to the fracture data. This information was collected primarily in order to compensate for biases that result from scanline sampling of fractures (La Pointe and Hudson, 1985). All orientations were collected without adjustment for magnetic declination. A complete database consisting of all of the scanline data can be found in the project webpage, http://www.fracturedreservoirs.com.

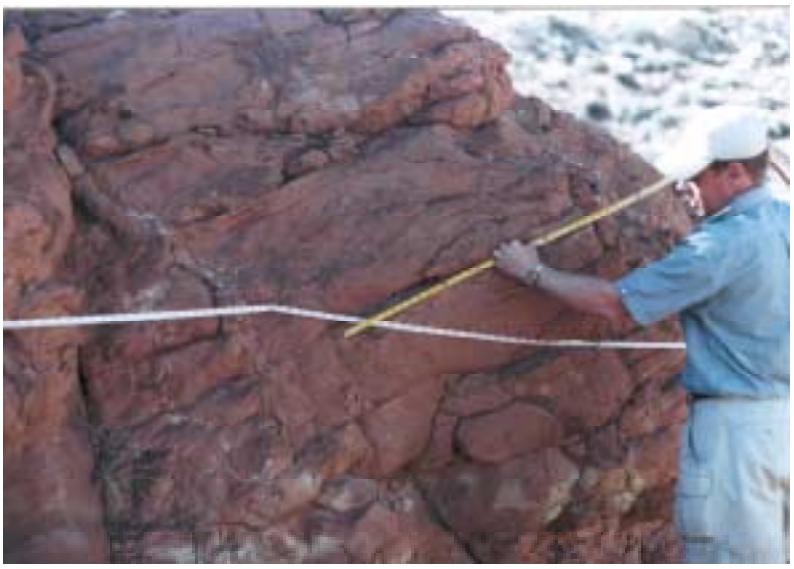

Figure 2-19. Detail of scanline measurements. The photo illustrates the measurement of fracture trace length for a specific fracture crossing the scanline.

Name: SCANLINE_8 **Date: 070600**

GPS points along the scan line

Waypoint	Altitude (ft)	Scanline dist. (ft)	Leg	Orientation		
134	7218	0				
135	7226	21	1	180	-5	
136	7225	36	2	165	2	

Rocktype Read Peak
Stratigraphic thickness
Bedding orientation N6W, 11N

Scanline length ft (decimal)	Leg	Orientation		Trace length		Terminations		Movement	Comments
		Strike	Dip	ft	in	upper	lower		
0.5	1	N85W	78S	2	7	T	U		
0.8	1	N86W	80S	0	9	T	A		
0.9	1	N84W	82S	0	7	B	B		
1.5	1	N89E	85S	1	8	B	B		
1.1	1	N58W	90S	3	8	A	U		
2.5	1	N80E	90S	10	0	U	U		CaCO3 filled
2.7	1	N71W	74N	2	0	B	A		
3.1	1	N76W	86N	4	0	A	U		
3.4	1	N85E	85N	1	5	B	U		
3.8	1	N70E	90S	5	4	A	U		
3.2	1	N76W	74N	5	7	A	U		
4.4	1	N90W	66S	1	3	A	B		
4.9	1	N89W	67N	7	10	U	U		
5.2	1	N79W	88N	2	0	A	U		
5.5	1	N65E	66N	1	3	H	T		
6.6	1	N72W	68S	1	4	T	B		
6.4	1	N24W	81S	4	2	T	T		

Figure 2-20. Example of data recorded for each scanline.

2.4.2 STATISTICAL ANALYSIS TECHNIQUES

2.4.2.1 Fracture Orientations

The method adopted in this project for characterizing fracture orientations consists of plotting all geologically similar fractures on a stereoplot, correcting for magnetic declination, and then correcting for orientational biases using the Terzaghi correction (Terzaghi, 1965). Additionally, all fractures were rotated relative to bedding in such a way that measured bedding strike was rotated about the Z-axis so that it was north-south. Then the fractures were rotated about the north-south axis until bedding dips were horizontal. These rotations make it possible to compare fracture orientations with bedding orientation, to assess whether there is a consistent pattern as would be expected if fractures were formed due to folding (Stearns and Friedman, 1972).

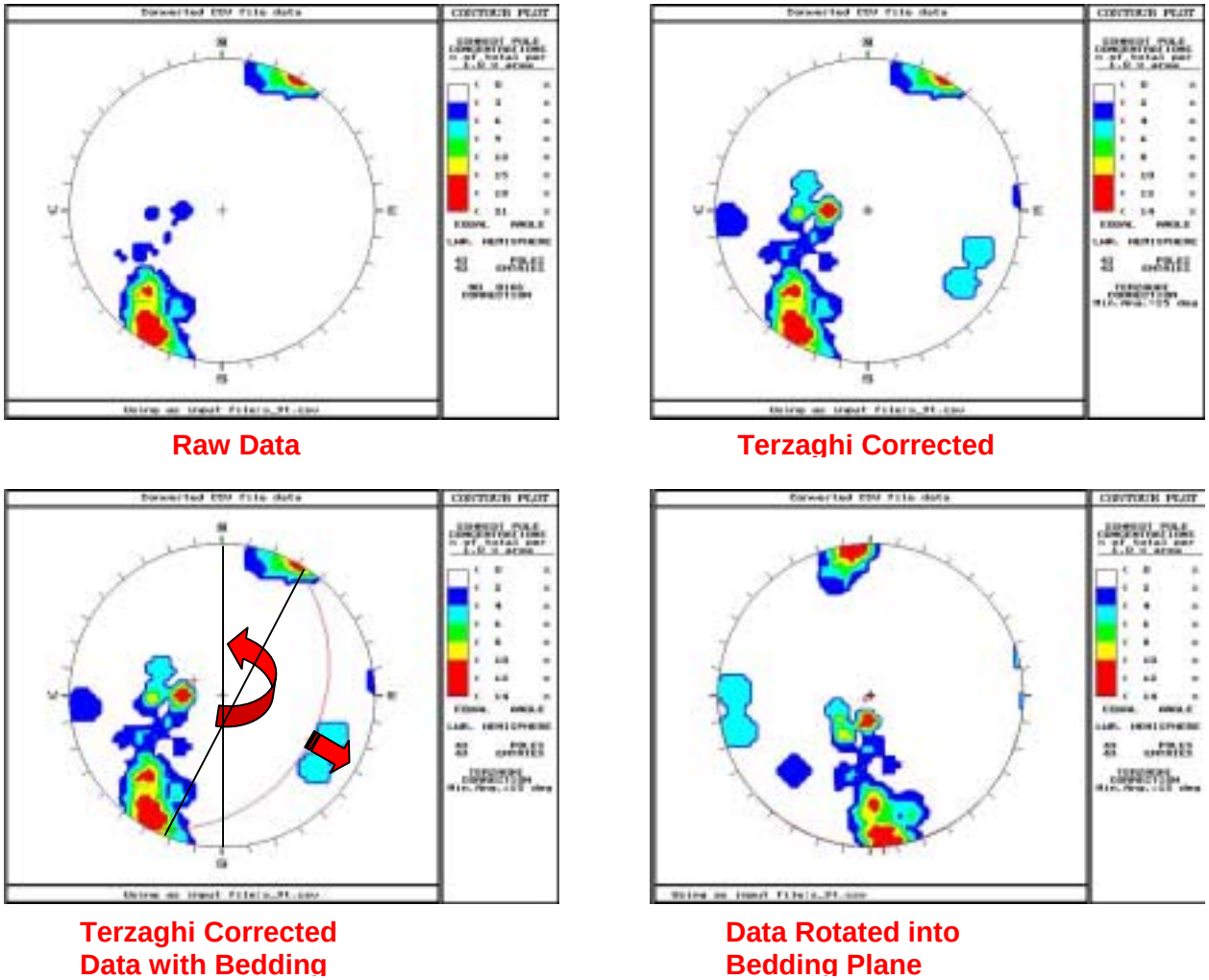

Figure 2-21. Analysis of fracture orientations, including rotation into bedding plane.

These steps are shown in Figure 2-21.

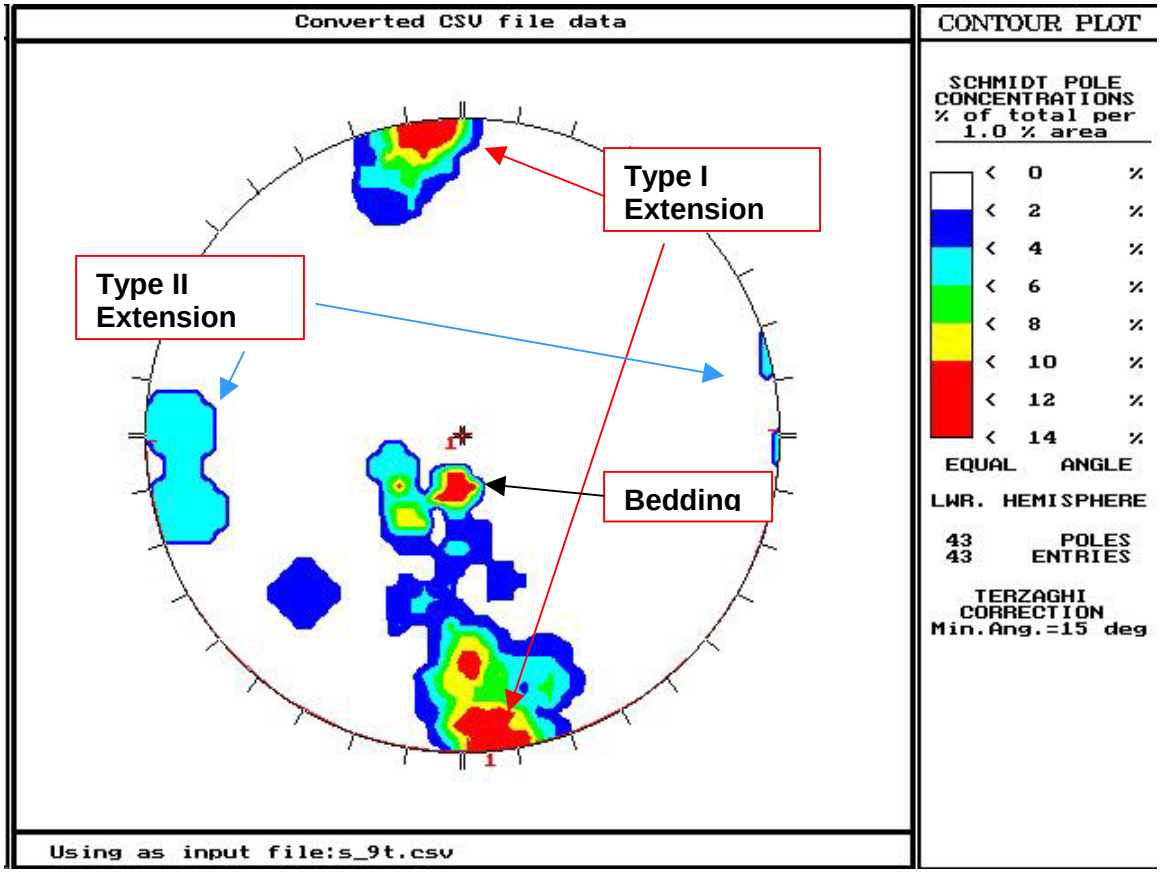

Figure 2-22. Example of possible interpretation of fracture orientations relative to bedding orientation.

Figure 2-22 shows how the fracture orientations may be interpreted once they have been rotated into the bedding plane. In this example, there are three concentrations of poles to fractures. The greatest concentration (the red contours) occurs near the top and bottom of the equal-area stereoplot. This indicates a modal fracture orientation that strikes parallel to te dip direction of bedding and is also orthogonal to bedding. This orientation is sometimes referred to as a Type I extension fracture (Stearns and Friedman, 1972). Another major concentration occurs near the center of the diagram. This concentration of fracture poles indicates an orientation nearly parallel to bedding. A third, much weaker, concentration is shown by the cyan contours near the left and right edges of the stereoplot. This concentration of fracture poles indicates an orientation orthogonal to bedding and in a strike direction parallel to bedding strike. This orientation is often referred to as a Type II extension fracture set (Stearns and Friedman, 1972). Thus, the orientations shown in the this diagram, taken from Scanline #9, show two sets of

fractures that are in orientations that are commonly predicted to occur during folding of rock (the Type I and Type II extension sets), while a third set is subparallel to bedding.

2.4.2.2 Fracture Intensity

Fracture intensity has been defined in many different ways for different purposes. In this project, the nomenclature of Dershowitz and Herda (1992) has been adopted.

In order to generate a DFN model, it is necessary to know the value of the volumetric fracture intensity, P_{32}, which is defined as the fracture surface area per unit volume of rock for the rock volume in which fractures are to be generated. This cannot be directly measured in the field, but instead, is calculated from P_{10} (number of fractures per unit length) or P_{21} (total fracture trace length per unit area of rock surface). For scanline data, the natural measure of fracture intensity is P_{10}.

Many studies have shown that fracture intensity, including P_{10}, often varies with the scale of measurement (Barton and La Pointe, 1995). Since the scale of the scanline (tens of meters) differs from the scale of the reservoir (hundreds or thousands of meters), it is essential to quantify the intensity scaling behavior of fracture intensity so that the scanline calculations can be correctly upscaled to the reservoir.

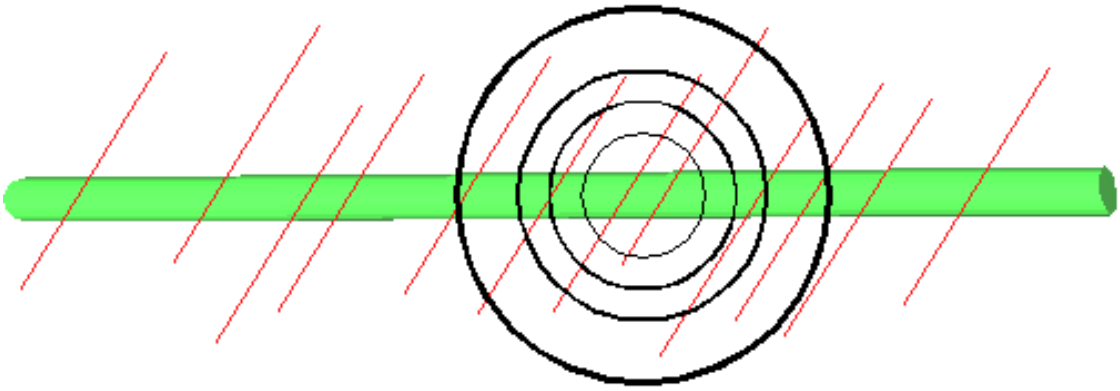

Figure 2-23. Methodology for calculating intensity scaling parameters.

Figure 2-23 shows how the intensity scaling parameters are calculated for scanline or wellbore data. A series of nested circles of different radii are centered on each fracture intersecting the scanline or wellbore. The number of fractures within each circle is counted. This series of calculations is repeated for every fracture intersecting the scanline, and the results for each specific radius value are averaged over all fractures. The results are plotted on doubly logarithmic axes, with the number of fractures plotted on the vertical axis and the radius on the horizontal axis. This type of plot can be used to test whether the scaling of intensity follows a fractal or a Poissonian process, because both can be represented as a power law of the form:

$$N(R) = \rho R^{D}$$ Equation 2-12

where R = the radius of the circle,
$N(R)$ = the mean number of fractures in a circle of radius R,
ρ = a constant, and
D = the scaling exponent.

In the above equation, D is often referred to as the *mass* dimension (Mandelbrot, 1983).

For a scanline, D typically varies between 0.0 and 1.0. If D is not equal to 1.0, the scaling law is a fractal or power law relation. If D = 1.0, then the scaling law is Poissonian. The importance of Poissonian vs. fractal scaling behavior is significant when the intensity of fracturing is being estimated at a scale different than the one over which the data was collected. This can be seen by deriving the expression for P_{10} from Equation 2-12:

$$P_{10}(R) = \frac{N(R)}{2R} \propto R^{D-1}$$ Equation 2-13

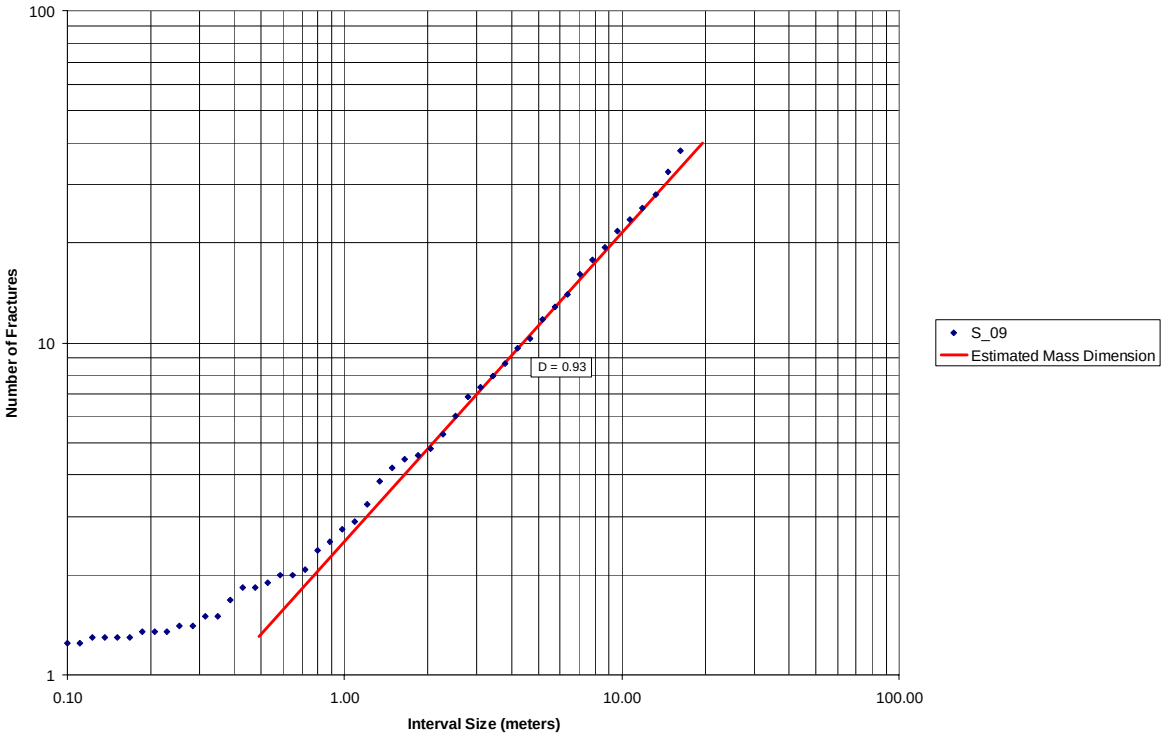

Figure 2-24. Example of a plot to determine the intensity scaling characteristics of fracture data collected along a scanline.

This equation shows that the value of P_{10} depends upon scale, except when *D = 1.0*. In this case, the P_{10} intensity is scale-independent.

Figure 2-24 shows an example of plotting the average number of fractures as a function of circle radius from scanline data. The departure from linearity at small circles (radii less than about 1 m) is due to the circle size approaching the minimum fracture spacing. This represents the lower limit of fractal scaling behavior, and so is not considered when fitting a straight line to the data. The figure shows a straight line fit through non-linear regression to the data for circles larger than the minimum fracture spacing. In this example, the data are well approximated by a straight line. The slope of this line is the scaling exponent or mass fractal dimension.

This type of scaling calculation was carried out for every scanline.

2.4.2.3 Fracture Trace Length

In order to generate a DFN model, it is necessary to specify the size distribution for each fracture set. This is done by specifying a radius distribution for the fractures, and specifying a fracture shape.

Size or fracture radius are not directly measured in outcrop fracture data; only fracture trace lengths can be measured. The trace length distribution differs from the radius distribution. Fortunately, the radius distribution can be derived from the trace length distribution either through analytical equations or by simulation.

An important and related issue is to compare size distribution information among different scanline sites. This is necessary for two purposes:

1) To assess whether there are differences in size distributions that can be related to strain or other geological factors; and
2) To determine a size distribution for the fractures that represents fractures at a larger size than encountered in the scanline data sets.

The process for evaluating this issue is to examine the number of fractures greater than or equal to a specific size based on all of the data from the different sources. Since each data set may pertain to a scanline with a different length, the number of fractures must be normalized for the scanline length.

The common way for carrying out this normalization is to divide the number of fractures by the length of the scanline. This type of length normalization is essentially Euclidean, since it assumes that if the scanline length were doubled, the numbers of fractures would also double. A Poissonian spatial model, typified by *D = 1*.0, is the only power law

model for which the Eudlidean length renormalization is correct. For other values of *D*, a different type of length renormalization is required, one that uses Equation 2-12 .

Fracture trace lengths often follow a relation given by:

$$N(X > x) = \left(\frac{x_0}{x} \right)^{D_l} \qquad \text{Equation 2-14}$$

where x_0 = the minimum trace length considered,
x = a trace length of size greater than x_0,
$N(X>x)$ = the number of fractures with a trace length greater than a specific length x, and
D_l = the trace length scaling exponent.

The trace length scaling exponent in Equation 2-14 is not related to the intensity scaling exponent in Equation 2-12.

The procedure to commensurate fracture trace length data from different scanline sites is to renormalize them to a common length. For example, if there are 50 fractures found on a 100 meter scanline, then the number of fractures for a 200 meter scanline would be calculated by using Equation 2-12. The values of $N(X>x)$ in Equation 2-14 would then be scaled by this ratio, rather than by a simple (Euclidean) doubling of the number.

3 RESULTS AND DISCUSSION

3.1 Overview

This section discusses the results of the three main active subtasks within Task 2 that were the focus of work during the 2nd six-month project period. These tasks comprise the acquisition of subsurface flow, transport and fracture data; the three-dimensional structural reconstruction of the Circle Ridge Field; and the analyses of the the outcrop fracture data.

3.2 Task 2.1 – Compilation of Existing Data and Task 2.2 – Core/FMI Data Analysis

This section describes the results of the subsurface field data acquisition carried out for the project. These two tasks are discussed in the same section since the image log data of Task 2.2 and the flow data of Task 2.1 have been gathered in the same wells and are analyzed together.

Approximately 17.9 MMCF of nitrogen was injected into an upstructure Overthrust Tensleep well, Shoshone 65-2, during September, 2000. A total of 66 Circle Ridge wells were monitored for gas breakthrough. Bottom hole pressures (BHP) were monitored at the injector, Shoshone 65-2 and seven offset wells (Figure 3-1and Figure 3-2):

- Shoshone 65-3: Overthrust Tensleep
- Shoshone 65-3: Overthrust Phosphoria
- Shoshone 66-3: Overthrust Tensleep (Lost BHP data)
- Shoshone 66-8: Overthrust Tensleep
- Shoshone 66-49: Overthrust Tensleep
- Shoshone 66-68: Overthrust Tensleep
- Shoshone 66-69: Overthrust Tensleep

All of these wells showed pressure response, although the response was minor in the Shoshone 63-3 Phosphoria interval. In addition, there was a BHP response in Shoshone 66-68, but no gas breakthrough was observed.

The nitrogen was injected at rates ranging from 1.6 to 2.1 MMCFPD over a 9.3 day period. Surface injection pressure at Shoshone 65-2 rose to 240 psi by the end of the test. Overthrust Tensleep gas cap pressure increased from approximately 3 psi to over 140 psi, as monitored in Shoshone 66-69, an offsetting observation well.

The gas initially broke through down structure to the east at Shoshone 66-69 and 66-40. This breakthrough was along a high directional permeability trend, which had previously been determined from multi-well pressure interference testing. The down structure gas coning occurred prior to gas breakthrough at Shoshone 65-3, an observation well to the north. Shoshone 65-3's open hole completion interval included Overthrust Tensleep at approximately the same structural elevation as the nitrogen injector.

Gas breakthrough was noted at over twenty monitor wells during and following gas injection. Times for breakthrough were noted whenever possible. Gas breakthrough occurred in both the Overthrust Tensleep and Overthrust Phosphoria reservoirs. The communication between the Overthrust Tensleep and the Overthrust Phosphoria may have occurred through reservoir pathways or at individual wellbores. .

A block of Overthrust Tensleep with apparently little or no effective fracturing was also highlighted by the nitrogen test. This block surrounds Shoshone 66-68. While liquid pressure response was observed at this well, no gas breakthrough occurred. Shoshone 66-68 is located up structure of other gas breakthrough wells (Shoshone 66-8 and Shoshone 66-55) and down structure of the gas injector, Shoshone 65-2.

A dual porosity reservoir simulator is being used to pressure match the Overthrust Tensleep gas cap pressure build-up and falloff as observed from the nitrogen injection test. Future plans also include utilizing this simulator to match bottom-hole pressures responses observed at several wells during the test. Fracture property adjustments required to obtain these matches will be used to help calibrate the models developed in Tasks 3.1, 4.2 and 4.3

Falloff data has been obtained at Shoshone 65-2, Shoshone 66-69, and Shoshone 66-2 and in the Overthrust Tensleep following nitrogen injection. Interpretation of this fall-off data is being performed using an Eclipse reservoir simulator and commercially available pressure transient interpretation software. Eclipse simulation results are shown in Figure 3-3, Figure 3-4 and Figure 3-5. The Eclipse match was obtained by including gas losses to the Overthrust Phosphoria. A classic fall-off interpretation was also performed. The interpretation match used a dual porosity model with intersecting faults at approximately 200/450 feet. The well had a skin of –2.5 and a kh of 1340 md-ft.

The FMI obtained from Shoshone 66-7 has been analyzed. This image covers the depth range of 720 ft to 973 ft, and is in the Overthrust Tensleep portion of the reservoir. The analysis of the image shows that there are 34 fractures that may have permeability: 6 that are open, 23 that are partially open (appearing like the image for Tribal C#38 in Figure 3-6, and 5 that are lithologically-limited or solution enhanced. If the partially open and open fractures are grouped together, then there are 0.11 fractures/ft or 0.035 fractures/m, which represents the potential conductive P_{10} intensity for this well and interval.

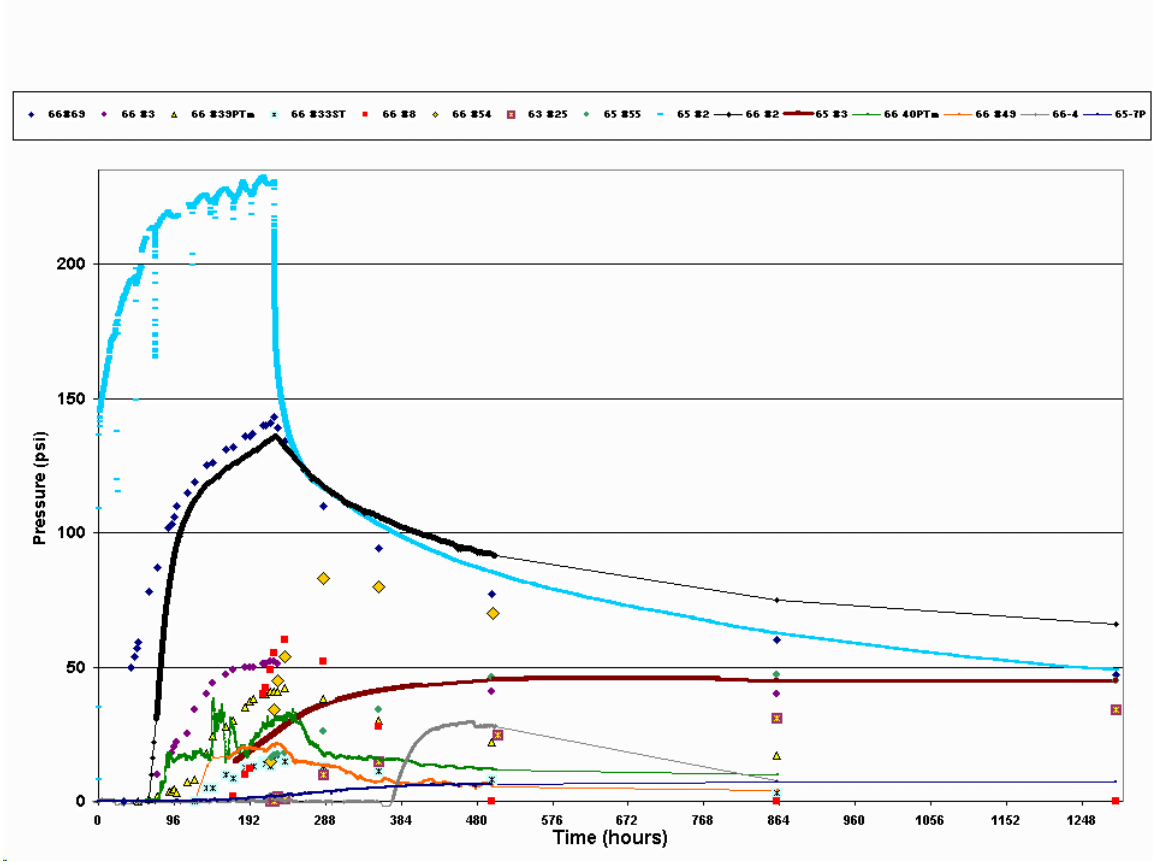

Figure 3-1. Measured surface pressures, all wells, nitrogen injection test.

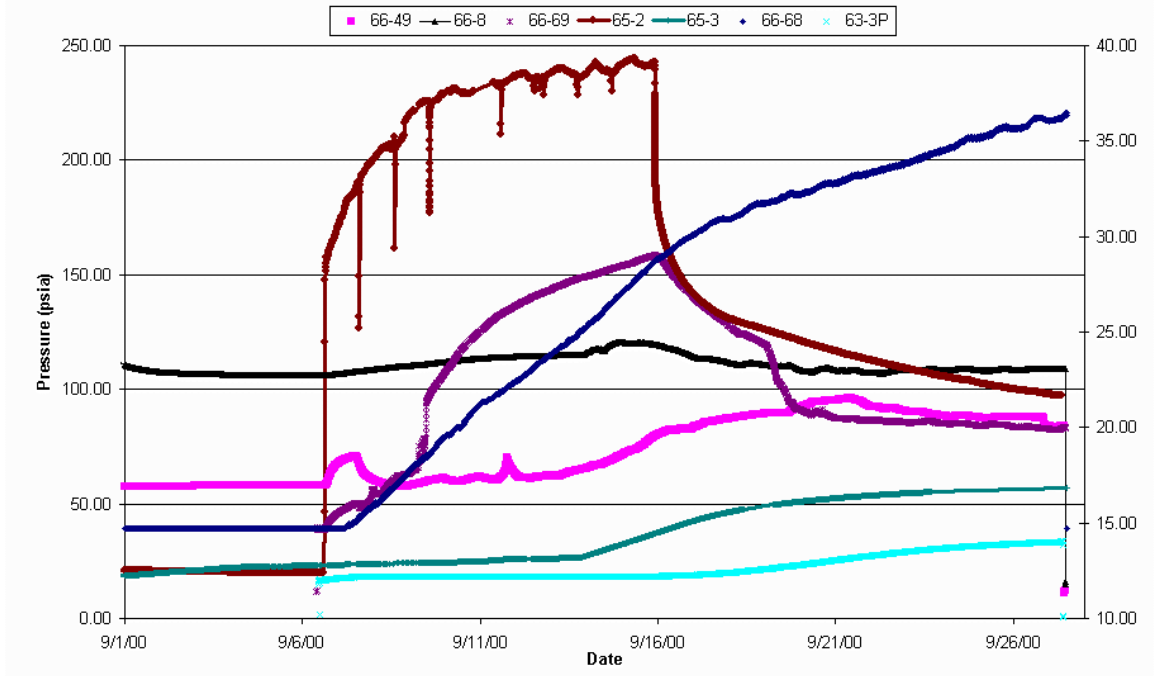

Figure 3-2. Measured bottom hole pressures, all wells, nitrogen injection test.

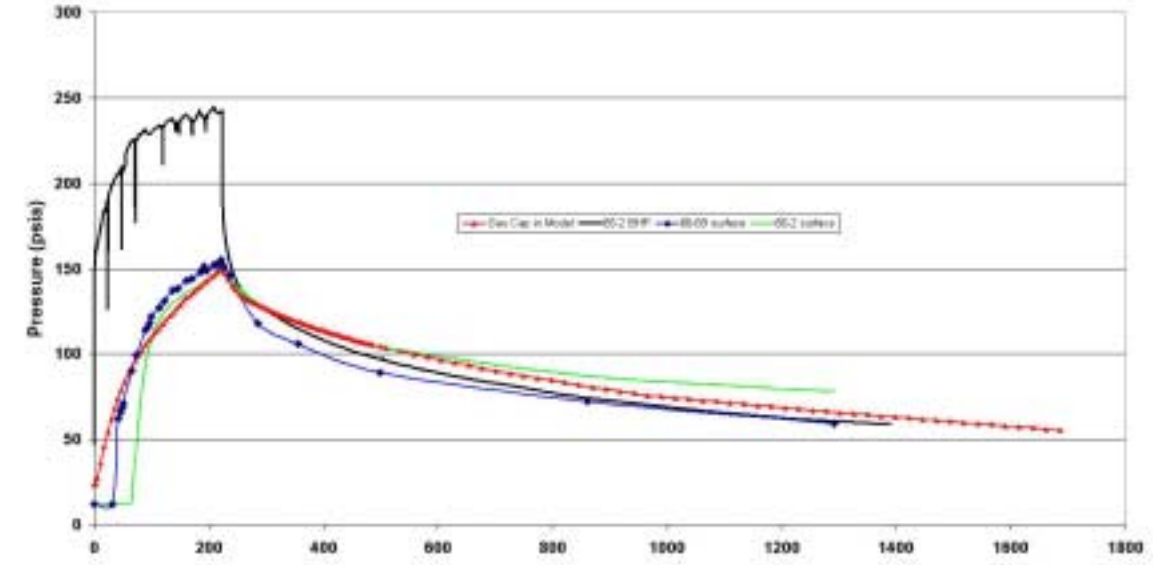

Figure 3-3. Gas cap, predicted vs. actual pressure responses during nitrogen injection test.

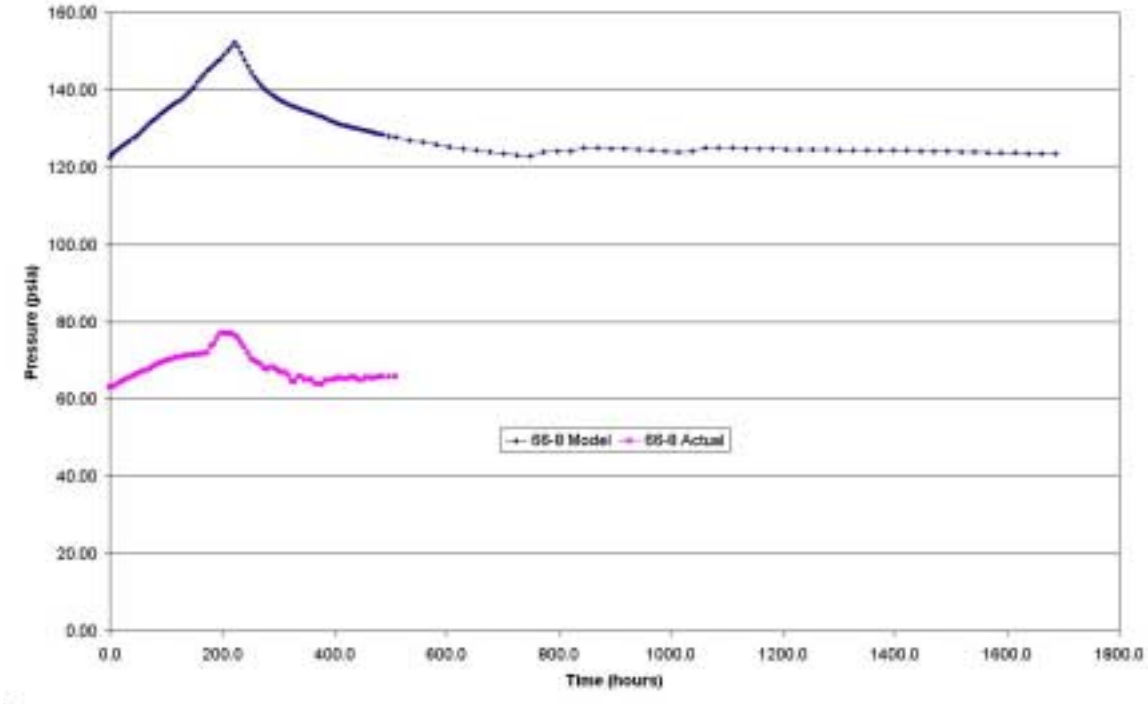

Figure 3-4. Predicted vs. actual pressure response in Shoshone 66-8 during nitrogen injection test.

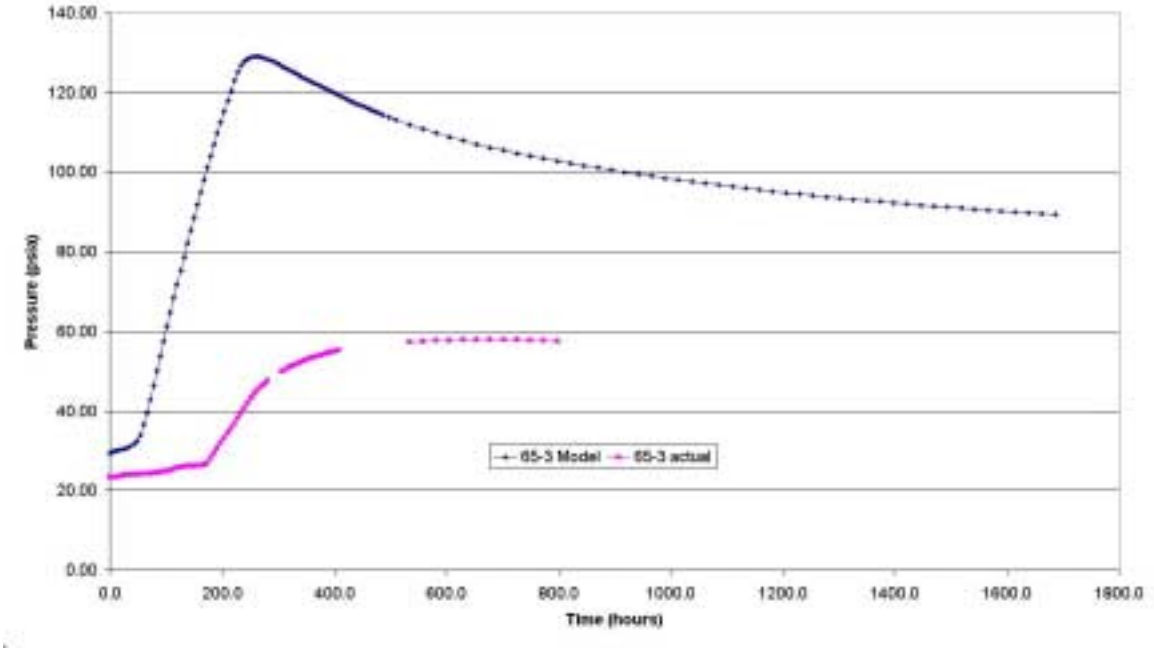

Figure 3-5. Predicted vs. actual pressure response in Shoshone 65-3 during nitrogen injection test.

In addition, there were 13 partial or completely resistive fractures which would probably not be effective in enhancing reservoir permeability.

Breakout data shown in Figure 3-8 and interpreted according to the method in Figure 3-7 indicate current in situ stress directions. The azimuths of the seven breakouts strike consistently to the west-northwest, indicating a maximum horizontal stress striking to the north-northeast/south-southwest. This direction is somewhat oblique to the northwest/southeast structural grain and to the Red Gully Fault.

Open and partiually open fracture dip very steeply in this well, typically on the order of 70 to 80 degrees. The fracture strike east-west to west-northwest for the most part, and dip steeply to the south. These fractures have a strike consistent with the breakouts/drilling induced fractures, and therefore might be related. There are two fractures that have a more northerly strike that subparallels the Red Gully Fault strike. Closed fractures tend to have a northeasterly strike, and in this way differ from the open, partially open and enhanced fractures.

A high resolution spinner survey was also obtained in this well (Figure 3-9). The injection rate was 5700 BWPD. Over 95% of the losses were in the interval from 761 ft to 790 ft, with a peak loss of 496 BPD between 764.1 ft to 764.5 ft. Other than this one

Figure 3-6 Unrolled and 3D view of the FMI log for Tribal C-38, Open and Partally Open fractures, Tenslep Formation, porous matrix.

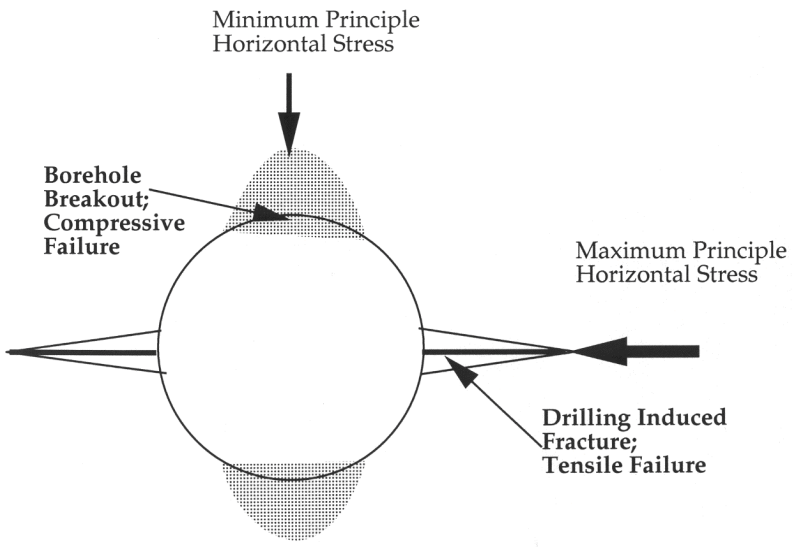

Figure 3-7. Interpreting stress directions from breakout data.

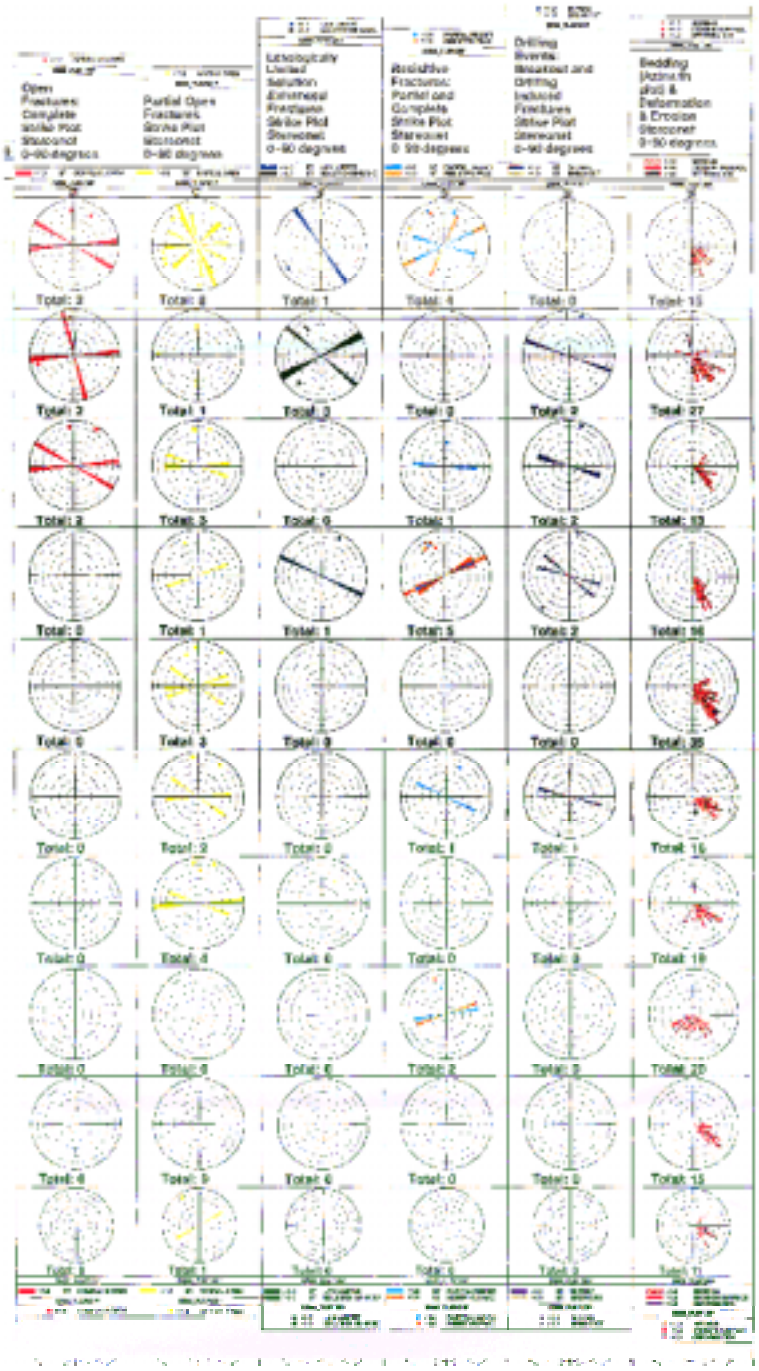

Figure 3-8. Interpretations of Shoshone 66-7 FMI log.

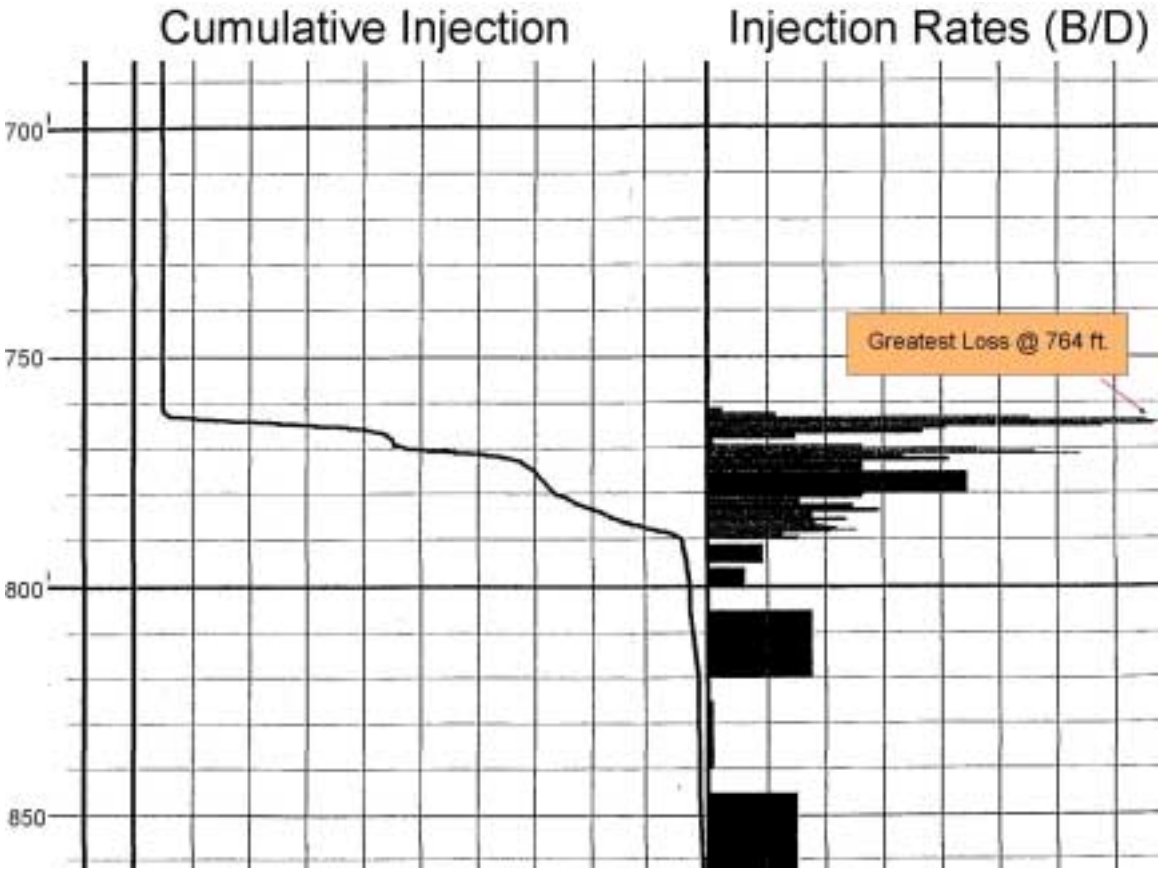

Figure 3-9. Spinner log (portion) for Shoshone 66-7.

0.4 ft interval, losses were spread relatively uniformly over the larger 29 ft interval. FMI logs show that this interval contains open, partially open and solution enhanced fractures. In the interval 790 ft – 880 ft, losses were minor, approximately 247 BPD total.

3.2.1 PLANS TO ACQUIRE REMAINING SUBSURFACE FLOW AND FRACTURE DATA

The following section describes the plans to acquire the remaining subsurface image log, single well and multiwell subsurface flow data. Note that all plans are dependent upon obtaining the required regulatory approval.

3.2.1.1 Tracer testing:

Marathon currently plans to perform a sodium bromide tracer test in subthrust Fault Block 1. The test will be performed by injecting a concentrated slug of sodium bromide into Shoshone 65-20, a subthrust Phosphoria water injection well. Offset subthrust and

overthrust producers will be monitored for breakthrough time and bromide concentration. Mass balance calculations, concerning tracer recovery, will also be performed. If problems are encountered, making injection into Shoshone 65-20 unfeasible, the tracer will be injected into Shoshone 65-12. Shoshone 65-12 is a subthrust Fault Block 1 Tensleep water injector.

3.2.1.2 FMI and Spinner Logging:

Current plans are to run and FMI log and injection spinner survey in the open hole at Shoshone 65-37, a subthrust Fault Block 1, Phosporia/Tensleep open hole section. A second FMI log is planned for Shoshone 66-75, a 2001 Overthrust Phosphoria/Tensleep infield drill well. A second high resolution spinner survey will be run at Shoshone 65-17, a TA'd subthrust Fault Block 1 Phosphoria water injector, or at Shoshone 65-16, a TA'd subthrust Fault Block 1 Tensleep producer.

3.2.1.3 Falloff and Multi-well Interference Testing:

A pressure transient falloff test is slated for Shoshone 65-36, a subthrust Fault Block 1 Phosphoria injector. Alternative falloff testing may be performed at Shoshone 65-12 or Shoshone 65-20.

Multiwell interference testing will be performed in subthrust Fault Block 1 in either the Phosphoria formation or the Tensleep formation. The formation will be selected to coincide with the formation of the sodium bromide tracer test. Observation and active wells for this testing have yet to be selected.

The acquisition of this data will fulfill Marathon's in-kind commitment of of the subsurface data to be provided to this project.

3.3 Task 2.4 – Construction of Balanced Cross Sections

3.3.1 REGIONAL GEOLOGY AND TECTONIC HISTORY OF THE WIND RIVER BASIN

The tectonic history of the area around Circle Ridge began with an early Precambrian or Archeozoic orogenic deformation phase. Contractional mountain building, dike intrusion, and the development of several regional fracture systems subdivided the basement rocks in the area into a mosaic of blocks (Fanshawe, 1952). Post-orogenic crustal stability was achieved during the Late Precambrian as long periods of active erosion produced a lowland among the earlier-formed mountain ranges (Fanshawe, 1952).

From the Paleozoic Era until Late Cretaceous, central Wyoming was part of the continental shelf along the eastern side of the Cordillera (Keefer, 1969). Paleozoic and lower Mesozoic strata were deposited mainly in shallow seas, with the exception of Silurian units which were either deposited and eroded before the Devonian or were never deposited (Keefer, 1969). Widespread facies changes and unconformities commonly associated with fluctuations in sea level or low-amplitude tectonic movements created a spectacular, multi-colored stratigraphy. Some areas were periodically raised above sea level and eroded while surrounding areas remained submerged thus creating formations with widespread thickness variations (Keefer, 1969).

Deformation related to the subduction of the oceanic Farallon Plate underneath the continental North American Plate began roughly 80 million years ago (Coney, 1978; Stock and Molnar, 1988; and Brown, 1993). This tectonic event, known as the Laramide Orogeny, continued intermittently with increasing intensity through the Paleocene and ceased by the end of the Early Eocene. Structural deformation during the Laramide Orogeny is characterized by crustal shortening to produce giant fault-bounded, basement-involved uplifts along the perimeter of basins (Figure 3-10). Precambrian-cored uplifts

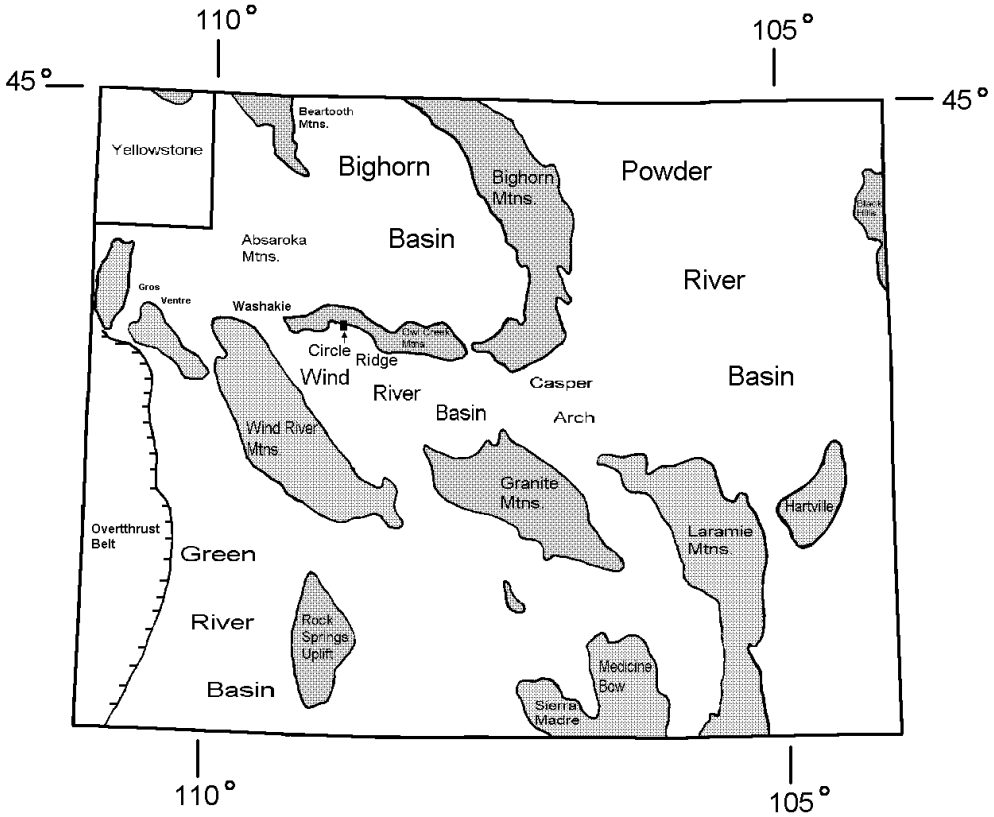

Figure 3-10 Index map of the Wyoming Foreland and adjacent areas showing principle Laramide uplifts (modified from Berg, 1962). Major Laramide uplifts are the speckled zones surrounding the inter-mountain basins.

separate basins that are filled with sediments accumulated during deformation. Brown (1993) characterized the Laramide Orogeny as a tectonic "front" that swept eastward across the Wyoming Foreland, creating crustal deformation sequences that grow progressively younger from west to east. Plate convergence during the Laramide Orogeny created structural deformation in a primary stress direction of N 40° to 50° E (Brown, 1988). Primary structures across the Wyoming Foreland, including Circle Ridge, trend northwest, perpendicular to the inferred direction of maximum principal stress (Brown, 1988; Figure 3-11). Northwest trending structures are generally thrusts, fold-thrusts, thrust-folds, and uplifted basement blocks (Brown, 1988; 1993).

Beginning in Late Cretaceous time, the seaways shifted east as Laramide deformation began downwarping the Wind River Basin and uplifting of the peripheral areas including the Owl Creek Mountains. The Wind River Basin is bounded by faulted and folded Paleozoic and Mesozoic sediments, but the basin is overlain by nearly flat-lying Eocene deposits that accumulated as a result of erosion of the surrounding areas since Laramide time. The arcuate-shaped basin encompasses approximately 8,500 square miles with a length over 135 miles and a width of as much as 35 miles. The Owl Creek Mountains are an east-west trending uplift thrust over the northern margin of the Wind River Basin. The Wind River cuts through this uplift, forming the Wind River Canyon.

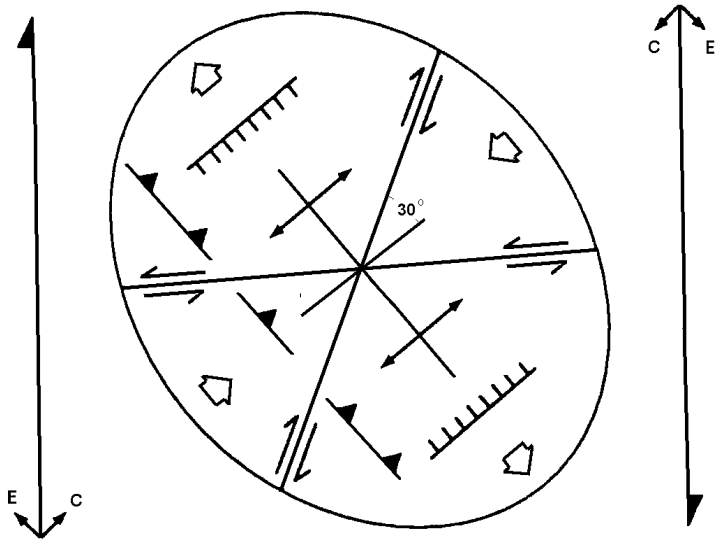

Figure 3-11 Schematic strain ellipsoid with σ_1 oriented parallel to the anticlinal axis of Circle Ridge (modified from Reading, 1980). Contractional structures, like reverse faults and anticlinal folds, are oriented parallel to σ_1. Extensional structures, like normal faults, are oriented perpendicular to σ_1. Oblique faults, indicated with arrows in the slip direction, are oriented 30° to σ_3.

3.3.2 RESERVOIR STRATIGRAPHY

Exposed stratigraphic units at Circle Ridge range from the Permian Phosphoria Formation to the Cretaceous Mowry Formation. Subsurface formations include all units from Precambrian basement to the Pennsylvanian Tensleep Formation.

<table>
<tr><th>Era</th><th>Period</th><th colspan="2">Unit</th><th>Symbol</th></tr>
<tr><td rowspan="15">Mesozoic</td><td rowspan="3">Cretaceous</td><td rowspan="2">Undifferentiated</td><td>Mowry Shale</td><td rowspan="2">Ku</td></tr>
<tr><td>Thermopolis Shale</td></tr>
<tr><td colspan="2">Cloverly Formation</td><td>Kcv</td></tr>
<tr><td rowspan="4">Jurassic</td><td colspan="2">Morrison Formation</td><td>Jm</td></tr>
<tr><td colspan="2">Sundance Formation</td><td>Js</td></tr>
<tr><td colspan="2">Gypsum Springs Formation</td><td>Jgs</td></tr>
<tr><td colspan="2">Nugget Sandstone</td><td>Jn</td></tr>
<tr><td rowspan="5">Triassic</td><td rowspan="3">Chugwater Formation</td><td>Popo Agie Member</td><td>TRpa</td></tr>
<tr><td>Crow Mountain Member</td><td>TRcm</td></tr>
<tr><td>Red Peak Shale</td><td>TRrp</td></tr>
<tr><td colspan="2">Dinwoody Formation</td><td>TRd</td></tr>
<tr><td rowspan="9">Paleozoic</td><td>Permian</td><td colspan="2">Phosphoria Formation</td><td>Pp</td></tr>
<tr><td rowspan="2">Pennsylvanian</td><td colspan="2">Tensleep Sandstone</td><td></td></tr>
<tr><td rowspan="2">Mississippian</td><td colspan="2" rowspan="2">Amsden Formation</td><td rowspan="2"></td></tr>
<tr><td colspan="2">Madison Limestone</td><td></td></tr>
<tr><td>Devonian</td><td colspan="2">Darby Formation</td><td></td></tr>
<tr><td>Ordovician</td><td colspan="2">Bighorn Dolomite</td><td></td></tr>
<tr><td rowspan="3">Cambrian</td><td colspan="2">Gallatin Limestone</td><td></td></tr>
<tr><td colspan="2">Gros Ventre Shale</td><td></td></tr>
<tr><td colspan="2">Flathead Sandstone</td><td></td></tr>
<tr><td colspan="5">PRECAMBRIAN</td></tr>
</table>

Figure 3-12 Stratigraphic column for the Circle Ridge Formation (from Smith 2000)

3.3.2.1 Madison Limestone

The Madison Limestone is a Lower Mississippian assemblage of carbonates that rests unconformably above the older Devonian Darby Formation. The Madison Limestone is

in general a massive limestone and dolomite unit deposited on the Wyoming shelf (Gower, 1978). In the Wind River Basin, thickness vary from 225 feet to 785 feet, reflecting minor tectonic movements (Gower, 1978). In addition, karsted zones in the upper part of the Madison Limestone may be former evaporitic zones that were leached either during or after Mississippian time, also accounting for thickness variations (Keefer, 1965). At Circle Ridge, the Madison Limestone measures about 690 feet and is known only in the subsurface (Olson, 1948). These shelf carbonates are generally homogenous in lithology with several porosity zones containing commercial petroleum accumulations (Stipp, 1952). Currently, the Madison Limestone is the deepest drilled reservoir at Circle Ridge. As of June of 1992, the Madison Limestone had produced 1.317 MMBO (Anderson and O'Connell, 1993).

3.3.2.2 Amsden Formation

The Amsden Formation is Late Mississippian to Early Pennsylvanian in age, and occupies the interval between the underlying Madison Limestone and the overlying Tensleep Formation. The contact of the Amsden Formation with the underlying Madison Limestone is an erosional unconformity, while the contact of the Amsden Formation with the overlying Tensleep Formation is conformable (Love, 1939). The Amsden Formation is a heterogeneous series of sandstone, shale, and limestone that was deposited under marine conditions (Keefer, 1965). It is separated into three members beginning with the Darwin Sandstone, which is a basal sandstone that fills the underlying karsted Madison (Olson, 1948). The middle member is the Horseshoe Shale. The upper member, the Ranchester Limestone, is a cherty carbonate. Within the Wind River Basin, the Amsden Formation varies in thickness from 200-400 feet (Gower, 1978). They are known only in the subsurface (Olson, 1948). Anderson and O'Connell (1993) reported that 3.522 MMBO had been produced from all of the productive units within the Amsden Formation as of June of 1992.

3.3.2.3 Tensleep Formation

A conformable contact separates the Tensleep Formation and the Amsden Formations, indicating no significant withdrawal of the sea at the close of Amsden time (Love, 1939). The lower unit of the Pennsylvanian Tensleep Formation is dolomite and limestone (Agaston, 1952). Shales and fine- to medium-grained, cross-bedded sands make-up the upper clastic unit. The abundant medium-scale cross-beds, frosted quartz grains, and limestone cement were used to interpret the depositional environment as a beach (Agaston, 1952). The Tensleep is capped with an unconformity separating it from the overlying Phosphoria Formation. The Tensleep Formation is widespread in Wyoming and has a highly variable thickness, with a range of 215-600 feet in the Wind River Basin (Gower, 1978). At Circle Ridge, the Tensleep measures 295 feet (Olsen, 1948). The thickness variance is due to the loss of the upper sand, which was removed prior to deposition of the overlying Permian Phosphoria Formation (Pedry, 1975). The Tensleep Formation became exposed as the seas migrated eastward and the upper sand eroded

(Keefer, 1965).

The Tensleep Formation is the most productive reservoir at Circle Ridge. Anderson and O'Connell (1993) reported the Tensleep Formation had produced 16.313 MMBO as of June of 1992.

3.3.2.4 Phosphoria Formation.

An erosional unconformity separates the Pennsylvanian Tensleep Formation from the Permian Phosphoria Formation. A progressive withdrawal of the Paleozoic seas occurred between Late Pennsylvanian and Early Permian (Agaston, 1952). A new marine transgression deposited the Phosphoria. The Phosphoria Formation averages 210 feet thick at Circle Ridge, although within the Wind River Basin, the Phosphoria Formation can measure up to 1,300 feet in thickness (Andrews, 1944).

The Phosphoria Formation is the oldest formation exposed at the surface in the center of Circle Ridge, and can be subdivided into two units. The basal unit is primarily a cherty dolomite and thin, hard, brown limestone that was deposited in a shallow marine environment (Mills, 1956). The upper unit, as seen on the surface at Circle Ridge, contains red, phosphatic shales and sandstones that weather to a dark brown. The upper unit accumulated within an arid climate and shallow marine environment (Frielinghausen, 1952). The Phosphoria Formation is the second most prolific oil-producing unit at Circle Ridge. Anderson and O'Connell (1993) reported the Phosphoria Formation had produced 7.867 MMBO as of June of 1992.

3.3.2.5 Dinwoody Formation

The basal Triassic unit is the Dinwoody Formation. The contact between the Dinwoody Formation and the Phosphoria Formation appears continuous and conformable as it crops out in the central hill of Circle Ridge. The Dinwoody is composed of silts and sandy, anhydritic shale with a few interbedded gray dolomites and limestone. It has a unique white to yellow color. The 140-foot-thick Dinwoody Formation was deposited in semi-restricted marine or supratidal environment (Kinsman, 1969).

3.3.2.6 Chugwater Formation

Overlying the Dinwoody is one of Wyoming's thickest and most distinctive formations, the Triassic Chugwater Formation. The Chugwater Formation is separated into three members—Red Peak, Crow Mountain, and Popo Agie. The basal Red Peak Shale is the thickest at 1,030 feet (Anderson and O'Connell, 1993). It contains a blood-red, interbedded siltstone and sandstone that accumulated within a paralic and nearshore marine complex (Picard, 1978). The upper portion of the Red Peak weathers into shades of tan, gray, red and purple. The Crow Mountain is 210-feet-thick of purple, very fine-

grained sandstone, and gray to red siltstone (Anderson and O'Connell, 1993. The main depositional environment for the Crow Mountain Member was probably a tidal flat complex (Picard, 1978). The upper Chugwater member, the Popo Agie, is dark red to purple on the base, and weathers to a dark rust color or ochre color. The upper portion is a bright tan siltstone with sharp brittle edges. It sounds like glass when walked upon. The difference in color is probably from different amounts of iron oxides present. The Popo Agie Member represents dominantly fluvial conditions, whereas the ochre-colored unit was deposited in a lacustrine environment on a deltaic plain (Picard, 1978). At Circle Ridge, the Popo Agie Member measures 170 feet in thickness (Anderson and O'Connell, 1993).

3.3.2.7 Nugget Sandstone

Unconformably overlying the Popo Agie Member is the Lower Jurassic Nugget Sandstone. This formation is only present along the northwest corner of Circle Ridge and can be up to 48 feet thick when present. The base of the Nugget is a fine- to very fine-grained, tan to buff sandstone with interbedded red siltstone beds. Above the basal unit is a red sandstone of the same texture. Large- and small-scale cross-bedding structures were found that might indicate eolian deposition. Much controversy exists today concerning the discontinuous surface exposure of the Jurassic Nugget Formation in the Wind River Basin. Picard (1978) has suggested that regional and local tectonism may have contributed to the observed thickness variations.

3.3.2.8 Gypsum Springs Formation

The lower and upper contacts of the Gypsum Springs are unconformities (Anderson and O'Connell, 1993). The basal portion of the Gypsum Springs Formation at Circle Ridge is a 95-foot-thick massive layer of gypsum (Anderson and O'Connell, 1993). The upper portion contains a pink to red gypsiferous siltstone with interbedded shale measuring 105 feet thick (Anderson and O'Connell, 1993). The gypsum weathers to a dark, puffy texture similar to heads of broccoli. The abundance of gypsum with the interbedded siltstone and shale beds would represent deposits that accumulated on the continental platform with intervals of isolation from the main sea. Kinsman (1969) interpreted the depositional environment as a semi-restricted basin with sabka and tidal mudflat conditions.

3.3.2.9 Sundance Formation

The Sundance Formation and overlying Morrison Formation are the two Upper Jurassic units at Circle Ridge. A distinctive strip of grass is seen at the contact between the Sundance Formation and the Gypsum Springs Formation. At Circle Ridge, a series of shale, sandstone, and limestone beds compose the 315-foot-thick Sundance Formation (Anderson and O'Connell, 1993). Colors range from gray to light brown to green. The fine-grained sands and shale can be highly glauconitic with sedimentary characteristics

that include thin cross-beds, ripples, and planar beds. An abundance of Gryphea was found loosely atop the soils of the Sundance and cemented within beds. The combination of characteristics and different bed compositions lead to the interpretation that the Sundance represents a variety of marine depositional environments—open marine platform, lagoon, and barrier bar (Peterson, 1954; Keefer, 1965).

3.3.2.10 Morrison Formation

Overlying the Sundance Formation, and separated by a conformable contact, is the Morrison Formation. Along the northeast flank of Circle Ridge, a cherty conglomerate bed of the Morrison Formation marks the contact above the Sundance Formation. In the study area, the Morrison is 200 feet thick and comprised of white, fine-grained sandstones and tan shale (Anderson and O'Connell, 1993). It was deposited in a non-marine environment as intermixed lacustrine, swamp, flood plain, and river deposits (Downs, 1952). The Morrison Formation is a regionally extensive unit found throughout Colorado, Idaho, Utah, and Wyoming. Dinosaur bones have been found in this formation, most notably at Dinosaur National Park, Colorado.

3.3.2.11 Cloverly Formation

The types of environments and conditions in which the Morrison Formation was deposited are largely repeated within the Cretaceous Cloverly Formation. The basal fluvial unit is a distinctive light gray, pebbly conglomerate. Above the conglomerate unit is a cross-bedded, gray to dark brown sandstone with interbedded bentonitic shales, silts, and clays. The upper part of the Cloverly Formation is composed mostly of rust-colored silts and sandstones that are called the Rusty Bed Member. Structures include ripples and cross-beds. The sandstone is fluvial in origin and was probably deposited in stream channels cut into the underlying lacustrine deposits (Curry, 1962). At Circle Ridge, the Cloverly Formation is 285 feet thick (Andrews, 1944).

3.3.2.12 Cretaceous Undifferentiated

The dark, betonitic shales that form a gradational contact above the Cloverly belong to the Thermopolis Formation. The Thermopolis Shale and Mowry Shale have been mapped together in this study to form the Cretaceous Undifferentiated. The Thermopolis marine shale layer coincides with the transgression of the Early Cretaceous seas into the Wind River Basin (Burtner and Warner, 1984). The bentonitic shales are dark gray to black in color, and contain thin layers of sandy and silty claystone. About 45 feet from the top of the Thermopolis Formation rests the Muddy Sandstone Member of the Thermopolis Formation. The Muddy Sandstone Member contains a white to buff, fine- to medium-grained sandstone, which is sharply distinctive from surface exposure with the Thermopolis Formation. The sandstone in the Muddy Sandstone Member represents

overlapping marine and non-marine sandstone facies and therefore indicates a brief regression in the Cretaceous sea (Curry, 1962).

The other formation in the Cretaceous Undifferentiated (Ku) in this study is the Mowry Formation. The contact between the Thermopolis Shale and the Mowry Shale is often difficult to locate. Generally, the base of the Mowry Shale is recognized as porcelaneous shale that conformably overlies the Muddy Sandstone Member. This hard shale is gray, fissile, organic-rich, and locally sandy. Numerous bentonite beds within the Mowry and the other Cretaceous formations indicate episodic volcanic activity at the same time from the northwest corner of Wyoming (Downs, 1952). The Mowry is 640 feet thick at Circle Ridge, and is a structurally incompetent unit that slumps frequently, producing uneven topography (Andrews, 1944).

3.3.3 THE GEOLOGICAL MODEL

3.3.3.1 Available data

There have been two previous attempts to interpret the geological character of the Circle Ridge Field by constructing cross-section through the anticlinal structure. The first attempt was made by Anderson and O'Connell (1993), who published two cross-sections through the Field and interpreted the tectonic evolution of the Field based on these sections. Later Smith (2000) remapped the surface geology of the Circle Ridge Field and combined the Anderson and O'Connell's cross-sections to create a 3D structural model which was used for computing reservoir volumes and to look for untested fault blocks.

For this project, Anderson and O'Connell's cross-sections where digitized and imported into 3Dmove™ (Midland Valley Ltd). The cross-sections are used as guides for the construction of the 3D geological model. Smith's model was imported piece-by-piece into 3Dmove and was used as guiding surfaces for the 3D interpretation of faults and geological formations. Well trajectories for approximately 200 wells were used to correctly place well data into the model.

In addition to previous interpretations of geological formations, well formation top data from 184 wells were used and incorporated into the 3D geological model. Part of the well data that was used by Anderson and O'Connell has been re-evaluated as part of the petrophysical analysis that was carried out in the first 6-month period of this project (Task 1). Specifically, fifty of the existing wells in the Circle Ridge Field were re-analyzed petrophysically, of which thirty-nine were in the overthrust and eleven in the subthrust portions of the reservoir. These wells were also re-analyzed with respect of the formation top of each geological unit. This data set was imported to the 3D geological model.

The assembled well information consists of 184 wells containing top information from 12 geological formations with 1296 control points throughout the Field. All tops were subject to a rigorous quality control which revealed about 120 tops records which had

either abnormal depth values beyond the trajectory of the well, or were labeled with non-existing geological formations names (considered typo's).

Three new cross-sections were completed and digitized as part of Task 2.4. These new cross- sections formed valuable information about the complex geological situation in the northern pat of the Circle Ridge Field. The cross-sections were imported into the 3D geological model and were used as guides for extending surfaces between wells.

Table 3-1 presents all used data for the 3D geological model.

Data type	**Comments**
Spatial location of wells and geological map by Anderson, 1993	Wyoming State Plane coordinate system, West-Central Zone
Geological formations	Formation top in well (184 wells)
Faults	Fault location in well
Field observations	Fault locations (GPS)
Cross sections by Anderson, 1993	Twenty two cross sections across the oilfield out of which three are complete and partially restored by Anderson
New cross sections from field campaign, 2000	Three cross sections across the central and northern part of the oilfield
Re-interpreted well tops as part of Task 2.2	Formation top in well (50 wells)

Table 3-1. Geological data sources from surface and wells in the Circle Ridge field

3.3.4 CROSS-SECTIONS

The Anderson and O'Connell (1993) study produced a number of cross-sections out of which two where balanced (P-P' and T-T') and published (Figure 3-13). The background material for their study also contained another cross-section (Z-Z') in the complex northern part of the block that was initially used in the interpretation the Circle Ridge structure. However, it was soon discovered that the interpretation of the northern part of the field needed to be revisited and re-evaluated and this cross-section was not used further.

The field campaign from the summer of 2000 produced three new cross-sections (Figure 3-13), two from the northern part of the field (H01-H01' and H02-H02') and one E-W trending section through the southern most productive part of the field (H03-H03'). These sections where complemented with subsurface information from nearby wells and coupled to the 3D interpretation of the formation surfaces.

The new cross-sections have been incorporated and balanced together with the 3D palinspastic reconstruction of the whole model. However, if scrutinized in detail each of

the H01 to H03 cross-sections contain fault movements of layers above the Phosphoria Formation that do not entirely balance. This is partly due to lack of surface (formation extension) control and as a result, have not been used in the balancing of the model. Only Phosphoria, Tensleep and Amsden Formations have been used in the reconstruction work as will be explained below.

All cross-sections are presented in Figure 3-14 through Figure 3-18.

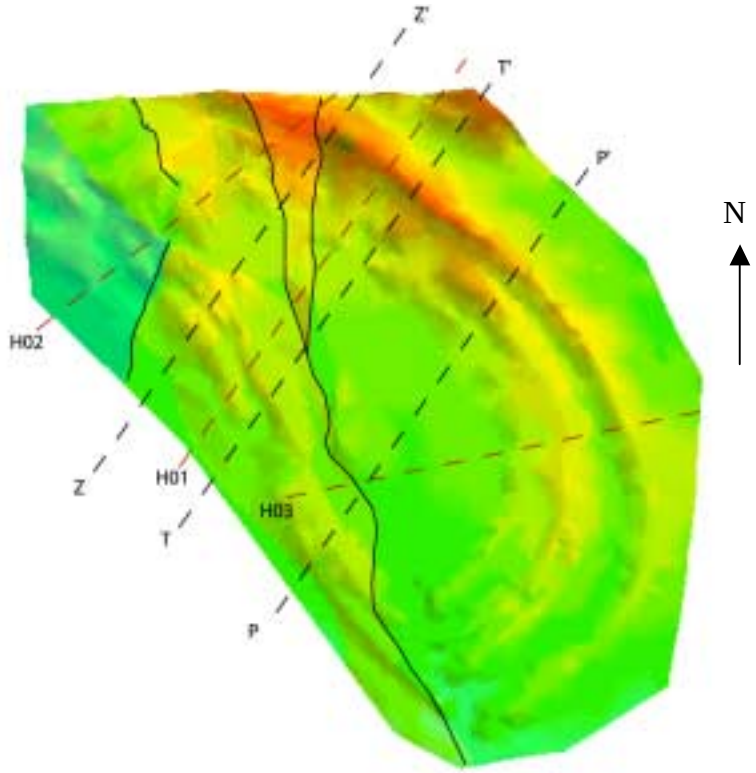

Figure 3-13 The location of the Anderson and O'Connell cross-sections (P-P', T-T' and Z-Z') and the new cross-sections assembled during the 2000 summer field campaign (H01 to H03). The black lines represent the main fault traces of the Red Gully, Green Valley, Orange Canyon and Blue Draw faults.

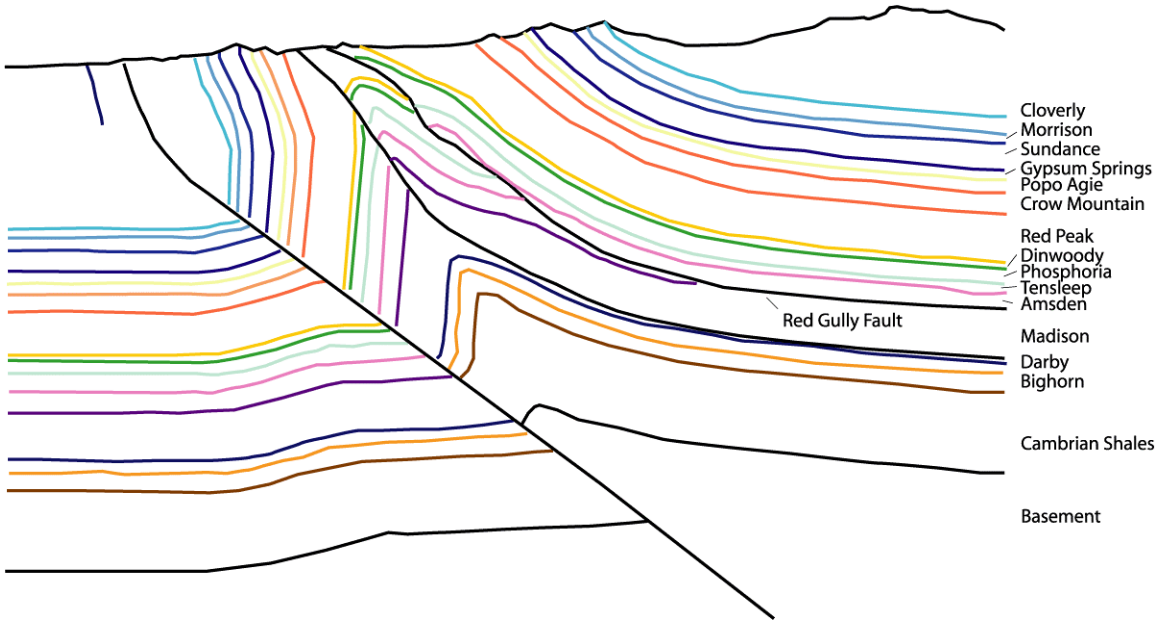

Figure 3-14 Cross-section P to P' after Anderson and O´Connell (1993)

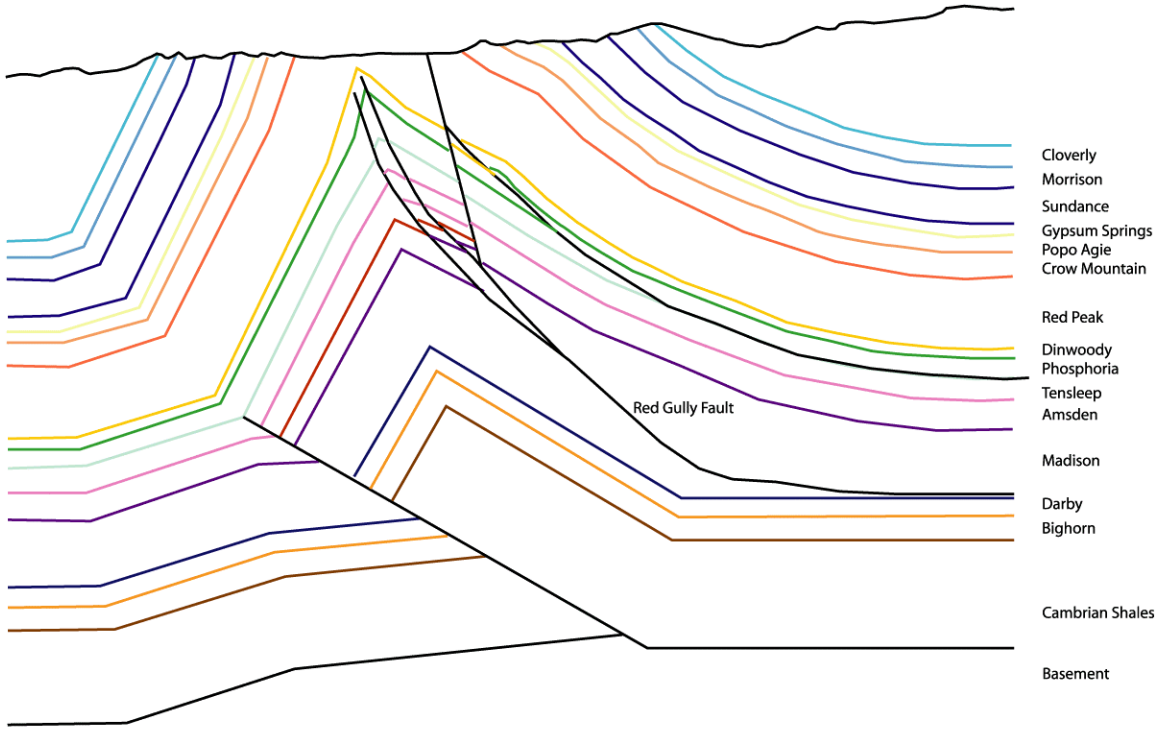

Figure 3-15 Cross-section T to T' after Anderson and O'Connell (1993)

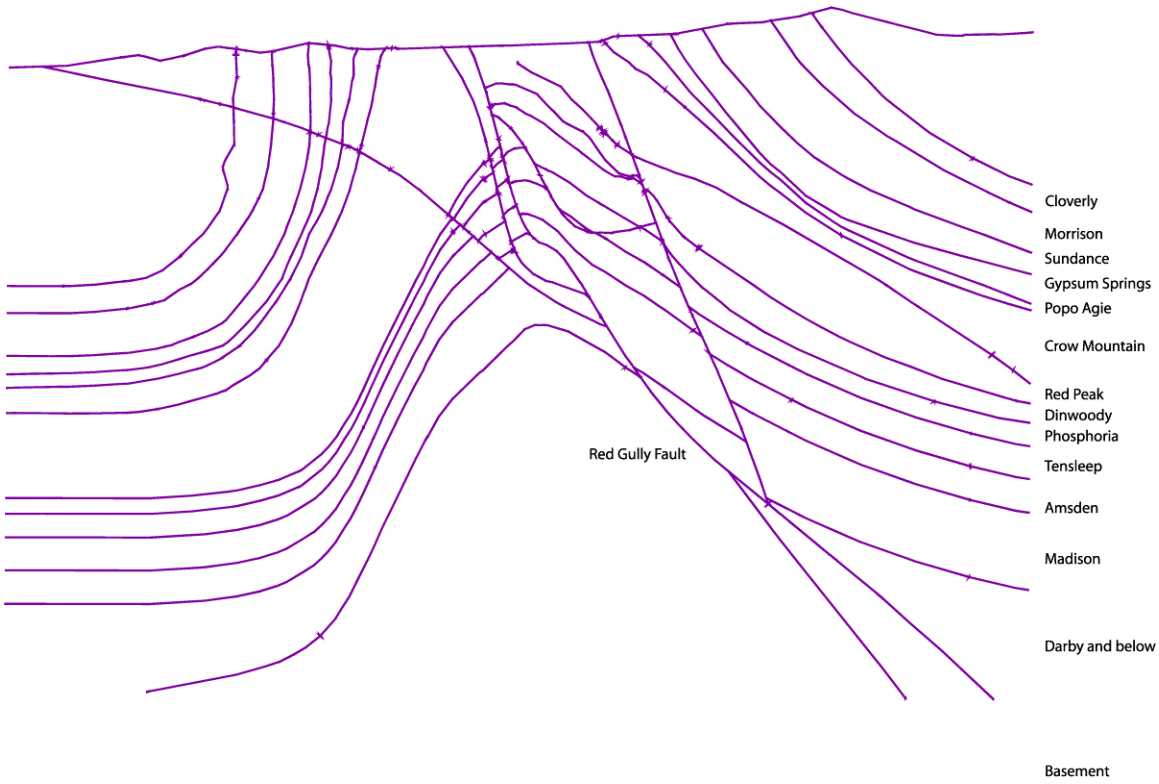

Figure 3-16 The H01-H01' cross-section

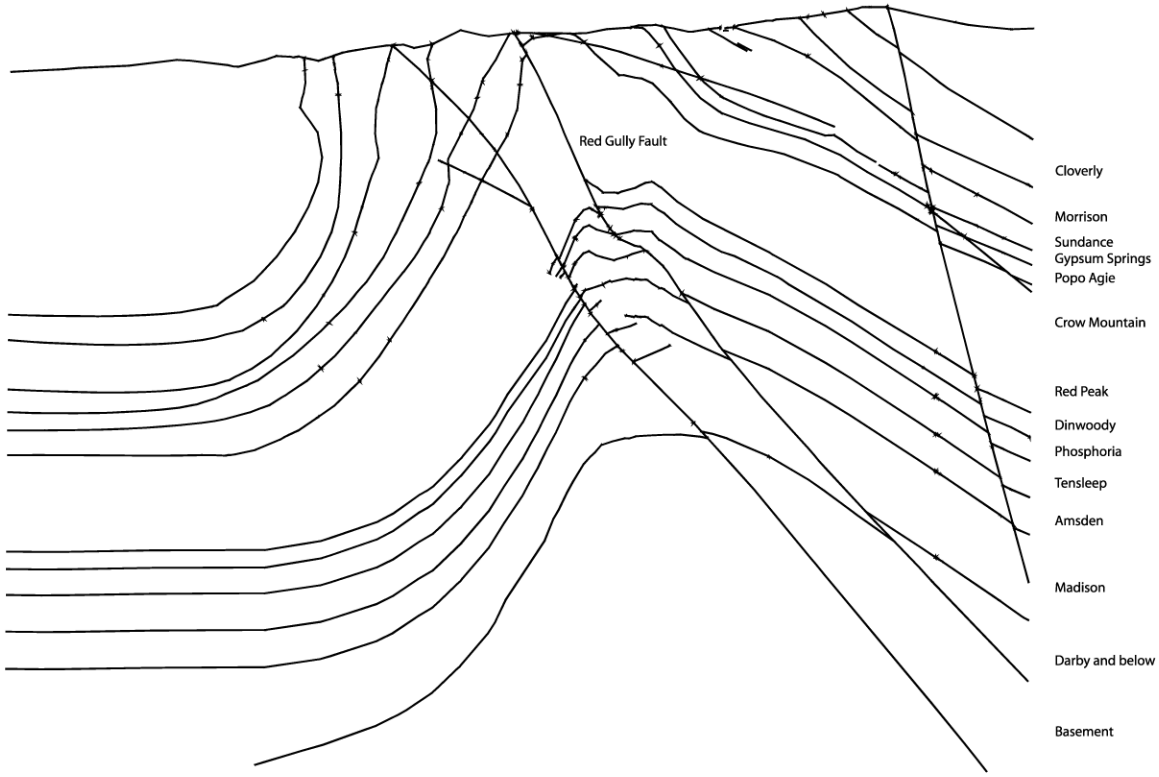

Figure 3-17 The H02-H02' cross-section

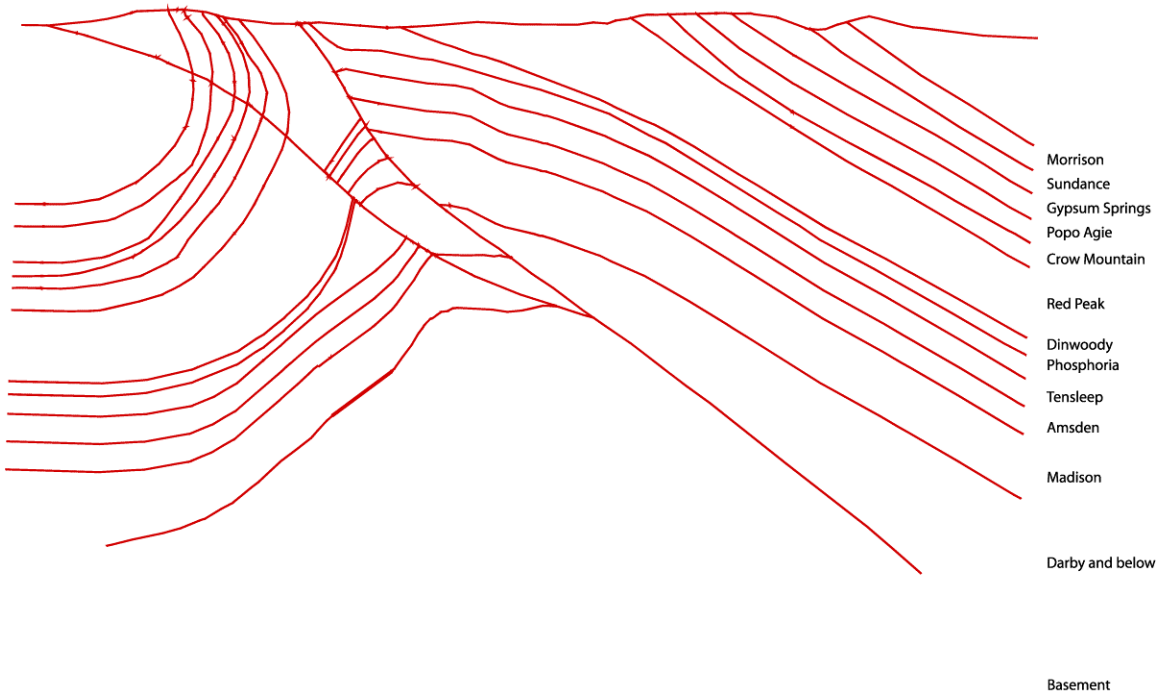

Figure 3-18 The H03-H03' cross-section

3.3.4.1 The Anderson Model

The Anderson Model (Anderson and O'Connell, 1993) consists of 2D interpretations along cross-sections across the Field. As a basis to the graphical interpretation Anderson and O'Connell produced an extensive database of formation tops from over 200 wells penetrating the Circle Ridge anticline. The database contains information of the depth of the top of each formation as well as the location of identified faults. Smith (2000) used the cross-sections and the tops to extend surfaces according to the Anderson and O'Connell (1993) interpretation and visualized the model using the EarthVision™ software (Figure 3-19 and Figure 3-20).

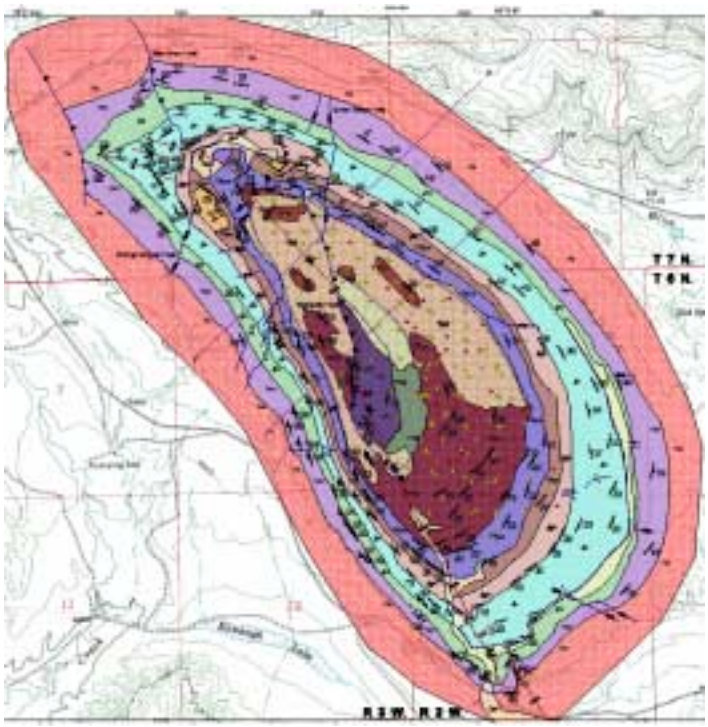

Figure 3-19 The Geological Map of the Circle Ridge Field after Anderson and O´Connell (1993) and Smith (2000). For legend see Figure 3-20.

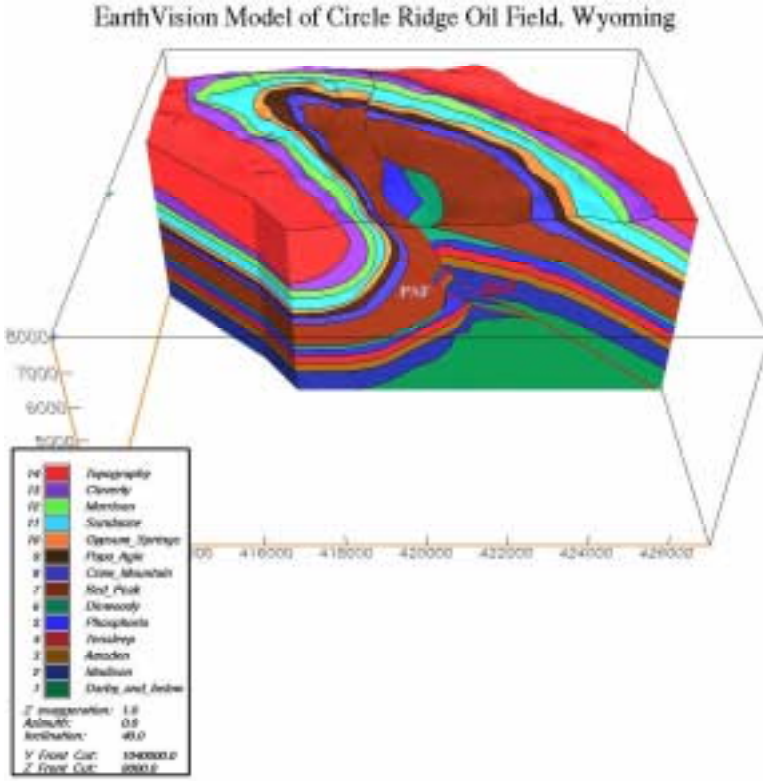

Figure 3-20 The Anderson Model after interpretations by Anderson and O'Connell (1993) visualized by Smith (2000) using EarthVision™ from Dynamic Graphics Inc.

3.3.4.2 Faults

Faulting observed on the surface falls into two main categories: reverse faults and strike-slip faults (both synthetic and antithetic). Minor normal faults have also been observed, mainly at high angles to the main anticline (Figure 3-21). A few large faults dominate the geology of the Circle Ridge field and are illustrated in Figure 3-29. Below follows a brief description of each larger fault.

Figure 3-21 Example of minor normal and strike slip faults in the northeastern corner of the field. Gypsum Springs is offset in several sections by less than 20 ft.

3.3.4.2.1 Red Gully Fault

The Red Gully Fault forms the main thrust through Circle Ridge. Anderson and O'Connell (1993) report that the reverse Red Gully Fault has a surface displacement of at least 1000 feet (305 m) along the western side of the central Dinwoody/Phosphoria hill in the core of the anticline. It juxtaposes Permian Phosphoria over Triassic Red Peak shales and sands that are overturned and dipping 50 degrees towards the east. The Fault is also observed in the north end of the anticline, offsetting Popo Agie and Nugget (Figure 3-22). It is not observed above Gypsum Springs. Quaternary alluvium conceals much of the central portions of this fault but its location is known from several well bores. Several splay structures relate to the Red Gully Fault; i.e. the Yellow Flats, Blue Draw and Gray Wash faults.

3.3.4.2.2 Green Valley Fault

The reverse Green Valley Fault is possibly a direct splay to the Red Gully Thrust. The fault is observed east of the northern part of the Red Gully fault, and offsets Popo Agie and Gypsum Springs (Figure 3-22). Beautiful examples of imbricated Popo Agie show the intense deformation along this fault. The displacement is in the same order as the Red Gully Fault. The fault dies out in the Sundance Formation, with several small folds to accommodate the movement.

Figure 3-22 Photograph showing the Green Valley Fault offset in the Gypsum Springs and the Popo Agie where finger is pointing. The Red Gully Fault runs through the larger gap in the Popo Agie member below the hand.

3.3.4.2.3 Orange Canyon Fault

The orange Canyon fault is a right lateral strike-slip fault with an additional normal fault component. The fault runs through a NE-SW trending drainage canyon in the northern part of the field that exposes orange sands and silts of the Popo Agie member. It is observed in all formations down to Gypsum Springs. This fault is possibly connected to the Blue Draw fault.

Figure 3-23 View down the Orange Canyon with Red Peak shales and sands to the left and Gypsum Springs to the right.

3.3.4.2.4 Blue Draw Fault

This is a reverse fault in the extreme northern end of the anticlinal structure and in the Blue Draw, which is the strike valley formed on Mowry shales north of Circle Ridge. As mapped it cuts through the Mowry – Muddy – Thermopolis section, the Rusty Beds and Morrison, then dies out toward the southeast within Sundance failing to offset basal Sundance limestones or the Gypsum Springs.

3.3.4.2.5 Other Subthrust Faults

The Subthrust Block (footwall block of the Red Gully Fault) consists of several sub-blocks divided by the Blue Draw Fault, Gray Wash Fault, Purple Sage Fault, and Yellow Flats Fault that compartmentalize the reservoirs. The Blue Draw Fault (as explained above), like the Red Gully Fault, has surface exposure while the others are recognized only from well top data.

However, these subthrust faults play an important role in the sequence of restoration of the Circle Ridge structure as will be explained below

3.3.4.3 Fault blocks

The Anderson Model contains sixteen fault blocks according to the original interpretation. However, seven of these blocks are very small or does not involve the producing formations at depth, i.e. Phosphoria, Tensleep and Amsden formations. The following fault blocks have been included in the palinspastic reconstructions; Block 1, 6, 8, 9, 11, 12, 14, 15 and block 16 as illustrated in Figure 3-24.

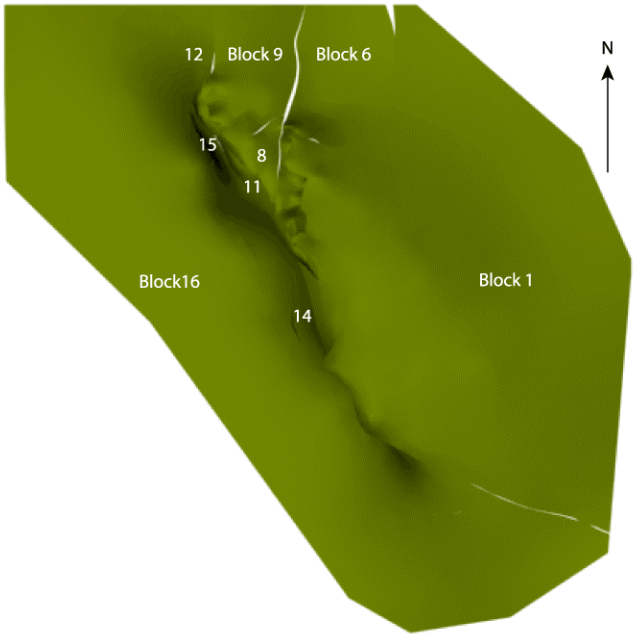

Figure 3-24 Top view of the location of major fault blocks in the Phosphoria formation.

The surfaces of most formations of the Anderson Model are complex and exhibit dramatic undulating geometries to honor all well information. The interpreted extension of surfaces between wells are questionable many times when wells at close distance have tops with large differences in elevation. As the undulations occur mostly in the northern end of the reservoir where faulting is most intense, it is more likely that the elevation differences are due to minor fault movements between wells. However, these small faults are too minor to be included into the reservoir scale model.

Figure 3-25 Illustration of the undulating extension of the top of the Phosphoria formation. The undulation of the surface is controlled by well top information from the Anderson and O'Connell database.

3.3.4.4 Observations in the field: Update of fault extensions

The field work during the summer of 2000 updated the extension of some of the faults in the Anderson Model. The Anderson and O'Connell (1993) extension of The Red Gully Fault up into the northern part of the field is questionable from observations in the field. Tracing the extension of both the Green Valley Fault and the Red Gully Fault suggests that the main plane of movement could be accommodated along the Green Valley Fault and not along the northern part of the Red Gully Fault. Observations of the well top information does not reject this interpretation, but shows that the Green Valley Fault need to have a steeper inclination than the Red Gully Fault.

Based on the 3D extensions it seems plausible that the Red Gully continues as Anderson and O'Connell have proposed but that the Green Valley Fault is interpreted as an imbricate to the Red Gully Fault. This interpretation fits very well with Anderson and O'Connells interpretation that the Circle Ridge structure is a fault propagation fold. The steeper angle of the Green Valley Fault is also supported by the mechanisms of fault propagating folds as proposed by Mitra (1990) where shortening of lower units during the propagation produces high angle fold hinge planes and faults above the basement fault.

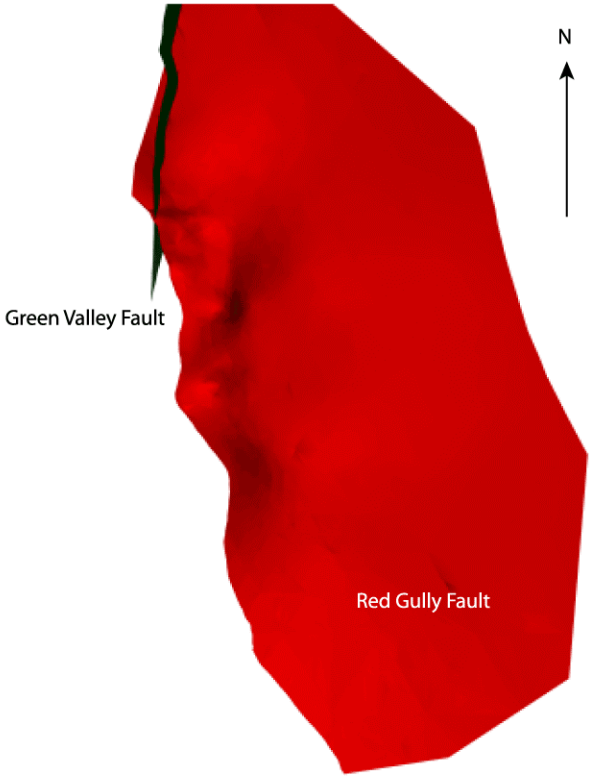

Figure 3-26 3D Illustration of the extension of the Red Gully Fault and the Green Valley Fault based on the well tops and the surface geology. The intersection between the two shows that the Green Valley Fault needs to be steeper than the Red Gully Fault in order to honor the well top data.

The original 3D interpretation of the Orange Canyon Fault extends in a bow like shape below the Circle Ridge structure, c.f. Figure 3-27. This interpretation has no basis in the well top data and does not show up in outcrops. The Orange Canyon Fault can only be observed in one location, running parallel to the Orange Canyon and in a few well tops. The orientation of the fault from field observations does not indicate any curvature at depth, nor does well intersections. This interpretation is therefore re-evaluated in such a way that the fault extension stops just below the last known intersection point in the wells and is indicated as a red line on the fault surface in Figure 3-27.

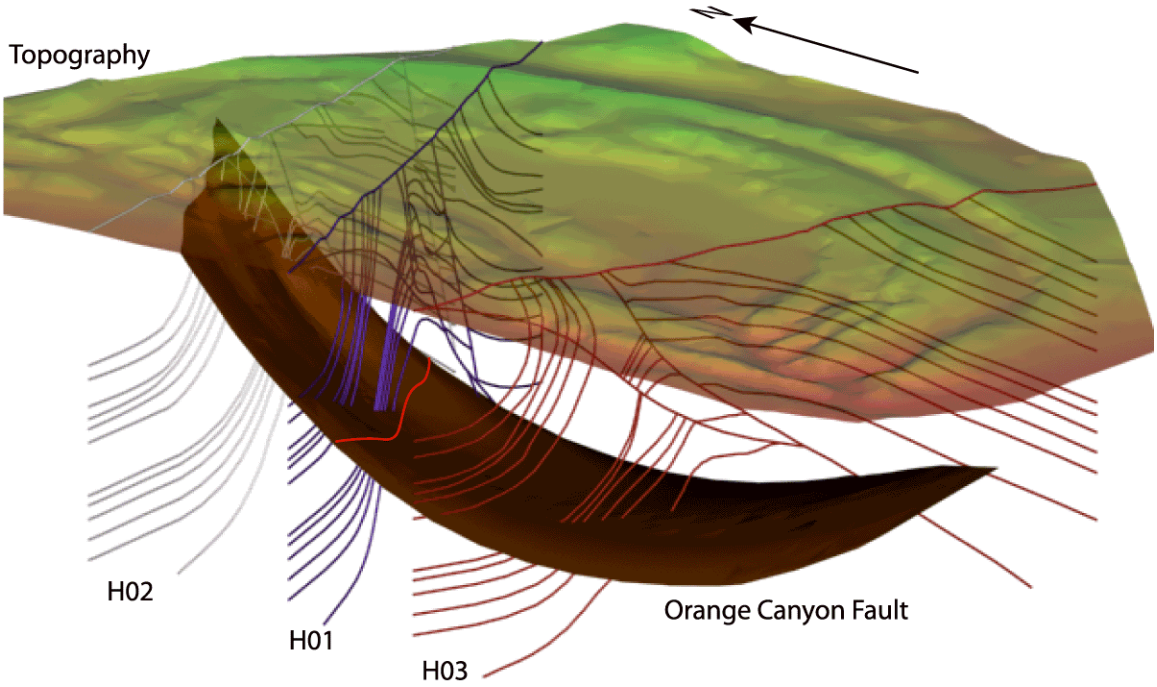

Figure 3-27 Illustration of the original extension of the Orange Canyon Fault in a bow shape below the Circle Ridge structure. This extension has no basis in well top information and has been excluded in the restoration process. The red line on the fault surface indicates where the new interpretation ends. Cross-sections are shown for a better 3D understanding of the extension of the fault.

3.4 Task 2.5 – Validation of Cross Sections Using Retrodeformation Software

3.4.1 OVERVIEW

The validation of the cross sections is accomplished through balancing then according to the experimental methods outlined in Section 2 of this report. Once these cross-sections have been validated, then the reconstructions can be used to calculate the strain parameters listed in Section 2.3.6 for use in Task 2.6 – Generation of the DFN model. It is important to note that, while many Formations are depicted in the cross-sections, the balancing focused only on the three most important reservoir units: the Amsden, Tensleep and Phosphoria Formations. Other units have not been subjected to balancing requirements; their deformation is calculated by allowing them to deform passively according to the deformation of the three key reservoir units.

Circle Ridge produces oil from five Paleozoic reservoir units, the Phosphoria, Tensleep, Amsden, Darwin and Madison formations, ranging from 300 feet to 1500 feet depth. The main reservoirs are the Phosphoria, Tensleep and Amsden (Figure 3-28), which produces about 95% of the oil in the field.

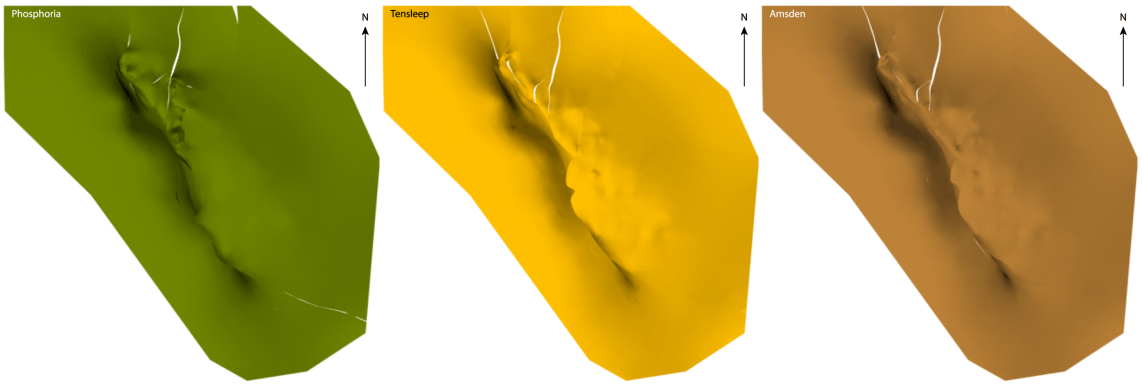

Figure 3-28 The Phosphoria, Tensleep and Amsden formation top surfaces

The palinspastic reconstructions of the Circle Ridge structure have been constrained only by the Phosphoria, Tensleep and Amsden Formations due to two reasons;

1. The complexity of the reconstruction is minimized with limited amounts of formations involved
2. The computer resources limits the number of geometric elements that can be involved in the restoration process
3. These three formations contribute 95% of the production.

The three chosen formations have been reconstructed down to its pre-deformations state with the following assumptions;

- The formations were deposited horizontally throughout the field
- The sedimentary deposition was completed by the time of the folding and faulting deformation events

These two assumptions are supported by the background geological history as presented by Anderson and O'Connell (1993), Agaston (1952), Brown (1988), Downs (1952), Fanshawe (1952), Frielinghausen (1952) and Keefer (1965).

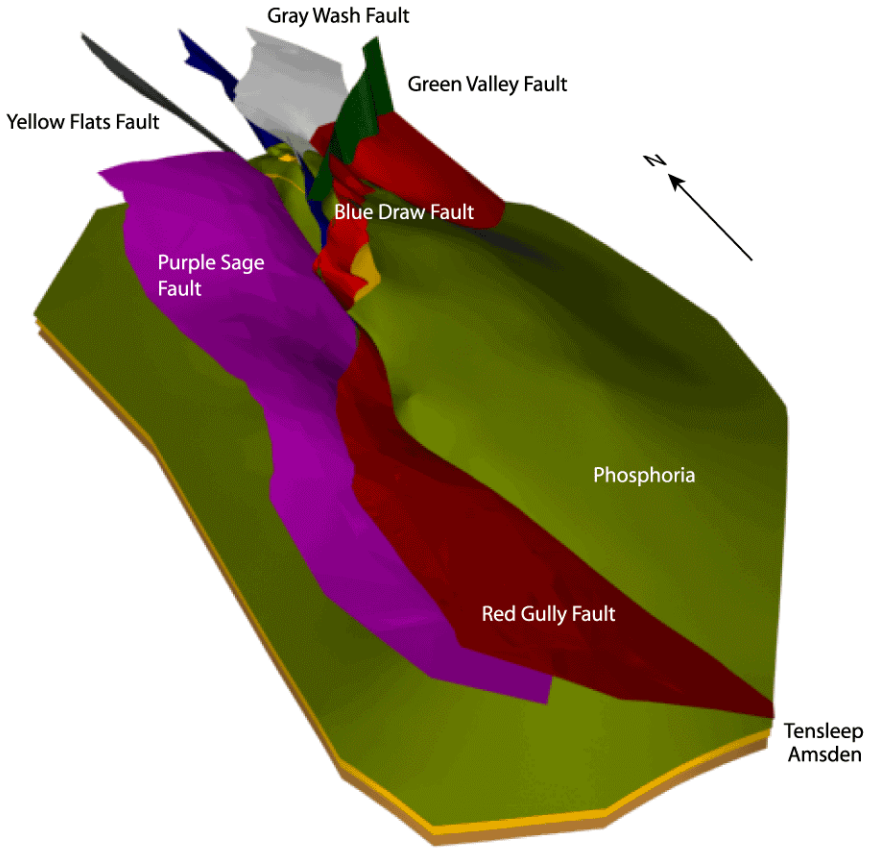

Figure 3-29 Illustration of the faults and formations that take part in the palinspastic reconstructions of the Circle Ridge structure.

3.4.2 IMPLICATIONS OF RESTORING THE GEOLOGICAL MODEL

The calculation of retro-deformation during the reconstruction requires that each polygon of the geometric representation of the surface or volume are tracked. The number of polygons directly effects the processing time of the strain calculations and is thus a major constraint in the restoration process. In the original Anderson Model, as represented by Smith (2000), the Phosphoria surface contains about 12000 polygonal elements. The polygonal surfaces are irregular, with most of the polygons along the borders of the surfaces (Figure 3-30), making unnecessarily complex surfaces, which will slow down strain calculations.

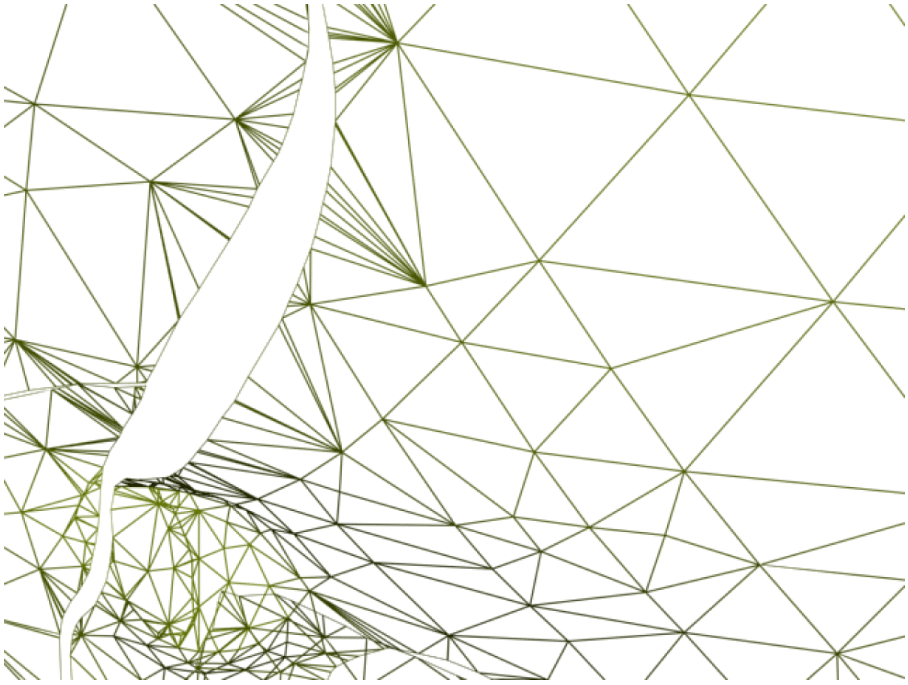

Figure 3-30 Close-up of the polygons of fault blocks 6 and 9 on the Phopshoria surface as defined by Smith (2000).

Further, the interpreted extension between wells of the chosen formations results in surfaces with very complicated undulations. The reasons for the undulations may be several as discussed in section 3.3.4.1;

- Limited surface control due to few well tops
- Minor scale faulting between wells
- Variable thickness of the units
- Poor knowledge of exact depth of tops in old wells

To achieve a good understanding of the large scale strain pattern and how this affects the formation of the fracture network in the reservoir, it is important to minimize the effect of anomalous strains generated by unknown small scale undulations of the formation surfaces. Each formation surface have therefore been smoothed to minimize the undulations, but also to minimize the potential deviation from the actual well top data.

The smoothing process is also performed in conjunction with making a more regular grid of each formation surface by using the method of resampling of the grid.

The Resample algorithm used in 3DMove, when decreasing data density, uses a grid (oriented parallel to the regional plane of the surface). The resampling methodology seeks to:

- maintain volume: Resampling attempts to maintain the volume between the resampled surface and a datum. In attempting to maintain the volume the

overall shape of the surface is maintained, though local shape changes will occur.

- minimize lateral spreading: In the down sampling mode, the boundary of a resampled surface may spread laterally, as can be seen if a resampled surface's edges are compared to the original surface edges.

The end result of the resampling exercise is a regular grip with fewer polygons which is smoother and exhibits less undulation than the original surfaces.

3.4.3 CREATION OF POLYGONAL VOLUMES

To be able to calculate all three principal components of strain during retro-deformation, it is necessary to create volumes between the formation top surfaces. The volumes are created by populating the space between the surfaces with polygonal elements, c.f. Figure 3-31. All three principal axes of strain is recorded in each polygonal element during the restoration process.

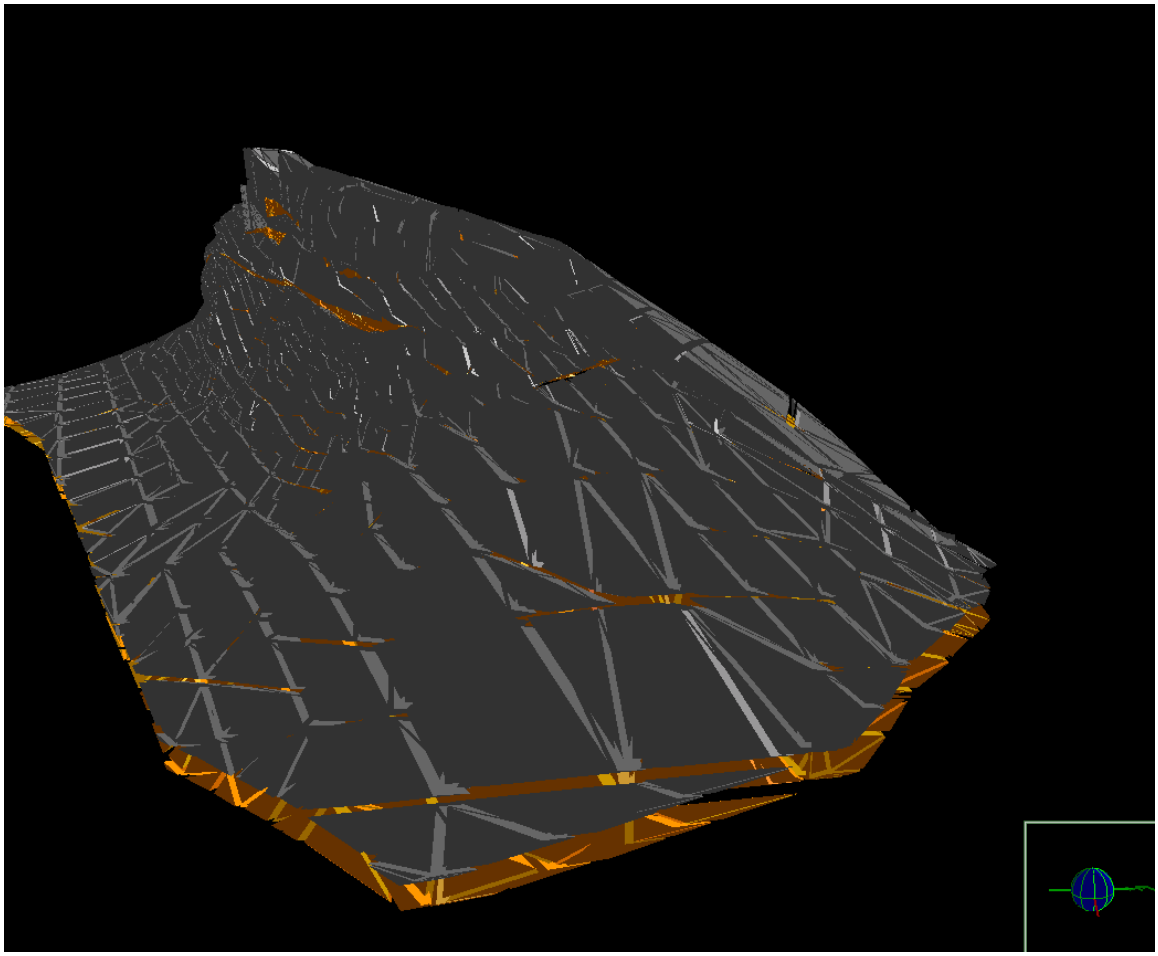

Figure 3-31 Phosphoria and Tensleep volume elements

3.4.4 RESTORING FAULTS AND THRUSTS

The faulting and thrusting sequence of Circle Ridge has been suggested by Anderson and O'Connell (1993) to start with the movement of the Gray Wash fault that is the lowest structurally. This initial faulting occurred subsequent to most of the folding found at the Circle Ridge anticline. Upon encountering some obstacle or reaching the stress limit of strain release, the stress field then broke higher in the sequence, creating the Blue Draw Fault. Towards the south both these faults merge into the Red Gully Fault system, which at this time continued to move along an earlier established thrust plane. The imbrication process in the northern end of the field is repeated once again with the formation of the Yellow Flats fault higher in the section. The final thrust displacement was focused on the Red Gully Fault that is structurally highest.

The Orange Canyon Fault obliquely cuts all these faults and was formed last of the great faults through the Circle Ridge anticline.

The palinspastic fault reconstruction was performed in the reverse order, restoring the fault movements fault by fault back to the unfaulted anticline.

The chosen process for fault movements was Fault Parallel flow (methodology described in section 2.3.4.1).

The Fault Parallel Flow process was performed on the Tensleep Formation, with all other formations following passively. This approach helps showing whether interpretations of the surface extensions are valid, or if other processes have to be involved in order to restore each hanging wall unit back to its matching level on the footwall.

The Tensleep Formation was chosen as the main restoration surface because of its relative competence compared to the more shaly and limestone rich formations of Phosphoria and Amsden and because its location in the middle of the restored pack of surfaces.

The unfaulted Tensleep Formation is illustrated in Figure 3-32. The recorded strain during the restoration is saved incrementally in each grid cell, both in the surfaces and in the volumes.

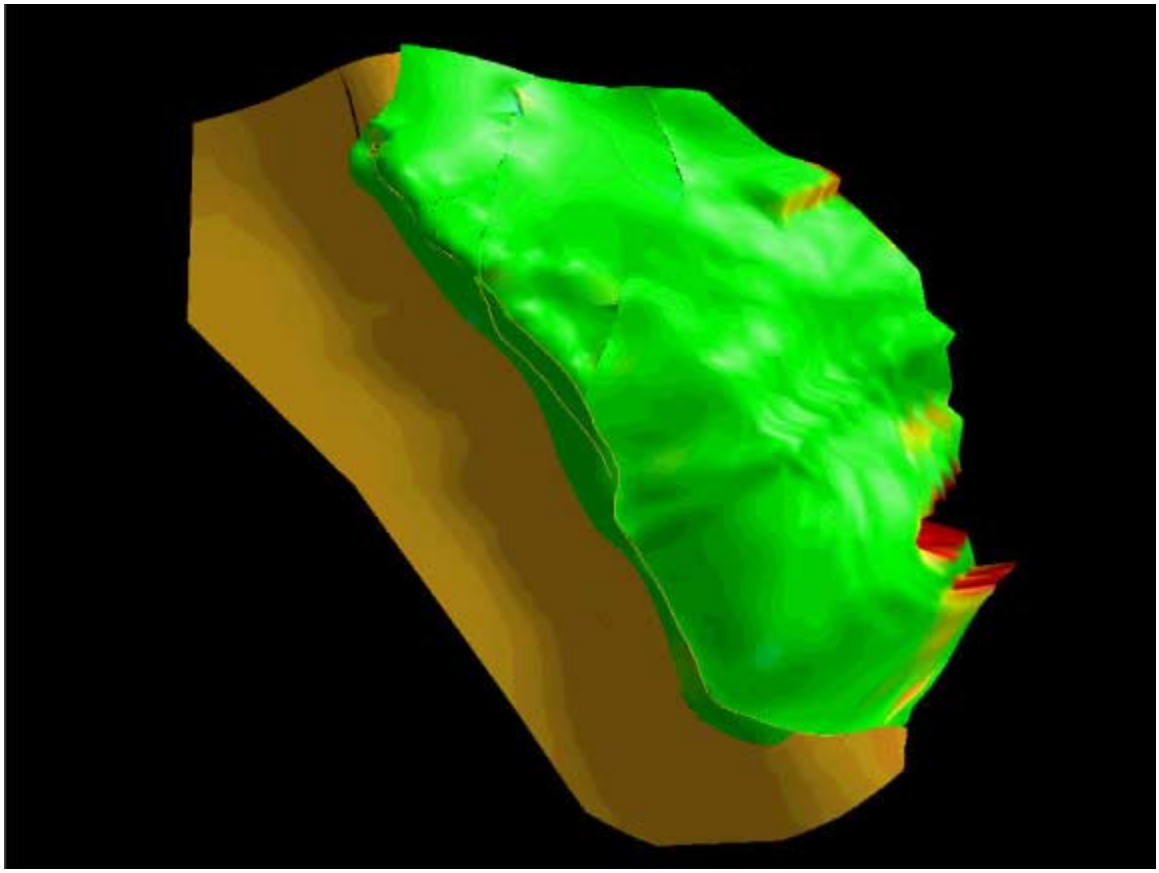

Figure 3-32 Illustration of the unfaulted Tensleep formation showing fault blocks 1, 6, 8, 9, 11 and 14 in green color as part of the overthrust and the top of the anticline.

3.4.5 RESTORING THE INITIAL FOLD STRUCTURE

The initial folding of the Circle Ridge anticline is restored back to its flat depositional state using two different methods: Vertical Shear Unfolding and Flexural Slip Unfolding.

The accumulated strain is recorded for each type of restoration and plotted on to of each formation surface after deformation, as illustrated in Figure 3-33.

The result of the Flexural slip unfolding shows that parts of the anticline still exhibit small-scale undulations that cannot be attributed to the main anticline folding. The perturbations on the surface reflects the fact that other smaller events has occurred, like smaller folds or minor faults which has not been part of the model. The important pattern to be distinguished is the highly deformed green-red band in the overturned limb of the anticline (left in Figure 3-33). Further, it is anticipated that the previously interpreted major fault block 1 (overthrust) are problematic to restore without generating large strains in bands across the block. This might suggest that there are other faults in this unit which have not been part of the model.

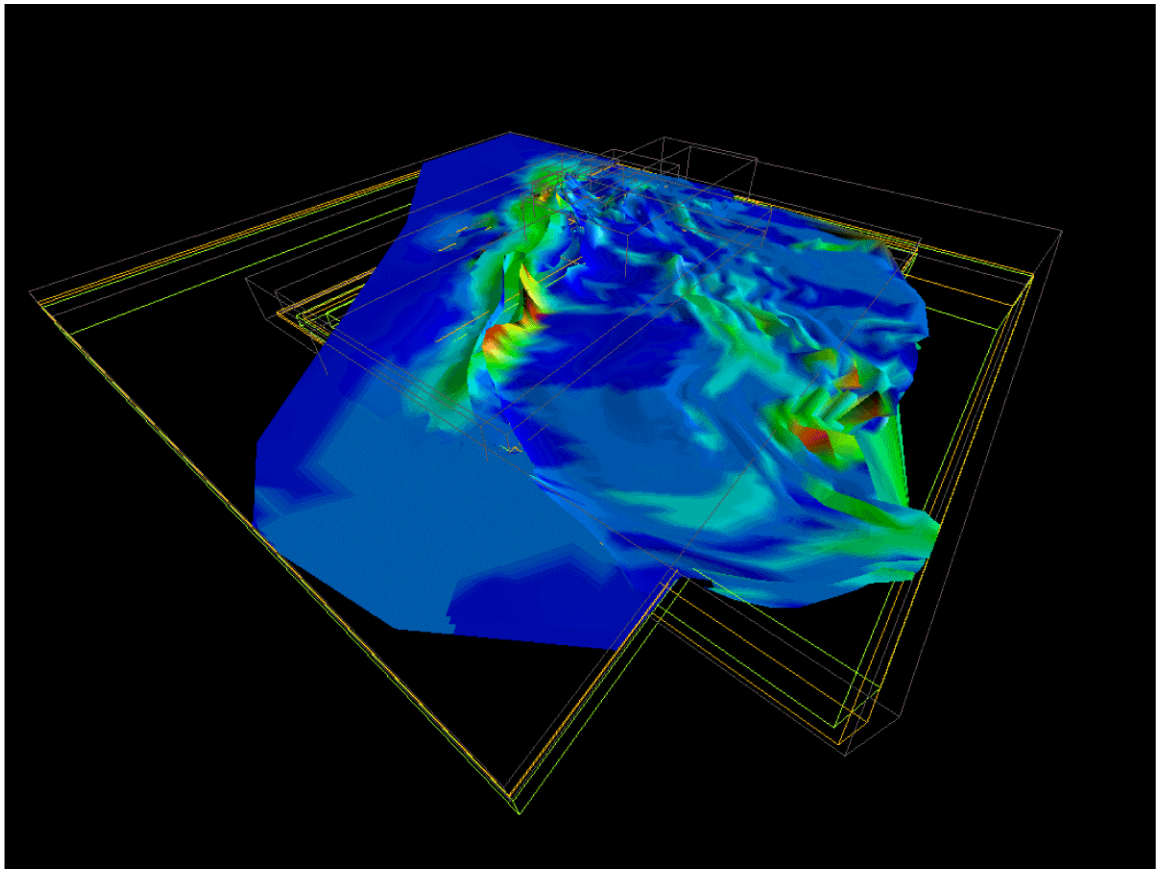

Figure 3-33 Completely restored Tensleep formation using Flexural Slip Unfolding. The color map reflect the amount of accumulated strain throughout the restoration process where blue colors are lowest recorded strains and the red are the highest.

The Vertical Shear Unfolding results are illustrated in Figure 3-34, Figure 3-35and Figure 3-36 for formations Tensleep, Phosphoria and Amsden respectively. The accumulated strain pattern shown in these illustrations are similar to that of using Flexural Slip Unfolding.

It is also possible to see the mismatches between fault blocks on the two formations that has been restored passively together with the Tensleep formation. These mismatches indicates that the interpretation of the fault blocks are not perfect. The reasons for the mismatches can be several;

1. volume changes in the formations during deformation have not been considered
2. the shape of the faults are different
3. the shape of the fault blocks are different
4. the extension of the surfaces between the well tops are different
5. the restorations processes requires more steps to restore minor structures like small faults or small scale folding
6. the thickness of the layers are not constant
7. the original depositional environment may not be planar

However, the mismatches are comparatively small and are interpreted to be of a minor effect to the understanding of the overall strain pattern of the Circle Ridge anticline. Most of the Strains are accumulated in the overturned limb which is exactly what to expect in a structure like this. The most interesting feature of the reconstructions is the accumulation of strain in the central part of fault block 1 which contains the most productive wells in Circle Ridge today. This is a likely place for a relativel higher intensity of fracturing, which seems to be reflected in the production history of the field.

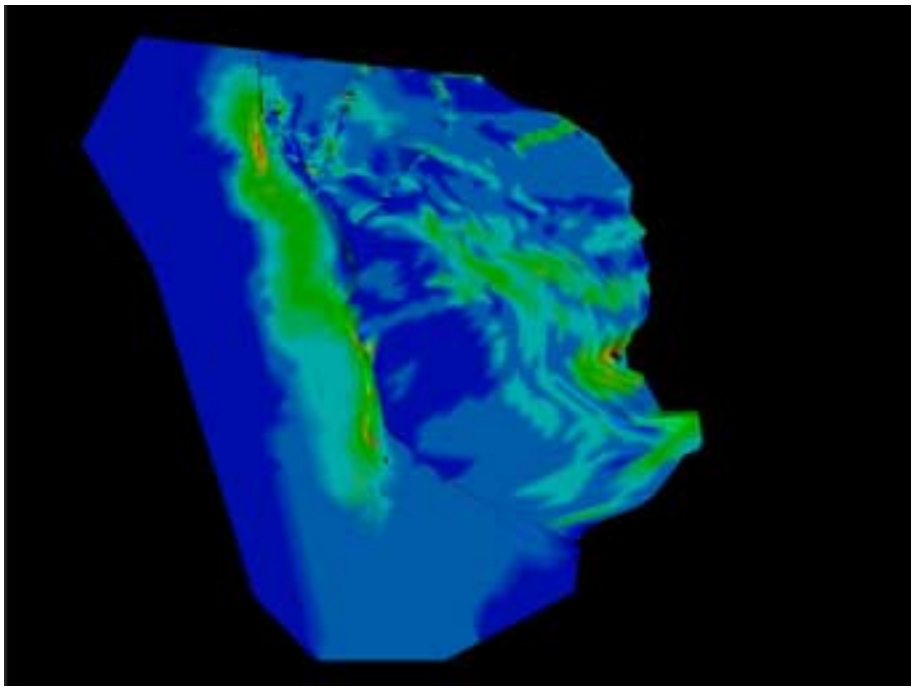

Figure 3-34 Vertical Shear Unfolding of the unfaulted Tensleep formation (top view). The color map shows the accumulated strain, with blue colors showing the lowest recorded strains and the red colors the highest.

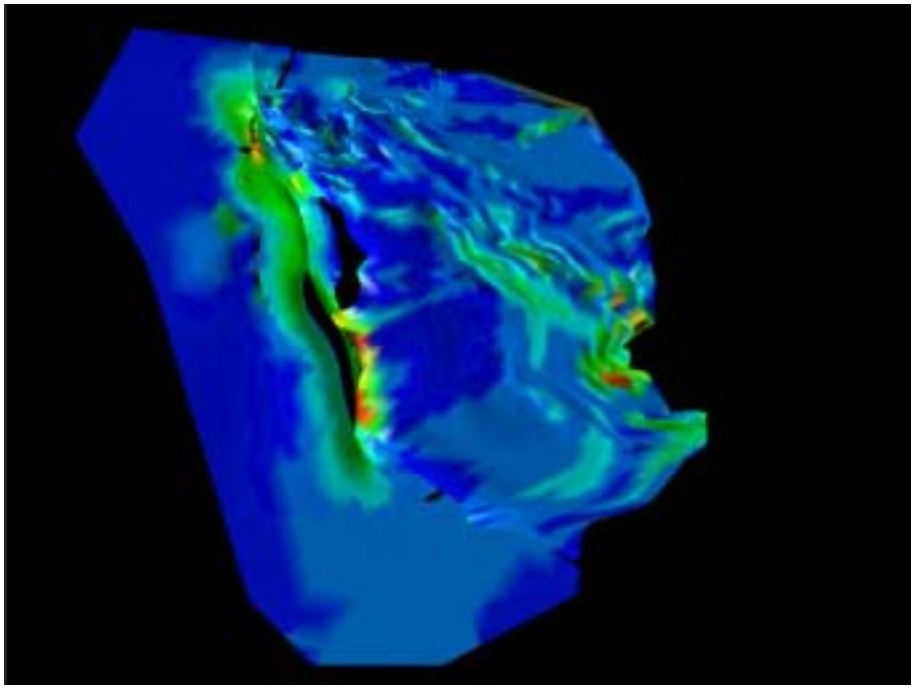

Figure 3-35 Vertical Shear Unfolding of the unfaulted Phosphoria formation (top view). The color map shows the accumulated strain, with blue colors showing the lowest recorded strains and the red colors the highest.

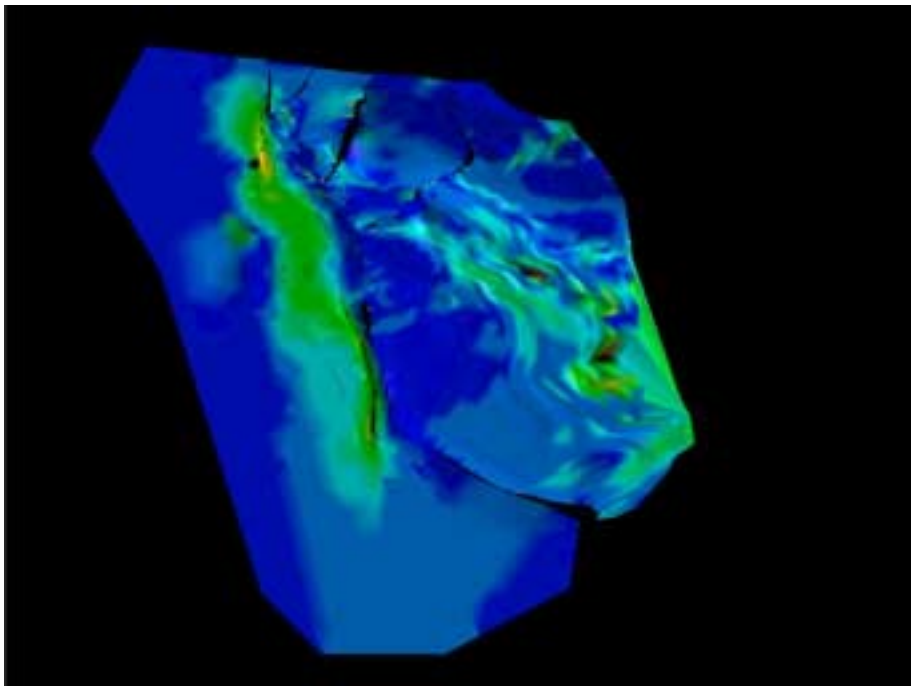

Figure 3-36 Vertical Shear Unfolding of the unfaulted Amsden formation (top view). The color map shows the accumulated strain, with blue colors showing the lowest recorded strains and the red colors the highest.

3.5 Task 2.3 – Field Data Collection & Analysis

3.5.1 PURPOSE OF TASK

The purpose of this Task is to analyze the fracture data obtained in outcrop to calculate the number of sets at each location, and for each set, the orientation distribution, the intensity and the trace length (size) distribution. This was done for all eleven scan line data sets using the methodology described in Section 2.4.2.

3.5.2 SETS & ORIENTATIONS

The orientation and number of fracture sets has been determined for all of the scanline sites, and results summarized in Figure 3-37 through Figure 3-46.

Many of the stereoplots show fracture sets, that when rotated relative to bedding, plot as pole concentrations at the top and bottom of the plot (indicating a fracture set orthogonal to bedding and striking parallel to bedding dip), or on the left and right sides (indicating a fracture set orthogonal to bedding and striking parallel to bedding). These fracture sets are evident in the plots for Scanlines 4,5,6,7,8,9 and possibly 11. The fracturing extant at Scanlines 1,2 and 3 differ. Scanlines 1 and 2 are similar in that they show evidence for a set orthogonal to bedding, but the strikes are at substantial angles from the strike and dip of the bedding. The fracturing at Scanline 3 differs the most: the one set present is neither orthogonal nor parallel to bedding, nor does its strike appear to be related in any way to bedding strike or dip.

Scanlines 1 and 2 are also in a more highly faulted and folded area of the Field. these two scanlines are located in the area where the Red Gully Fault cuts the section, and also where the anticline is more tightly folded. Scanline 3 is located in the nose of the tightly folded northwesterly part of the anticline, and so also may have a more complex strain history. The other scanline sites, particularly sites 5 through 9, are located along the eastern and northern flanks of the anticline where there is little large-scale faulting and folding is much more gentle and regular. Scanline sites 10 and 11 are near the southeastern end of the Red Gully Fault, in the subthrust portion to the southwest, and although not as tightly folded as the rock in the vicinity of scanlines 1-3, still may be in an area of increased strain.

The results of these stereoplots suggest that at least some of the fracturing is probably due to the strain produced by the folding that created the anticline. In regions where the folding is tighter and major faulting occurs, there may be additional fracture sets.

Since the comparisons to the strains calculated from the 3D palinspastic reconstruction has not been completed, it is not yet known whether these strain history will further clarify the controls on fracture orientation, but these preliminary observations on the relation of fracture orientation to bedding orientation suggest that the strain history may prove an excellent control on fracture orientations.

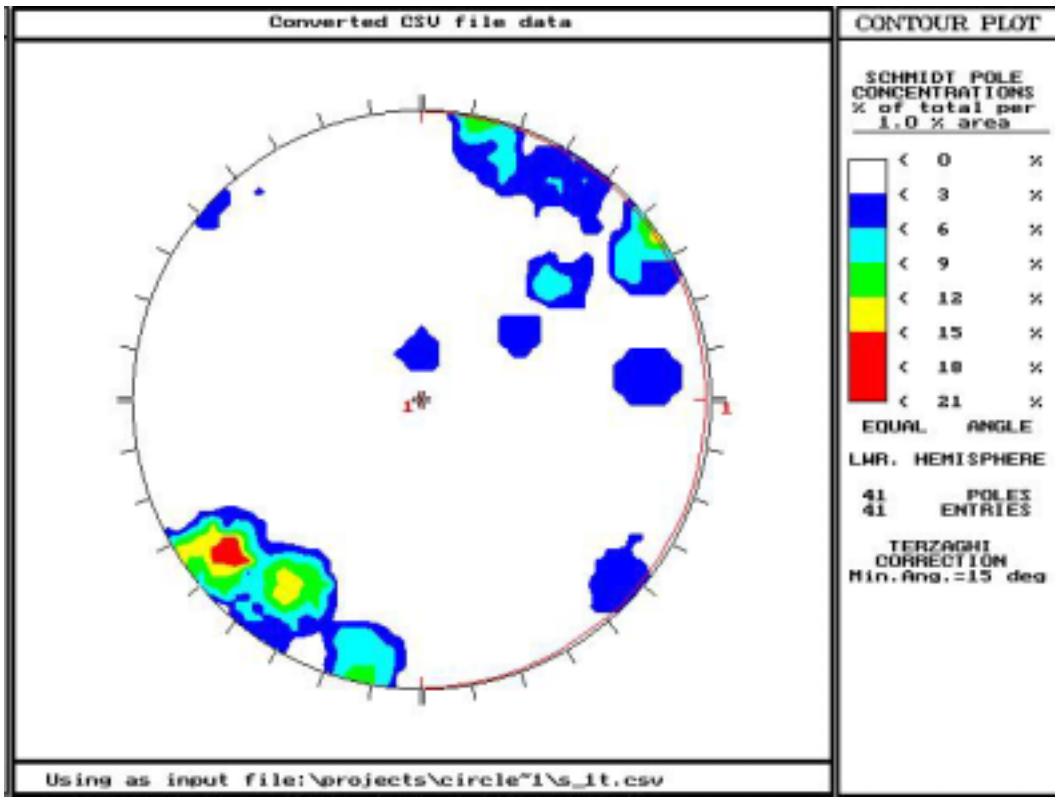

Figure 3-37. Stereoplot for Scanline 1, rotated relative to bedding plane.

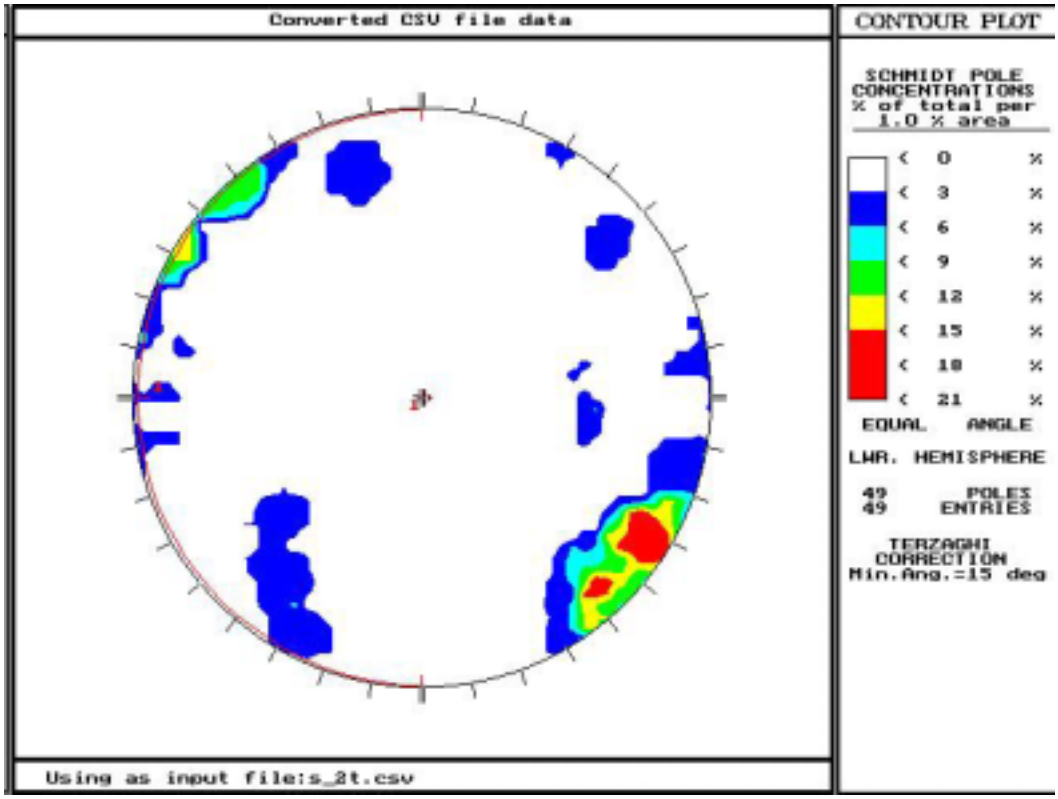

Figure 3-38. Stereoplot for Scanline 2, rotated relative to bedding plane.

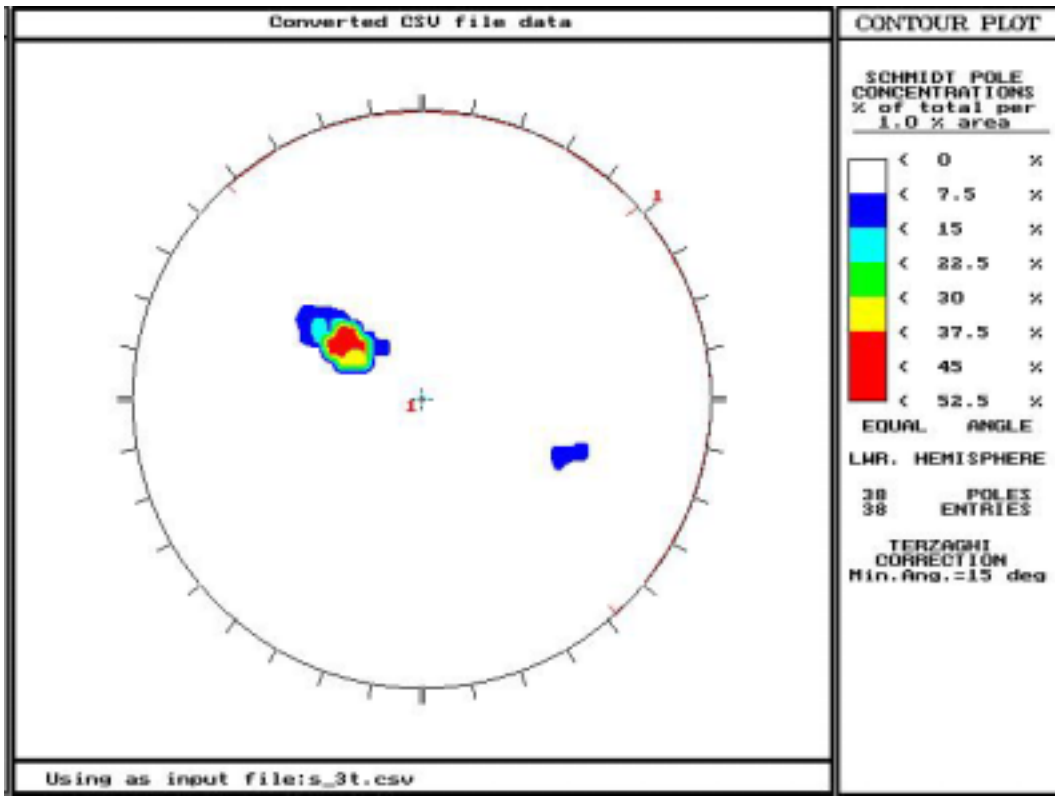

Figure 3-39. Stereoplot for Scanline 3, rotated relative to bedding plane.

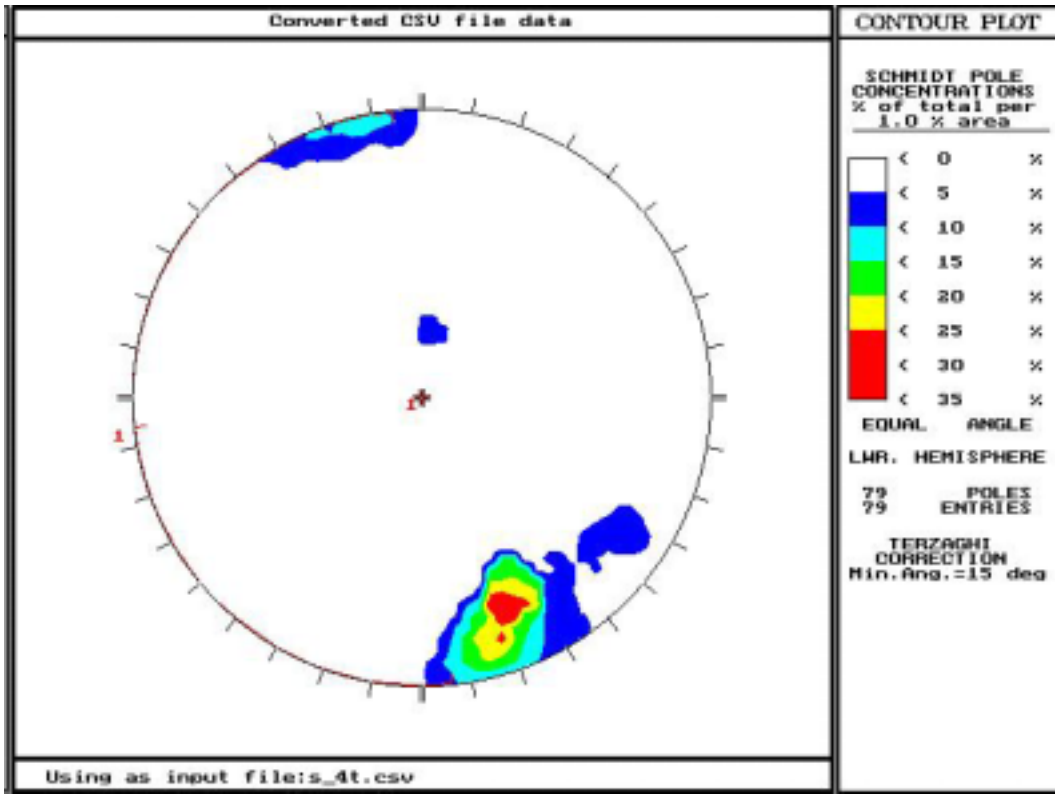

Figure 3-40. Stereoplot for Scanline 4, rotated relative to bedding plkane.

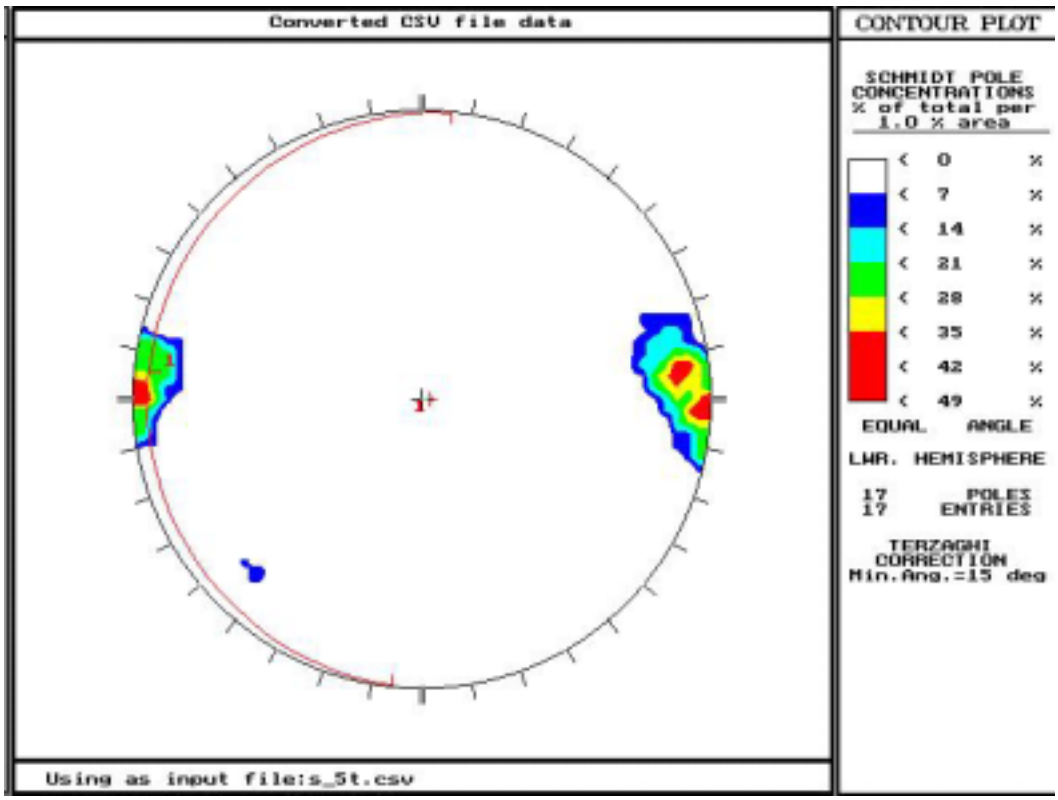

Figure 3-41. Stereoplot for Scanline 5, rotated relative to bedding plane.

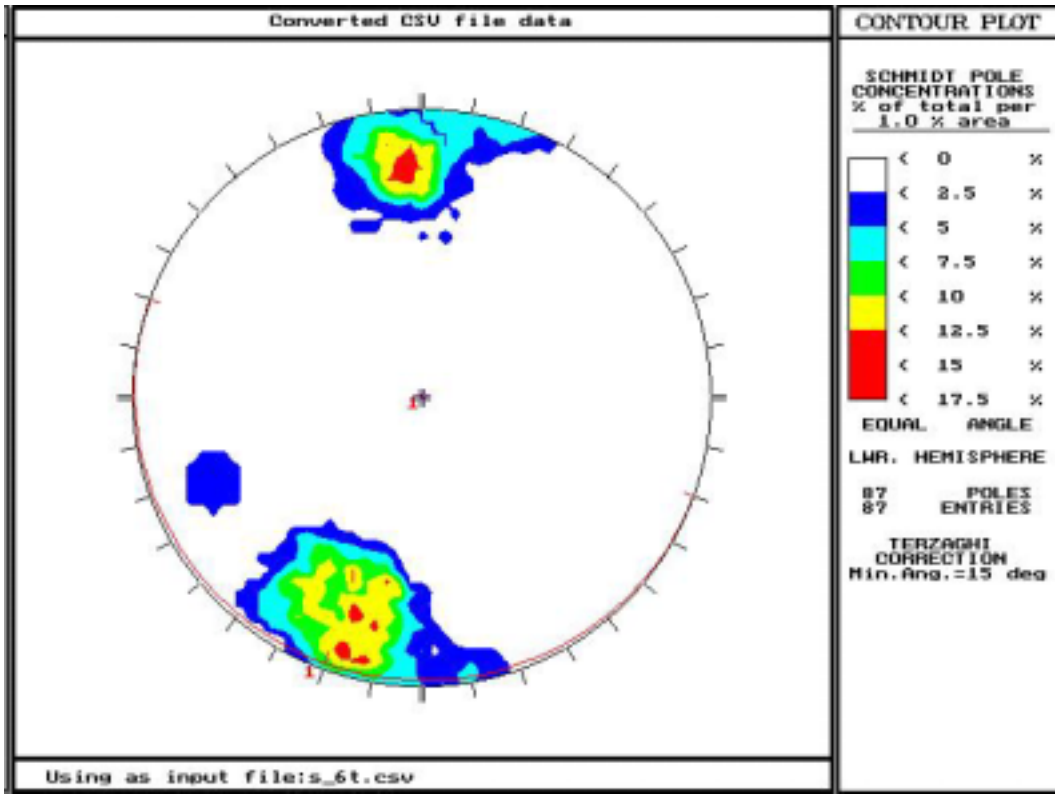

Figure 3-42. Stereoplot for Scanline 6, rotated relative to bedding plane.

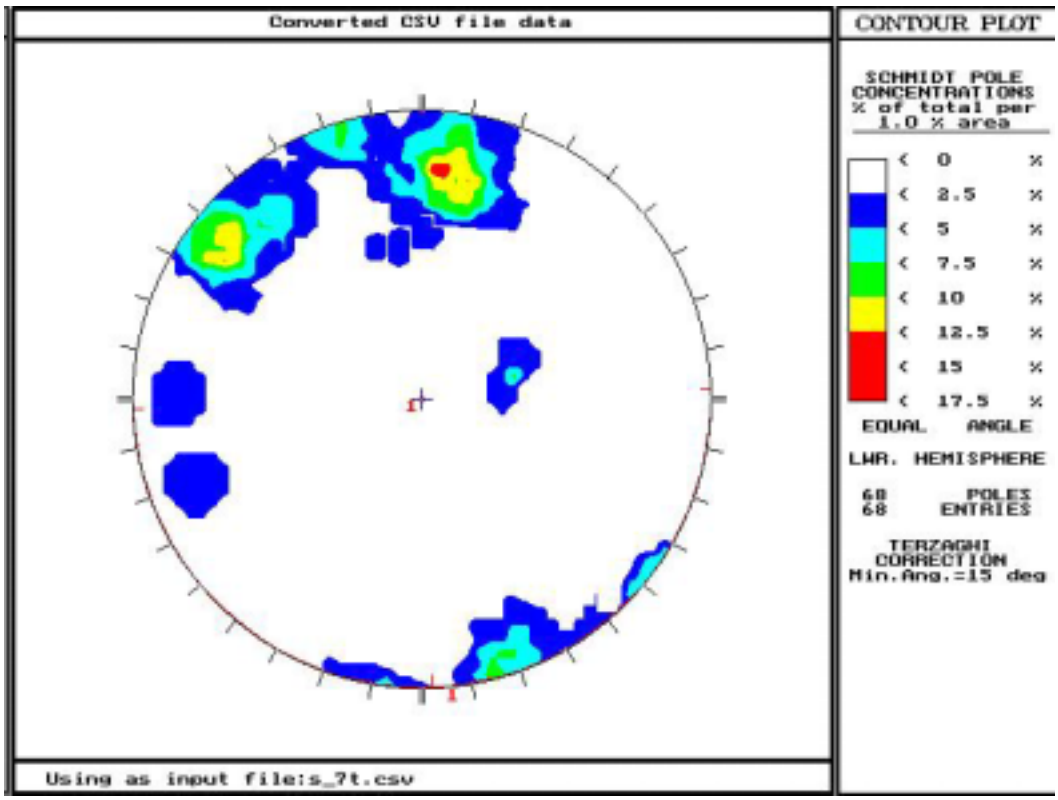

Figure 3-43. Stereoplot for Scanline 7, rotated relative to bedding plane.

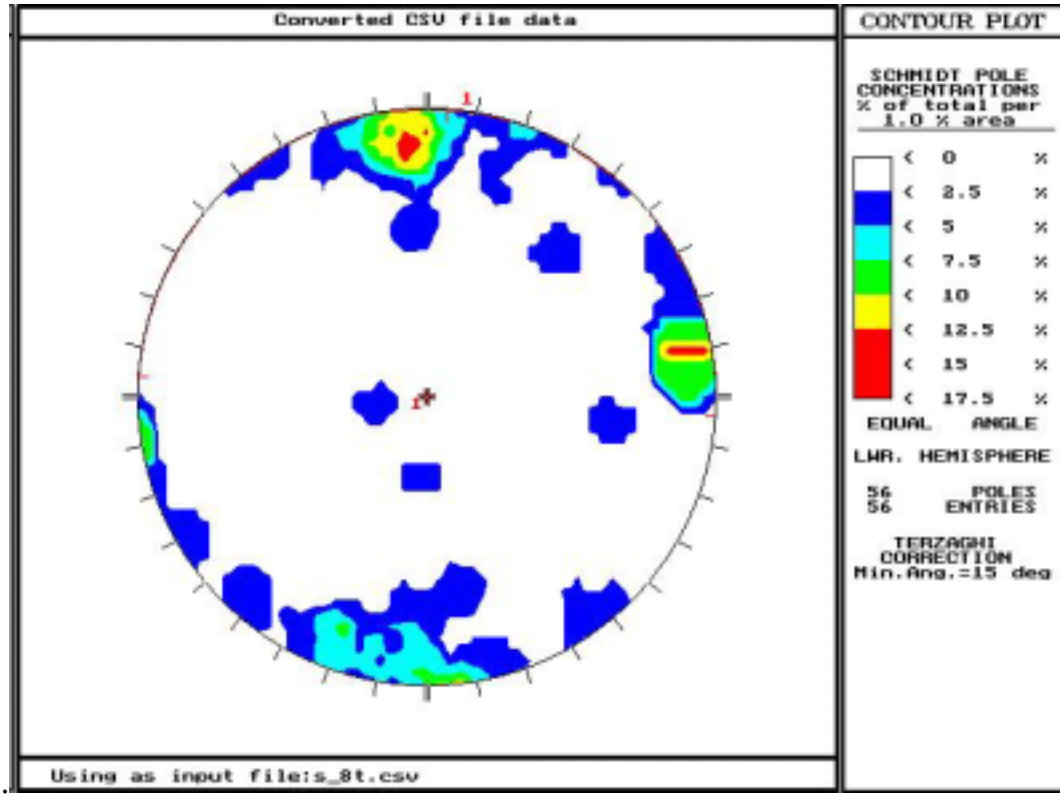

Figure 3-44. Stereoplot for Scanline 5, rotated relative to bedding plane.

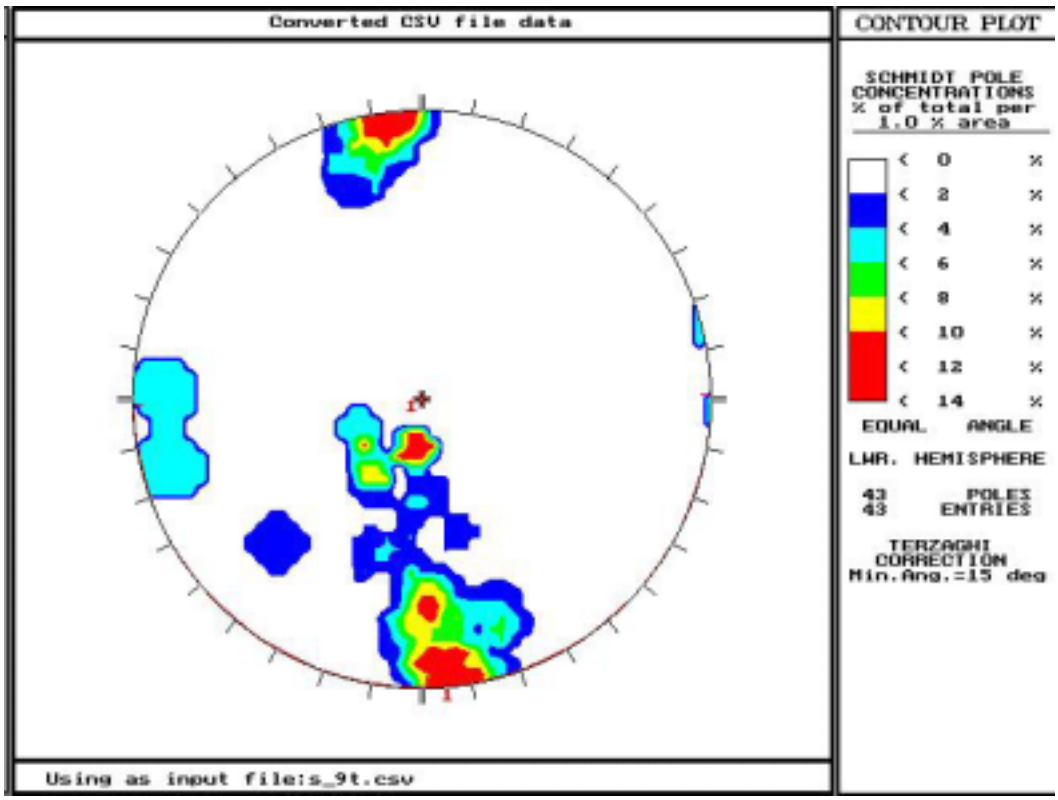

Figure 3-45. Stereoplot for Scanline 9, rotated relative to bedding plane.

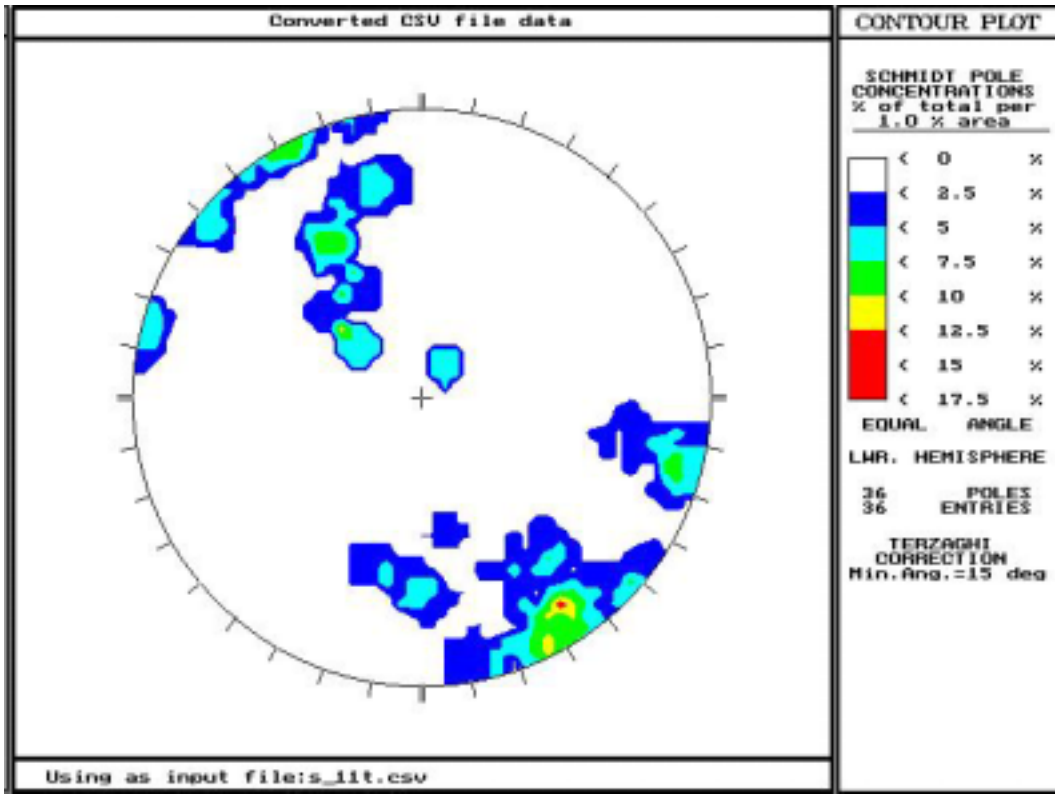

Figure 3-46. Stereoplot for Scanline 11, rotated relative to bedding plane.

3.5.3 FRACTURE INTENSITY

Fracture intensity is another important component in building the discrete fracture reservoir model. Fracture intensity was studied at each of the scanline sites.

One of the goals of these analyses was to establish whether there is a single intensity value that characterizes fracturing at each site, whether for all scales or only for scales above a certain minimum size. This later case is what is often termed a Representative Elementary Volume, or REV. At the scale of the REV or at larger scales, parameter values do not change with the scale. At scales below the REV scale, parameter values show scale dependence.

The scaling properties of intensity are studied through the Mass fractal dimension. Mass dimension for scanline fracture data can vary between 0.0 and 1.0. A value of 1.0 indicates scale independence for intensity, so if a mass dimension plot has a slope approaching 1.0 for all or a threshold scale, then it is behaving as an REV. Values appreciably less than 1.0 indicate scale dependence for fracture intensity.

The mass dimension plots (Figure 3-47) show that, with the exception of Scanline 5, the slope of the mass dimension plot approaches 1.0 for scales 3 m and greater for all scanline sites. This indicates that, while fracture intensity shows some scale dependence for scales smaller than a few meters, intensity in the direction parallel to bedding behaves in a scale-independent fashion for scales greater than a few meters. Fracturing measured at Scanline 5 shows significant scale dependence up to the largest scale that could be measured – 10 m.

These results pertain only to intensity scaling parallel to bedding, and not to possible changes perpendicular to bedding, as the scanlines were set up to remain in mechanical layers defined by one or more beds. The implication of these results is that fracture intensity within a mechanical layer appears to be scale independent at scales of tens of meters. Intensity among different scanline sites, however, shows that there may be some variations at these larger scales (hundreds of meters). These results imply that intensity within a reservoir simulation grid cell, typically on the order of 50 m to 100 m in horizontal extent, should be homogeneous; but that variations among cells may occur. in other words, the measured horizontal variation in fracture intensity is at about the same scale of disrcetization as a typical reservoir simulation grid.

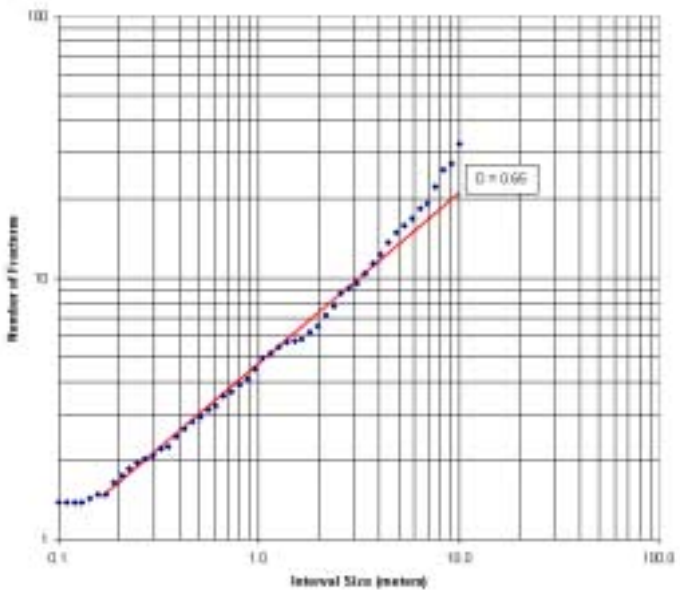

a)

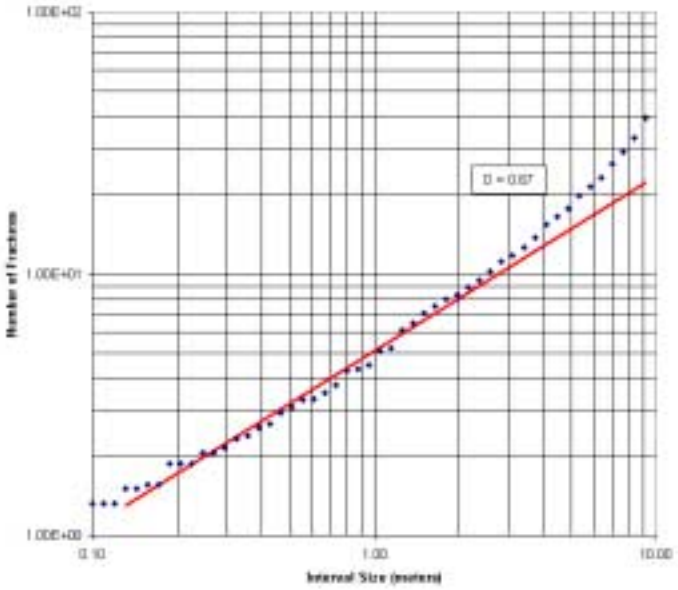

b)

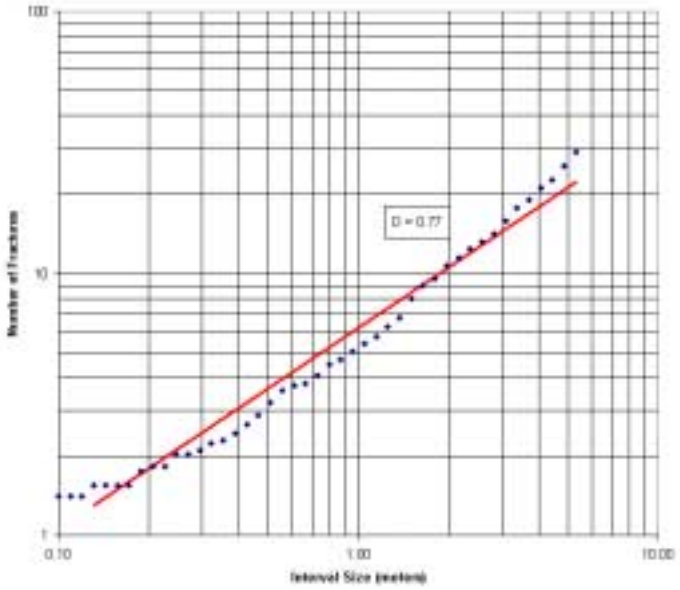

c)

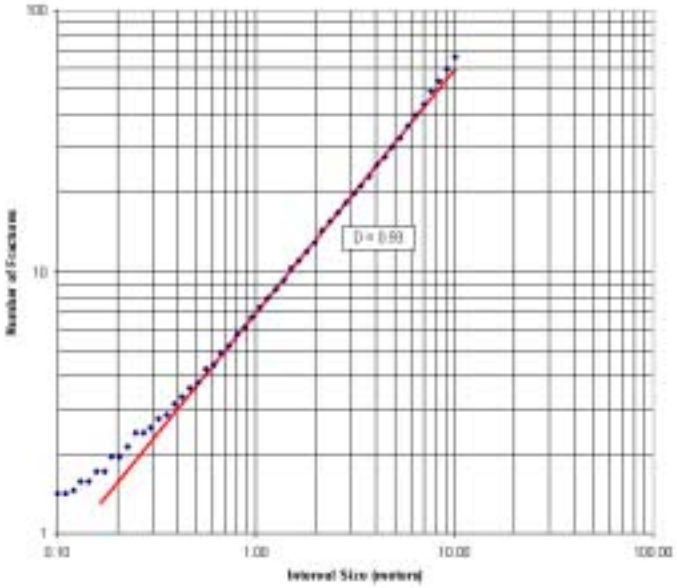

d)

Figure 3-47. Mass dimension calculations for the 11 scanline sites. Plots a through k are, in order, for scanlines 1 through 11.

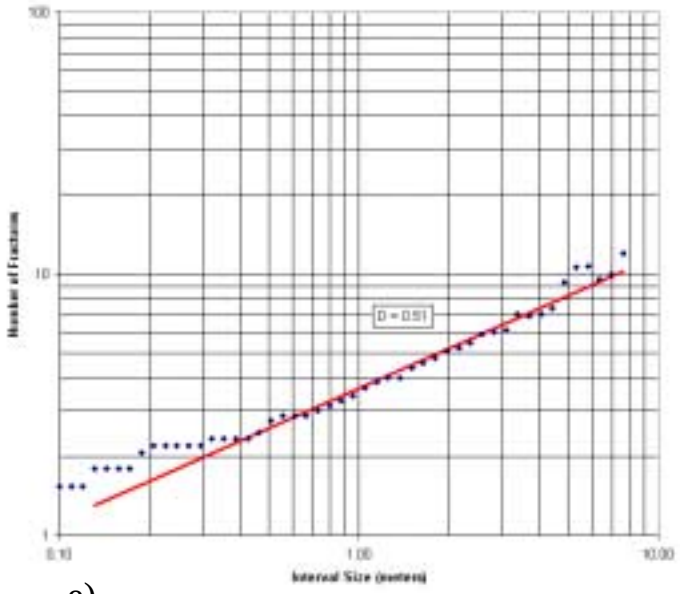
Number of Fractures
100
10
1
D = 0.91
0.10
1.00
10.00
Interval Size (meters)

e)

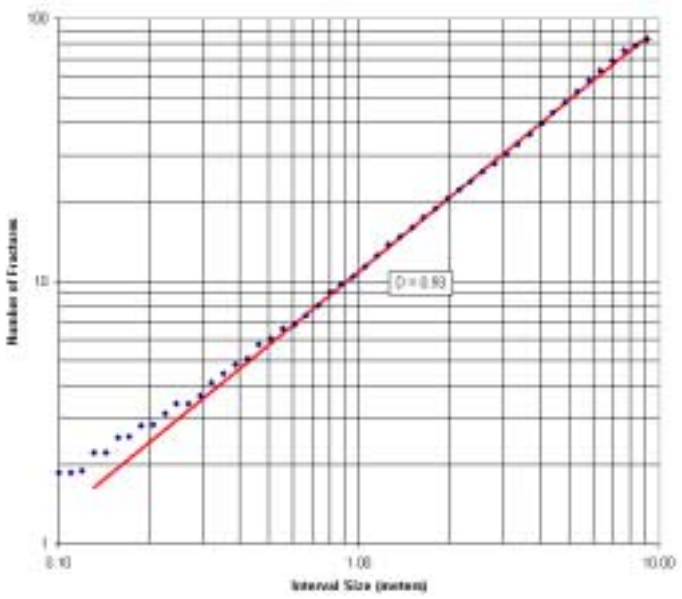
Number of Fractures
100
10
1
D = 0.93
0.10
1.00
10.00
Interval Size (meters)

f)

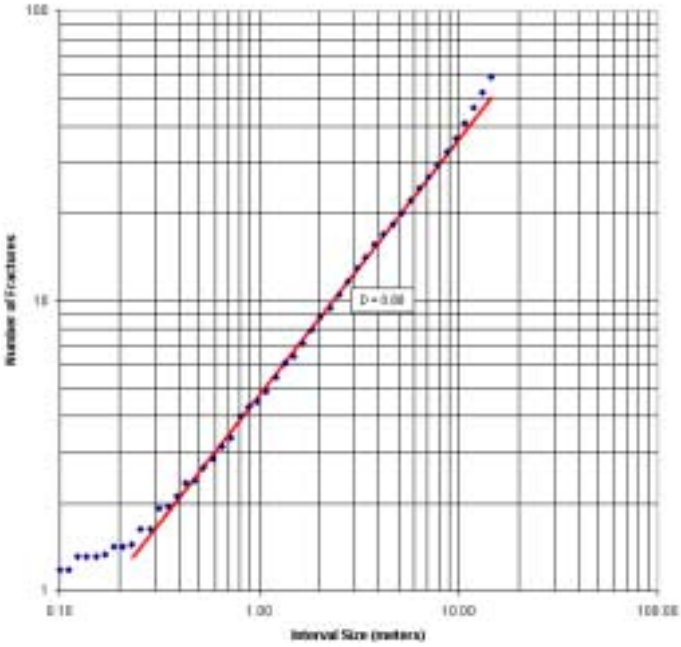
Number of Fractures
100
10
1
D = 1.08
0.10
1.00
10.00
100.00
Interval Size (meters)

g)

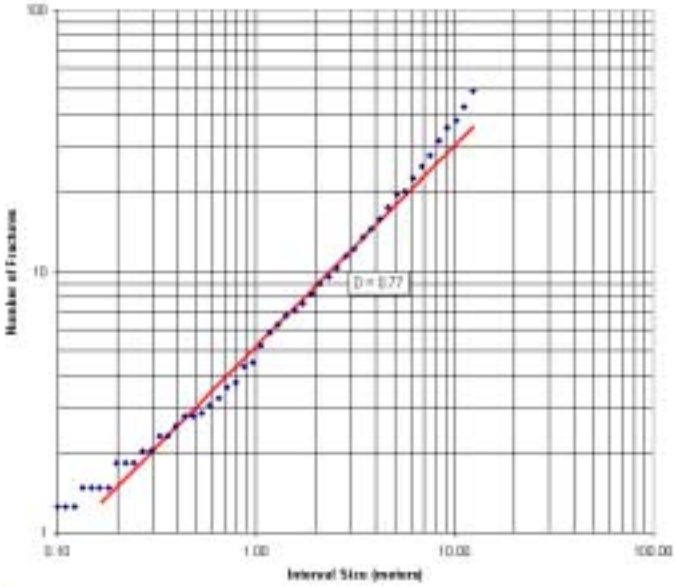
Number of Fractures
100
10
1
D = 0.77
0.10
1.00
10.00
100.00
Interval Size (meters)

h)

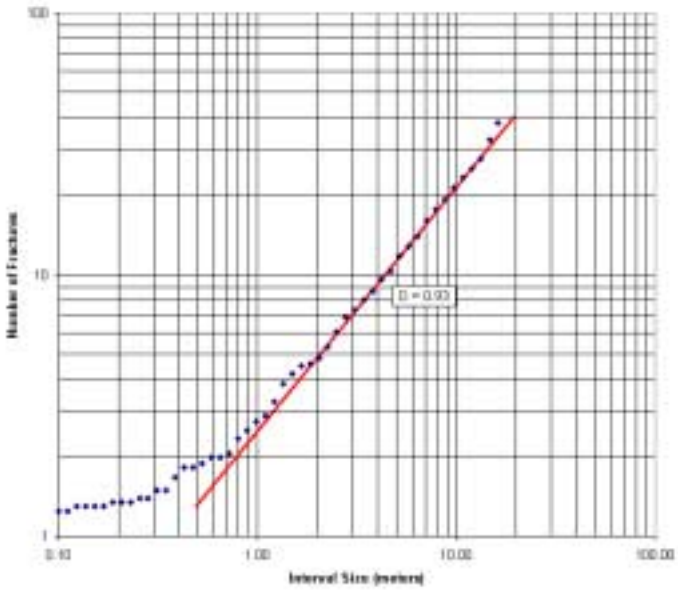
100
10
1
D = 0.93
0.10
1.00
10.00
100.00
Interval Size (meters)

i)

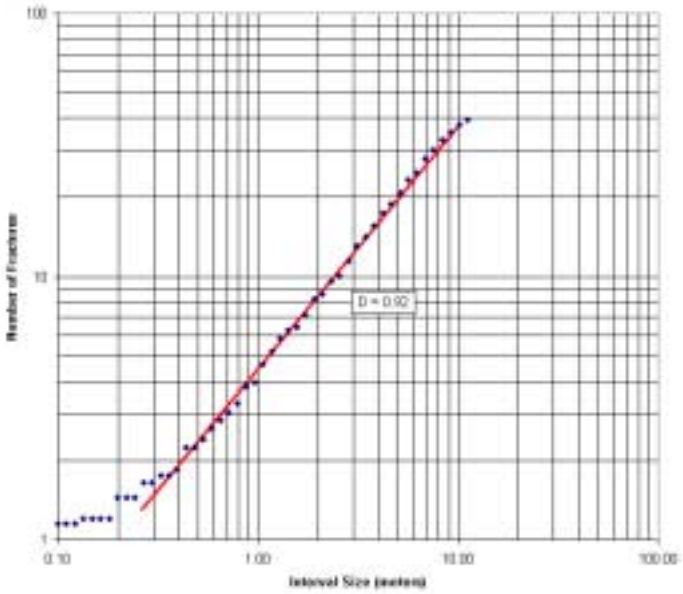
100
10
1
D = 0.92
0.10
1.00
10.00
100.00
Interval Size (meters)

j)

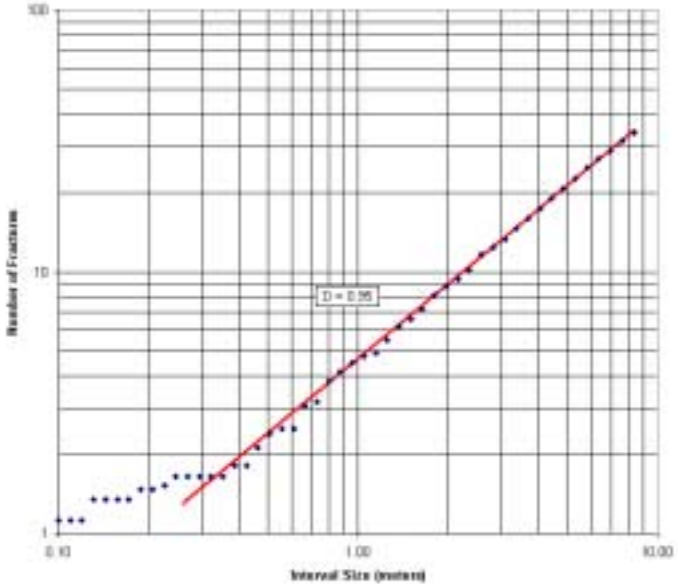
100
10
1
D = 0.95
0.10
1.00
10.00
Interval Size (meters)

k)

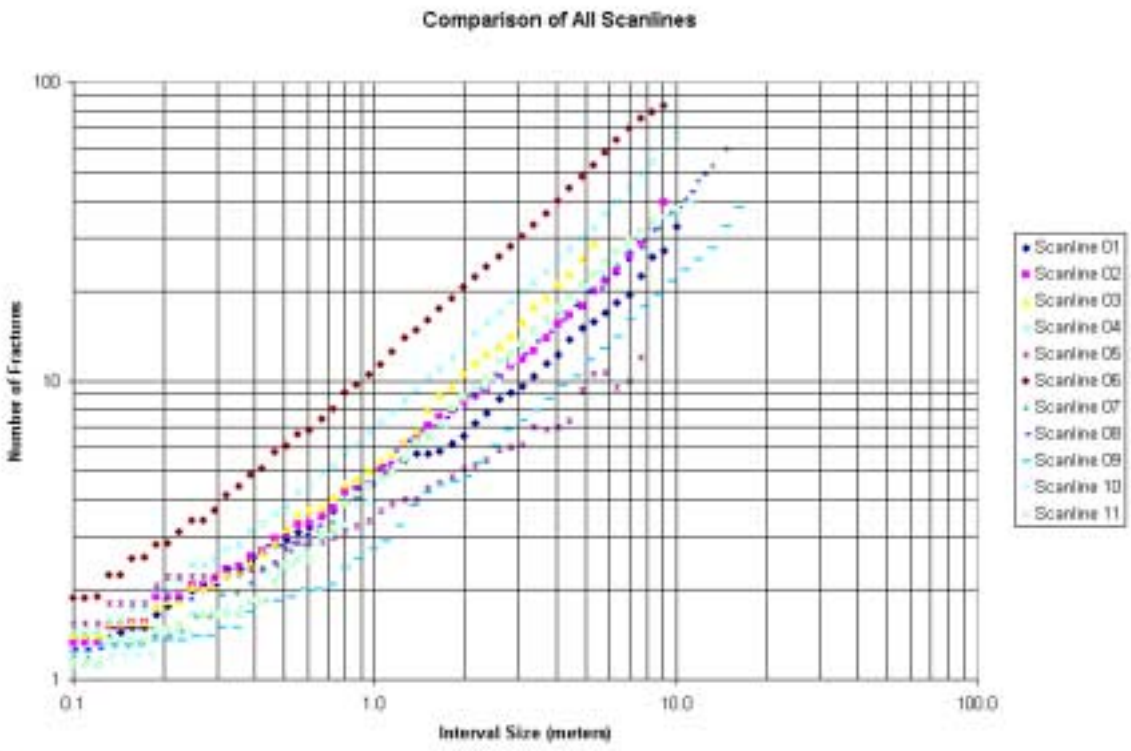

Figure 3-48. Composite plot of mass dimension calculations for all 11 scanlines.

Scanline	Mass Dimension
1	0.65
2	0.67
3	0.77
4	0.93
5	0.51
6	0.93
7	0.88
8	0.77
9	0.93
10	0.92
11	0.95

Table 3-2. Summary of mass dimensions for all 11 scanlines. Orange shading indicates Red Peak Member, while light blue shading indicates Crow Mountain Member.

Figure 3-48 and Table 3-2 summarize the mass dimensions calculated for all eleven scanlines. The values of the dimensions show groupings similar in some ways to the groupings of orientations.

For example, the mass dimensions for scanline sites 1 and 2 show values close to 0.66, which is distinctly different than for the other sites. With the exception of Scanline 5, the mass dimensions of the remaining scanlines are generally quite high. The reason for the low value (0.51) for Scanline 5 stands out. The reason for this may be due to the very low intensity of fracturing at this location.

Scanlines 4 through 7 are in the Crow Mountain Member, while the others are in the Red Peak Member. Table 3-2 indicates by colored shading which member the scanline was in. This Table does not show any obvious correspondence between the mass dimension and the Member.

The fracture intensity at scales above the REV threshold (essentially the value of the ordinate at the largest scales displayed in the plots) shows that Scanline 6 has the highest intensity, followed by 4 and 3. Slightly below these three scanlines are a group of five scanlines – 11,2,7,8 and 10 – that all have a nearly identical intensity. The scanlines with the lowest intensity, in decreasing order, are 1, 9 and 5. Once again, absolute intensity does not appear to correspond to whether it is in the Crow Mountain or Red Peak Member.

3.6 Task 2.6 – Generation of the DFN Model

3.6.1 PURPOSE OF TASK

Task 2.6 involves the comparison of the strain field predicted by the successfully-balanced restoration with the fracture geometry measured in outcrop in the subsurface, in order to determine how the strain field relates to fracture pattern development, as well as to the parameter values necessary to utilize strain information for developing the discrete fracture network (DFN) model.

In order to evaluate alternative improved oil recovery processes in fractured reservoirs, and to design these processes, it is important to understand the development of fractures throughout the reservoirs, not only in the vicinity of the wells.

To date, there has been no seismic acquired at the Circle Ridge Field that could be processed to yield the types of attributes that may correspond to fracture intensity or orientation. Moreover, the steep dips of the strata in some areas of the Field could make processing problematic, and the shallowness of the reservoirs would require a closely-spaced 3D survey, which would greatly increase the per-acre acquisition cost.

Fortunately, the Circle Ridge Field's fracturing most likely originated in response to the folding and faulting that has produced the present-day structure. Because of the excellent

well control on key horizons, and due to the successful acquisition of additional cross section data and successful cross-section balancing (Tasks 2.3 and 2.4, respectively), it is possible to determine whether and how the strains developed during folding and faulting have produced the current fracture pattern.. Thus, the two goals of this Task are to:

1) Determine if the strains related to folding and faulting are likely to have produced the observed fracture patterns in the Tensleep and Phosphoria; and
2) If there does appear to be a causal relation between the strain history and the fracture pattern, to quantify how the strain magnitudes, orientations, etc. relate to fracture intensity, orientation and other parameters.

Several of the key pieces of information for developing the DFN conceptual model have been completed. It has been determined that the scale of fracture intensity does not appear to depend upon scale for scales on the order of a few meters to some tens of meters, but may vary at scales greater than hundreds of meters. This variation is, fortunately, at the horizontal scale typical of many reservoir simulation discretizations, which suggests that the reservoir simulator input calculated from the DFN model should accurately reflect the in inherent scale of fracture variability.

Moreover, the intensity studies do not show variation as a function of whether the scanline was located in the Crow Mountain member or the Red Peak member. While this does not rule out variations as a function of lithology for other formations or members, it does indicate that the strain differences associated with deformation may play a greater role in controlling fracture intensity than the mechanical property variations attendant to different lithologies. This implies that the intensity variation of the fracturing in the DFN model may be controlled primarily or completely by the strain differences inferred from the palinspastic reconstructions.

While the final comparisons between the intensity and orientation of strain derived from the structural reconstructions and the scanline data have not been completed, the values do show orientations and orientation and intensity variations that are consistent with the fracturing having been generated by the folding and faulting. This suggests that the choice to carry out a palinspastic reconstruction of the Field will provide very useful and important controls on the development of the reservoir model.

3.7 Task 5.1 – Project Web Site

3.7.1 WEB SITE DEVELOPMENT

The project website, www.fracturedreservoirs.com, has been updated with additional data and reports during the project reporting period.

The contents of the web site are divided into the following sections:

Background	General information about the Circle Ridge

	project
History	Brief description of the history of the Circle Ridge Oil Field
Data	Project Data Warehouse
Documents	Progress Reports and Papers related to the Circle Ridge project
Presentations	Presentations given during the Circle Ridge project
Feedback	Form to provide feedback to the project team
Links	Links to related sites on the World Wide Web

Table 3-3. First-level organization of project web site content.

Table 3-4 lists the additions to the data made accessible to the public during the project's second six-month period.

Website Category	**Item Description(s)**
Background	no new updates
History	no new updates
Data	nitrogen injection test results; image log data and spinner data from well Shoshone 66-7; raw scanline data from all 11 scanline outcrop fracture study sites; stereoplots of fracture data from all 11 scanline sites petrophysical interpretations of 35 wells, complete with raw log curves; 3D strain output from palinspastic reconstructions
Documents	1st Progress Report, May 1, 2000 – Oct. 31, 2000.
Presentations	**Palinspastic Reconstruction Presentation, March 29, 2001, Fort Washakie, Wyoming** Core photographs for Shoshone 65-48

Table 3-4. Updates to website content during period Nov. 1, 2000 to April 31, 2001.

3.7.2 WEB SITE STATISTICS

Since October 31, 2000, there have been 490 hits on the project website (Figure 3-49).. This translates into between two and three external visits a day. This figure shows that there has been a progressive increase in the number of visits to the project page, particularly since the beginning of 2001.

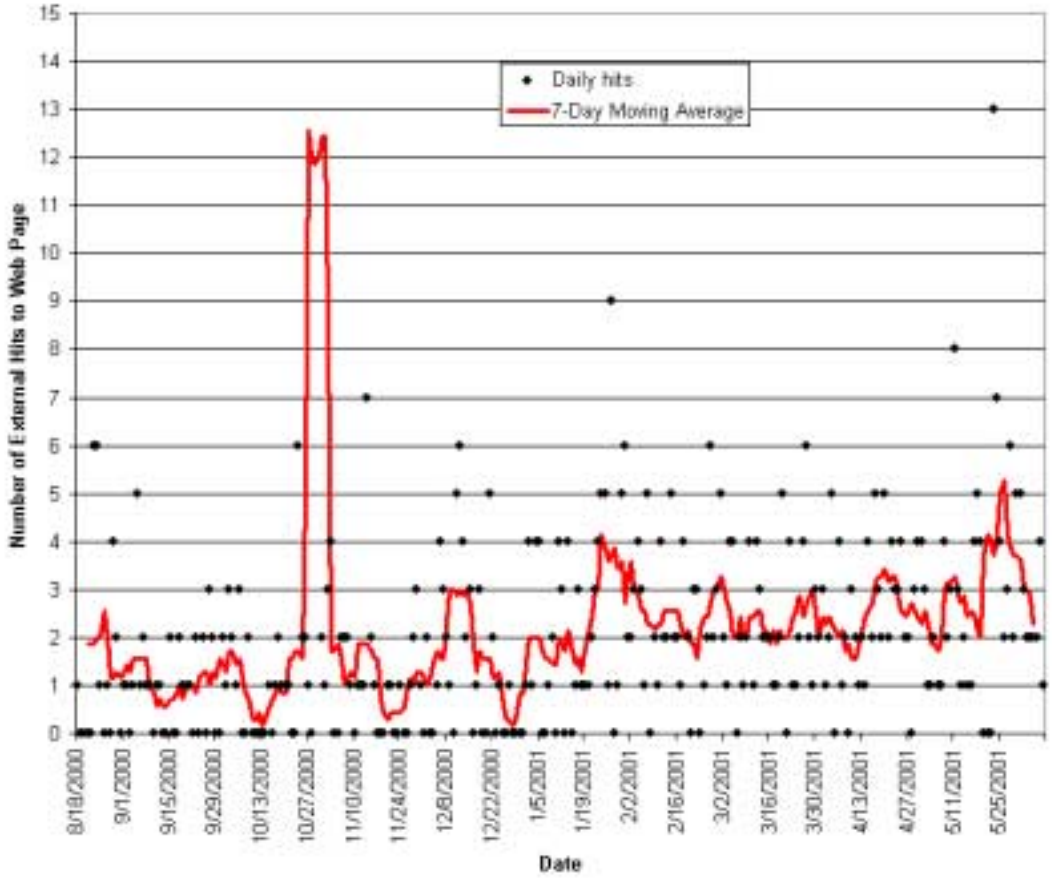

Figure 3-49. Number of external hits on project web page from initiation of web page on August 18, 2000.

3.8 Task 5.2 – Conferences and Papers

3.8.1 PURPOSE OF TASK

The purpose of this task is to help disseminate project results to all stakeholders and other interested parties in the public and private sectors. It is one of four ways in which project results are made available (the others being the project website, meetings for the Tribes, and reports). The workscope for this subtask called for one abstract to be submitted to a relevant national conference.

3.8.2 STATUS AND PLANS

With the completion of the 3D palinspastic reconstruction, it is now possible to prepare two conference contributions on the completed technical work. The first contribution will be on the three-dimensional reconstruction of the field; the second paper will focus on the relation of the surface and subsurface fracturing to the structural deformation. Both are in the process of being written, and will be submitted to the AAPG for next year's annual meeting in Houston, TX. The provisional titles and authorship for these two papers are:

Three-Dimensional Palinspastic Reconstruction of the Circle Ridge Oilfield, Wind River Basin, WY. J. Hermanson[1], P. La Pointe[1], R. Straub[2] and B. Curran[3]

[1]Golder Associates Inc., Redmond, WA
[2]GeoData Services, Coos Bay, OR
[3]Marathon Oil Company, Oklahoma City, OK

The Evolution of Fracturing and Fracture Controls in the Circle Ridge Oilfield, Wind River Basin, WY. P. La Pointe[1], J. Hermanson[1], M. Dunleavy[2] and K. Steel[2]

[1]Golder Associates Inc., Redmond, WA
[2]Marathon Oil Company, Cody, WY

4 CONCLUSIONS

4.1 Overview

This section summarizes the most important results obtained in the project during the six-month reporting period, and discusses what implications they have both for their influence on future project activities, and more importantly, on the goal of recovering additional oil from the Circle Ridge Field. The two key areas where significant technical results have been obtained concern the palinspastic reconstruction and the scanline fracture data analysis.

4.2 Palinspastic Reconstruction

4.2.1 ANALYSIS RESULTS

The 3D palinspastic reconstructions of the Circle Ridge Field has been performed using the major faults and thrusts identified by field observations by the authors and by previous investigations by Anderson and O´Connell (1993) and Smith (2000). The restoration process has been performed on the Tensleep formation as the controlling surface, with the Phosphoria and Amsden Formations moving as passive bodies and surfaces. All other geological formations above and below these three formations have not been included in the balancing process.

The 3D restoration along the major fault planes was successfully completed using the Fault Parallel Flow algorithm. The relatively good matches of footwall and hanging wall sections indicates that fault-parallel flow may be a useful model for the kinematic deformation process at Circle Ridge for these reservoir units. The mismatch in the formations that are immediately above and below the Tensleep formation indicates that there might be other processes involved as well, such as volume change during the deformation. The volume change is more or less evenly distributed throughout the formations.

The finite strain developed during the faulting process is highest along the main Red Gully Fault and the Blue Draw Fault, which are the faults with the largest displacements.

The resulting movements of Fault Block 1 (mainly the overthrust) show local anomalies of strain developing in the central part of the Block. This strain accumulation is due to a space problem as Fault Block 1 is moved against the Red Gully Fault and the lower faults. There may be several reasons for this strain anomaly, such as:

- The order of faulting may be different than assumed
- The movement along some of the faults may be simultaneous
- Small faults take no part in the restoration process
- Unkown faults may exist in Fault Block 1, particularly northeast or northwest trending structures

The strain accumulation becomes even more evident as the initial fold structure is restored back to its flat depositional origin.

The final stage of unfolding the Circle Ridge anticline was performed using the processes of Flexural Slip Unfolding and Vertical Shear Unfolding. Both methods show similar results:

- The overturned limb has the largest accumulated strains
- Fault Block 1 show large strain anomalies in its central part
- Boundary effects are evident along the outer boundary of especially Fault Block 1 and should be carefully removed when using the strain output from the model
- The observed mismatches of the Phosphoria and Amsden formations from the fault restoration process becomes evident when unfolding the anticline

The Vertical Shear Unfolding algorithm offers a slight advantage over the Flexural Slip unfolding algorithm that suggests that the results from the Vertical Shear Unfolding be used for future fracture generation calculation. Both algorithms produce a similar strain pattern, but Flexural Slip Unfolding is numerically less stable, resulting in local anomalies of extreme strain accumulations. This difference was evident when performing restoration calculation.

Although the details of the formation (and member) tops have been revised based upon the extensive well-reinterpretations in La Pointe and others (2000), and the geometry of the fault surfaces have been changed, the reconstructions shows that the order of faulting proposed by Anderson and O'Connell (1993) is kinematically reasonable in three, not just two dimensions, as is the overall first-order fold shape. However, there are mismatches between the footwall and hanging wall of the Phosphoria and Amsden formation which suggest that there are other processes involved as well. The strain accumulation in Fault Block 1 also points at alternative interpretations of how these units have moved, or if there are other faults involved which are not known or to small to be included at a reservoir scale.

In summary:

1) It was not known prior to the 3D reconstruction work whether it would be possible to successfully reconstruct the Tensleep and Phosphoria Formations in the Circle Ridge Field from just well data, as no seismic data is available for this purpose. A combination of the extensive well log reinterpretations and the power of reconstructing the reservoir units using three-dimensional balancing constraints made it possible to achieve this success.
2) The reconstruction process has led to a revision to the geometry of a number of the fault surfaces, but not to their chronological order of formation.
3) The results of the reconstruction indicate the usefulness and importance of obtaining subsurface flow and transport data in both the Tensleep and

Phosphoria Formations, as well as in the overthrust and subthrust portions of the Field, and has led to a clearer understanding and delineation of portions of the Circle Ridge Field that have experienced different strain histories. This understanding has been used to guide the selection and planning for the additional well data to be obtained as part of this project

4.3 DFN Reservoir Model Development

Final DFN reservoir model development will await the completion of the comparison between the 3D palinspastic strain history and the scanline and subsurface fracture data. However, the work thus far on the scanline data has led to some conclusions regarding the geological conceptual model. These are:

1) Structural controls appear likely to be the most important constraints on fracture orientation and intensity. Lithology variations within a formation or member may also have some influence. In terms of structural controls, it appears that the fracture orientations are typically orthogonal to bedding and strike parallel and/or perpendicular to dip along the flanks of the fold away from the more tightly contorted fold nose or from the major faults. In the more tightly folded areas, which are also generally areas proximal to faults, fracture orientations become more varied and include orientations that are not as simply related to bedding as on the flanks.
2) Horizontal variation in fracture intensity is at the scale of hundreds of meters, the typical disrcetization scale of a reservoir simulation grid. This suggests that a typical reservoir simulation grid will accurately represent the scale of variability inherent in the fracture pattern.

As previously discussed, the palinspastic reconstructions showed that there should be differences in the strain in the Tensleep vs. the Phosphoria, and in the subthrust vs. the overthrust portions of the reservoir. Thus, it will be important to making an accurate reservoir model of these regions to obtain subsurface data in each. The locations of the additional tracer, image log, spinner log and transient well test data have been planned with these specific requirements.

3) REFERENCES

Agaston, R. S., 1952, Tensleep Formation of the Bighorn Basin: Wyoming Geological Association 7th Annual Field Conference Guidebook, southern Bighorn Basin, Wyoming, p. 44-48.

Anderson, T. C., and O'Connell, P., J., 1993, Structural geology of the Circle Ridge Oilfield, Fremont County Wyoming, in Keefer, W. R., Metzger, W. J., Godwin, L. H. eds., Wyoming Geological Association Special Symposium on Oil and Gas and Other Resources of the Wind River Basin, Wyoming, p. 399-418.

Andrews, D. A., 1944, Geologic and structure contour map of the Maverick Springs area, Fremont County, Wyoming: U.S. Geological Survey Oil and Gas Investigations Preliminary Map 13.

Asquith. G. and C. Gibson (1982). Basic Well Log Analysis for Geologists. American Association of Petroleum Geologists, Methods in Exploration Series, Tulsa, OK (4th Printing), 216p.

Barton, C. C. and P. R. La Pointe, 1995. Fractals in the Earth Sciences. Plenum Press, New York. 265p.

Berg, R. R., 1962, Mountain flank thrusting in Rocky Mountain foreland, Wyoming and Colorado: Bulletin of the American Association of Petroleum Geologists, vol. 48, no. 11, p. 2019-2032.

Brown, W. G., 1988, Deformational style of Laramide uplifts in the Wyoming foreland: Geological Society of America Memoir 171, p. 1-25.

Brown W. G., 1993, Structural Style of Laramide basement-cored uplifts and associated folds, in Snoke, A. W., Steidtmann, J. R., and Roberts, S. M., eds., Geology of Wyoming: Geological Survey of Wyoming Memoir no. 5, p. 312-371.

Burtner, R. L., and Warner, M. A., 1984, Hydrocarbon generation in lower Cretaceous Mowry and Skull Creek Shales in the northern Rocky Mountains area; in Woodward, J., Meissner, F. F., and Clayton, J. L., eds., Hydrocarbon source rocks of the greater Rocky Mountain region: Rocky Mountain Association of Geologists Guidebook, p. 449-467.

Coney, P. J., 1978, Mesozoic-Cenozoic plate tectonics, Cenozoic tectonics and regional geophysics of western Cordillera: Geological Society of America Memoir no. 152, p. 33-50.

Curry, W. H., 1962, Depositional environments in central Wyoming during Early Cretaceous: Wyoming Geological Association 17th Annual Field Conference Guidebook, p. 118-123.

Dershowitz, W. S. and H. H. Herda, 1992, Interpretation of fracture spacing and density: *in Proc. 33rd U. S. Symposium on Rock Mechanics, J. R. Tillerson and W. R. Wawersik, eds.,* A. A. Balkema, Rotterdam, 757-766.

Downs, G. R., 1952, Summary of Mesozoic stratigraphy, Bighorn Basin, Wyoming: Wyoming Geological Association 7th Annual Field Conference Guidebook, southern Bighorn Basin, Wyoming, p. 26-31.

Fanshawe, J. R., 1952, Big Horn Basin Tectonics: Wyoming Geological Association 7th Annual Field Conference Guidebook, southern Bighorn Basin, Wyoming, p. 19- 21.

Flinn, D. (1962). On folding during three dimensional progressive deformation. Q.J. Geol. Soc. London, 118, 385 - 433.

Frielinghausen, K. W., 1952, The Phosphoria Formation of southern and southeastern Bighorn Basin, Big Horn, Hot Springs, and Washakie Counties, Wyoming: Wyoming Geological Association 7th Annual Field Conference Guidebook, southern Bighorn Basin, Wyoming, p. 55-57.

Gersic, J., 1993, Nonmetallic mineral resources of the Wind River Indian Reservation, in Keefer, W. R., Metzger, W. J., and Godwin, L. H. eds., Wyoming Geological Association Special Symposium on Oil and Gas and Other Resources of the Wind River Basin, Wyoming, p. 419-425.

Gower, M. A., 1978, Catalog of Paleozoic, Mesozoic, and Cenozoic rock names for the Wind River Basin: Wyoming Geological Association 30th Annual Field Conference Guidebook, Resources of the Wind River Basin, p. 39-45.

Keefer, W. R., 1965, Geologic history of Wind River Basin, central Wyoming: Bulletin of the American Association of Petroleum Geologists, vol. 49, no. 495-b, 58p.

Keefer, W. R., 1969, Geology of petroleum in Wind River Basin, central Wyoming: Bulletin of the American Association of Petroleum Geologists, vol. 53, no. 9, p. 1839-1865.

Kinsman, D. J., 1969, Modes of formation, sedimentary associations, and diagnostic features of shallow water and supratidal evaporites: Bulletin of the American Association of Petroleum Geologists, vol. 53, no. 4, p. 830-840.

La Pointe, P. R. and J. A. Hudson (1985). Characterization and Interpretation of Rock Mass Joint Patterns. Geological Society of America, Special Paper 199, 37p.

La Pointe, P. R., J. Hermanson and T. Eiben (2000). 3-D reservoir and stochastic fracture network modeling for enhanced oil recovery, Circle r\Ridge Phosphoria/Tensleep reservoir, Wind River Reservation, Arapaho and Shoshone tribes, Wyoming. Semi-

Annual Technical Report – May 1, 2000 through October 31, 2000. DOE Award Number: DE-FG26-00BC15190

Love, J. D., 1939, Geology along southern margin of the Absaroka Range, Wyoming: Geological Society of America, vol. 53, p. 830-840.

Mandelbrot, B. B., 1983. The Fractal Geometry of Nature, W.H. Freeman and Company, New York.

Medwedeff, D. A., 1989, Growth fault-bend folding at southeast Lost Hills, San Joaquin Valley, California: AAPG Bulletin, v. 73, p. 54-67.

Midland Valley, 2000, 3Dmove User Guide & Online help pages, Midland Valley Exploration Ltd.

Mills, N. K., 1956, Subsurface stratigraphy of the pre-Niobrara Formations in the Big Horn Basin: Wyoming Geological Association Nomenclature Committee, pt. 1, p. 8-22.

Mitra, S., 1986, Duplex structures and imbricate thrust systems: geometry, structural positions and hydrocarbon potential: AAPG Bulletin v. 70, p. 1087-1112.

Mitra, S, Namson, J., 1989, Equal-area balancing: American Journal of Science, v. 289, p. 563-599.

Mitra, S., 1990, Fault-propagation folds: Geometry, kinematic evolution, and hydrocarbon traps: Bulletin of the American Association of Petroleum Geologists, vol. 74, no. 6, p. 921-945.

Olson, W. G., 1948, Circle Ridge and Maverick Springs Oil Fields, Fremont County, Wyoming: Wyoming Geological Association 3rd Annual Field Conference Guidebook, p. 178-185

Pedry, J. J., 1975, Tensleep fault trap, Cottonwood Creek Field, Washakie County, Wyoming. Wyoming Geological Association Guidebook, 27th Annual Field Conference, Wyoming, p. 211-219.

Peterson, J. A., 1954, Marine Upper Jurassic, eastern Wyoming: Bulletin of the American Association of Petroleum Geologists, v. 38., p. 463-507.

Picard, M. D., 1978, Stratigraphy of the Triassic rocks in west-central Wyoming. . Wyoming Geological Association Guidebook, 30th Annual Field Conference, Wind River Basin, Wyoming, p. 101-130..

.

Smith, V. (2000). Surface Geologic Map of the Circle Ridge Oil Field, Wyoming. M. S. Thesis, Baylor University, Waco, TX.

Stearns, D. W. and M. Friedman, 1972, Reservoirs in fractured rock: AAPG Memoir 16, Stratigraphic Oil and Gas Fields, American Association of Petroleum Geologists, Tulsa, OK, 82-106.

Stipp, T. F., 1952, Paleozoic formations of the Big Horn Basin, Wyoming. Wyoming Geological Association Guidebook, 7th Annual Field Conference, Southern Big Horn Basin, Wyoming, 22-25.

Stock, J. and P. Molnar,1988: Uncertainties and implications of the Late Cretaceous and Tertiary position of North America relative to the Farallon, Kula & Pacific plates. Tectonics, Washington, 7, 1339-1348.

Suppe, J., 1983, Geometry and kinematics of fault-bend folding: American Journal of Science, v. 283, p. 684-721.

Suppe, J., 1985, Principles of structural geology: Englewood Cliffs, New Jersey, Prentice Hall, 537 p.

Suppe, J., 1989, Rates of fault slip and fold growth (abs): GSA abstracts with programs, v. 21, p. A28.

Suppe, J., Mount, V. S., Hook, S. C., 1990, A forward modeling strategy for balancing cross-sections, AAPG, v. 74 no. 5, p. 521-531.

Terzaghi, R. D., 1965, Sources of error in joint surveys: Geotechnique 15, 287-304.